FINAL REPORT ~ FHWA-OK-14-02

DRYING SHRINKAGE PROBLEMS IN HIGH PI SUBGRADE SOILS

Rifat Bulut, Ph.D.
Lizhou Chen
Sruthi Mantri
Omar Amer
Yi Tian
School of Civil Engineering and Environmental Engineering
College of Engineering, Architecture and Technology
Oklahoma State University

Musharraf Zaman, Ph.D., P.E.
School of Civil Engineering and Environmental Science
College of Engineering
The University of Oklahoma

January 2014

Oklahoma Department of Transportation

DRYING SHRINKAGE PROBLEMS IN HIGH PI SUBGRADE SOILS

FINAL REPORT ~ FHWA-OK-14-02

ODOT SP&R ITEM NUMBER 2236

Submitted to:
John R. Bowman, P.E.
Planning & Research Division Engineer
Oklahoma Department of Transportation

Submitted by:
Rifat Bulut, Ph.D.
Lizhou Chen, Ph.D. Candidate
Sruthi Mantri, M.Sc. Student
Omar Amer, Ph.D. Candidate
Yi Tian, M.Sc. Student
School of Civil and Environmental Engineering
Oklahoma State University
and
Musharraf Zaman, Ph.D., P.E.
School of Civil Engineering and Environmental Science
The University of Oklahoma

January 2014

TECHNICAL REPORT DOCUMENTATION PAGE

1. REPORT NO.	2. GOVERNMENT ACCESSION NO.	3. RECIPIENTS CATALOG NO.
FHWA-OK-14-02		

4. TITLE AND SUBTITLE	5. REPORT DATE
Drying Shrinkage Problems in High PI Subgrade Soils	January 2014
	6. PERFORMING ORGANIZATION CODE

7. AUTHOR(S)	8. PERFORMING ORGANIZATION REPORT
Rifat Bulut, Lizhou Chen, Sruthi Mantri, Omar Amer, Yi Tian, and Musharraf Zaman	

9. PERFORMING ORGANIZATION NAME AND ADDRESS	10. WORK UNIT NO.
Oklahoma State University School of Civil and Environmental Engineering 207 Engineering South, Stillwater, OK 74078	11. CONTRACT OR GRANT NO. ODOT SP&R Item Number 2236

12. SPONSORING AGENCY NAME AND ADDRESS	13. TYPE OF REPORT AND PERIOD COVERED
Oklahoma Department of Transportation Planning and Research Division 200 N.E. 21st Street, Room 3A7 Oklahoma City, OK 73105	Final Report Oct 2011 - Dec 2013
	14. SPONSORING AGENCY CODE

15. SUPPLEMENTARY NOTES

16. ABSTRACT

The main objective of this study was to investigate the longitudinal cracking in pavements due to drying shrinkage of high PI subgrade soils. The study involved laboartory soil testing and modeling. The shrinkage cracks usually occur within the vicinity of the edge of the pavement where moisture boundary conditions play a significant role in the behavior of expansive subgrade soils. The study investigated the shrinkage problems in pavement subgrade soils at four sites in Oklahoma. The soil specimens collected from the sites were tested for the basic index properties as well as soil suction and unsaturated diffusivity measurements. Various ranges of the test results have been implemented in suction profile and tensile stress prediction models for evaluating the typical suction changes and the corresponding tensile stresses in subgrade soils

17. KEY WORDS	18. DISTRIBUTION STATEMENT
Drying, shrinkage, pavement, suction	No restrictions. This publication is available from the Planning & Research Division, Oklahoma DOT

19. SECURITY CLASSIF. (OF THIS REPORT)	20. SECURITY CLASSIF. (OF THIS PAGE)	21. NO. OF PAGES	22. PRICE
Unclassified	Unclassified	141	N/A

SI* (MODERN METRIC) CONVERSION FACTORS

APPROXIMATE CONVERSIONS TO SI UNITS				
SYMBOL	**WHEN YOU KNOW**	**MULTIPLY BY**	**TO FIND**	**SYMBOL**
LENGTH				
in	inches	25.4	millimeters	mm
ft	feet	0.305	meters	m
yd	yards	0.914	meters	m
mi	miles	1.61	kilometers	km
AREA				
in^2	square inches	645.2	square millimeters	mm^2
ft^2	square feet	0.093	square meters	m^2
yd^2	square yard	0.836	square meters	m^2
ac	acres	0.405	hectares	ha
mi^2	square miles	2.59	square kilometers	km^2
VOLUME				
fl oz	fluid ounces	29.57	milliliters	mL
gal	gallons	3.785	liters	L
ft^3	cubic feet	0.028	cubic meters	m^3
yd^3	cubic yards	0.765	cubic meters	m^3
NOTE: volumes greater than 1000 L shall be shown in m^3				
MASS				
oz	ounces	28.35	grams	g
lb	pounds	0.454	kilograms	kg
T	short tons (2000 lb)	0.907	megagrams (or "metric ton")	Mg (or "t")
TEMPERATURE (exact degrees)				
^oF	Fahrenheit	5 (F-32)/9 or (F-32)/1.8	Celsius	^oC
ILLUMINATION				
fc	foot-candles	10.76	lux	lx
fl	foot-Lamberts	3.426	candela/m^2	cd/m^2
FORCE and PRESSURE or STRESS				
lbf	poundforce	4.45	newtons	N
lbf/in^2	poundforce per square inch	6.89	kilopascals	kPa

APPROXIMATE CONVERSIONS FROM SI UNITS				
SYMBOL	**WHEN YOU KNOW**	**MULTIPLY BY**	**TO FIND**	**SYMBOL**
LENGTH				
mm	millimeters	0.039	inches	in
m	meters	3.28	feet	ft
m	meters	1.09	yards	yd
km	kilometers	0.621	miles	mi
AREA				
mm^2	square millimeters	0.0016	square inches	in^2
m^2	square meters	10.764	square feet	ft^2
m^2	square meters	1.195	square yards	yd^2
ha	hectares	2.47	acres	ac
km^2	square kilometers	0.386	square miles	mi^2
VOLUME				
mL	milliliters	0.034	fluid ounces	fl oz
L	liters	0.264	gallons	gal
m^3	cubic meters	35.314	cubic feet	ft^3
m^3	cubic meters	1.307	cubic yards	yd^3
MASS				
g	grams	0.035	ounces	oz
kg	kilograms	2.202	pounds	lb
Mg (or "t")	megagrams (or "metric ton")	1.103	short tons (2000 lb)	T
TEMPERATURE (exact degrees)				
^oC	Celsius	1.8C+32	Fahrenheit	^oF
ILLUMINATION				
lx	lux	0.0929	foot-candles	fc
cd/m^2	candela/m^2	0.2919	foot-Lamberts	fl
FORCE and PRESSURE or STRESS				
N	newtons	0.225	poundforce	lbf
kPa	kilopascals	0.145	poundforce per square inch	lbf/in^2

*SI is the symbol for the International System of Units. Appropriate rounding should be made to comply with Section 4 of ASTM E380.

TABLE OF CONTENTS

LIST OF FIGURES

LIST OF TABLES

ACKNOWLEDGEMENTS

The financial support for this project was provided by the Oklahoma Department of Transportation (ODOT) under Grant No. SPR 2236 and Oklahoma Transportation Center (OkTC) under Grant No. OTCREOS11.1-09. The authors would like to express their appreciations to ODOT for providing the soil specimens for the study.

1. INTRODUCTION

The problems associated with shrinking and swelling soils are worldwide. In the United States, approximately 20 percent of the area is underlain by moderately to highly expansive soil. The annual cost of damage in the United States from shrinking and swelling soils is estimated at over $15 billion, and close to half this damage is attributed to highways and streets. Longitudinal cracking in pavements due to drying shrinkage of high PI subgrade clays has been a major problem in Oklahoma. Annual maintenance to seal and repair these distress problems can cost millions of dollars statewide. It has been well established in the literature that the mechanisms of shrinkage cracks due to high PI clay soils are governed by the principles of unsaturated soil mechanics, the suction stress being the major part of the cracking mechanism. These longitudinal cracks occur usually within the so-called edge moisture variation distance, where the moisture boundary conditions play a significant role in terms of changes in water content (or suction).

The current study investigates the subgrade soils at four sites in Oklahoma that have experienced drying shrinkage problems. Thin-walled tube soil specimens were obtained from the sites in Norman, Lake Hefner, Ardmore, and Idabel in Oklahoma for laboratory testing. The soil specimens were tested for the basic index properties as well as suction and unsaturated diffusivity measurements. The average values of the test results have been implemented in a suction prediction model for evaluating typical suction profiles in subgrade soils. An existing, water-content based analytical model was modified for unsaturated soils for prediction of tensile stresses in subgrades. The tensile stress predictions have been made using the new model for different moisture boundary conditions. The commercially available finite element method software package Abaqus was also employed in studying the suction, tensile stress, and deformation profiles in the subgrade soils. The main purpose of the study was to focus on improving our understanding of the mechanism of drying shrinkage problems in high PI soils using the unsaturated soil mechanics principles. The study attempted to provide a rational approach in predicting the suction change underneath the pavement and corresponding

tensile stresses in subgrade soils in response to various surface moisture boundary conditions.

2. BACKGROUND

High PI shrinking clay soils are encountered in many parts of Oklahoma. These subgrade soils support transportation infrastructure, which include pavements, runways, parking lots, bike and walking trails at the recreational areas, etc. Damages to civil infrastructures due to shrinking soils have been increasing each year as a result of large volumetric strains experienced by these soils from moisture content fluctuations. Longitudinal pavement cracking on the local road network in Oklahoma is one of the most prevalent pavement distresses caused by volumetric changes of shrinking high PI subgrade soils (Nevels 2006). These cracks occur close to the shoulder of the pavement and represent a significant problem for Oklahoma Department of Transportation (ODOT) as well as other state agencies. Annual maintenance to seal and repair these distress problems can cost millions of dollars statewide. In the United States, volumetric changes due to shrinking and swelling soils cause extensive damage, which costs about $7 to $15 billion annually (Nuhfer et al. 1993; Wray and Meyer 2004).

Desiccation of clay soils causes shrinkage cracks which is a major problem in pavement engineering as well as in some other disciplines (Jayatilaka et al. 1993; Puppala et al. 2009). Shrinkage cracks have the potential to cause severe damage to the serviceability of the transportation infrastructure. In recent years, a significant effort is directed to better analyze ground and climate interactions as applicable to a range of transportation structures. It has been well established in the literature that the mechanism of shrinkage cracks due to high PI clay soils are governed by the principles of unsaturated soil mechanics, the suction stress being the major part of the cracking mechanism (Luo and Prozzi 2008; Puppala et al. 2009).

In many cases, this type of cracking initiates in the drying subgrade soil and reflects from the highly plastic subgrade through the pavement structure. These longitudinal cracks occur usually within the so-called edge moisture variation distance (e_m), where the climate plays a significant role in terms of changes in water content (suction). Climatic effects have long been recognized as being influential in the construction and performance of pavements (Lytton et al. 2005). Consequently, the drying shrinkage

problem should be investigated based on the unsaturated soil mechanics principles and the climatic surface and subsurface boundary conditions. The mechanism of crack development is rooted in the moisture variation in shrinking high PI subgrade soil. The impermeable pavement surface layer has a significant impact on water migration out of the shrinking subgrade beneath the pavement, which results in the non-uniform moisture change in the subgrade (Luo and Prozzi 2009). The gradients of moisture variation, together with the soil volume change characteristics, determine the tensile stress distribution and shrinkage crack initiation.

If the initial condition is considered after the subgrade construction when the subgrade soil is intact without any cracks, the initial strains are zero in all three directions (Luo and Prozzi 2009). During the desiccation process of the soil in the pavement subgrade, the lateral strains (the strains in horizontal directions) remain zero before crack initiation because of lateral constraint (Luo 2007). The field data collected by Konrad and Ayad (1997) confirmed that drying soils experience a restrained desiccation so that the lateral strains were maintained zero until a crack initiated in the soil. As a result, the incremental horizontal strains in both transverse and longitudinal directions remain zero before cracking. However, soils are considered to have a certain amount of tensile strength, and this tensile strength has been used in the crack initiation criterion that predicts the onset of large tensile cracks by comparing the tensile strength with the net normal horizontal stress (Ayad et al. 1997).

In order to study the development of desiccation cracks in the subgrade soil during the reduction in water content and increase of matric suction, it is desirable to estimate the shrinkage stresses generated between two steady state matric suction profiles. Lytton et al. (2005) used a volumetric strain based model for the computations of displacements between two suction profiles (e.g., dry suction profile and wet suction profile). Sumarac (2004) presented a simpler approach for the prediction of the tensile stresses based on the elastic theory in response to moisture content changes.

Consequently, the shrinkage stress produced by the matric suction change can be estimated using the stress-strain constitutive relationships of the subgrade soil. Based on the stress distribution, the development of shrinkage cracks can be analyzed. A

theoretical, but practical, approach is needed to identify and analyze the mechanisms of the longitudinal crack development and to minimize this type of crack by means of economical and practical means. An understanding of these mechanisms is necessary to design economical remedial maintenance programs and to alter future designs, construction methods, and material specifications to reduce or eliminate this type of pavement stress. To understand the mechanisms of pavement cracking, it is necessary to understand the major variables which initiate the cracks. In the mechanisms mentioned here, it is evident that climatic effects (surface moisture boundary conditions) have a major influence on the behavior of pavements.

2.1 Moisture Diffusion in Unsaturated Soils – Matric Suction Profiles

The matric suction profile in the soil can be predicted theoretically by solving the moisture diffusion equations that governs the matric suction distribution in the soil. Mitchell (1979) proposed solutions to the general moisture diffusion equation for several different boundary conditions to simulate the effects of climate on matric suction at the ground surface, and with depth at any time. The magnitude and rate of transient moisture flow in an unsaturated soil in response to suction changes is controlled by the unsaturated moisture diffusion coefficient, which is a fundamental soil parameter in Mitchell's model (Mabirizi and Bulut 2010).

The equilibrium matric suction is usually estimated for different climatic regions based on the Thornthwaite Moisture Index (TMI). The TMI has shown promise in relating climate to pavement performance (Jayatilaka et al. 1993). The TMI is a climatic parameter introduced by Thornthwaite (1948) to characterize the moisture balance in a specific location taking into account climatic variables as rainfall, potential evapotranspiration and the depth of available moisture stored in the root zone of the vegetation. The original Thornthwaite (1948) approach for computing the TMI maps were later simplified further by Thornthwaite and Mather (1955) and Witczak et al. (2006). As a result of the revision, the modified TMI is only related to the precipitation and potential evapotranspiration at monthly intervals in evaluating the annual soil moisture balance. The Witczak et al. (2006) study was conducted as part of the Enhanced Integrated Climatic Model (EICM) in the Mechanistic Empirical Pavement

Design Guide (MEPDG), and correlations were established between TMI and equilibrium suction at depth in the pavement profile. The equilibrium suction can also be measured in the field, or estimated from Mitchell's model.

2.2 Unsaturated Soil Volumetric Strains

In unsaturated soils, two stress state variables (i.e., matric suction and mean mechanical stress) play a significant role in determining shear strength and volume change characteristics of soils (Fredlund and Morgenstern 1977). Luo and Prozzi (2009) indicated that the Lytton's model (e.g., Lytton et al. 2005), incorporating the two stress state variables for volumetric strains and Mitchell's diffusion equations for suction profiles, provides a reasonable and relatively simple relation for studying the longitudinal shrinkage cracks in pavement subgrade soils. However, in their study, Luo and Prozzi (2009) did not consider the effects of the mean mechanical stress, only suction stresses were considered. This was a reasonable assumption because in pavements the effects of mean mechanical stresses on the development of shrinkage cracks are probably small and negligible, as compared to the effects of suction stresses.

This stress-strain analysis uses unsaturated soil mechanics principles to analyze the suction stress distribution in the pavement structure over shrinking subgrade soils. The matric suction stress distribution before crack initiation is critical in order to investigate the potential location and propagation of the shrinkage crack. As the moisture content decreases in the subgrade soil, the matric suction increases, which results in volumetric changes of the soil (Sabnis et al. 2010). If the matric suction change is uniform and the soil is not constrained, normal strains will occur in each direction unaccompanied by normal stresses (Kodikara et al. 2002; Luo and Prozzi 2009). However, because the pavement is an impermeable cover, the matric suction change is not uniform in the subgrade soil. In addition, the lateral confinement does not allow the soil to have free expansion or shrinkage. Therefore, tensile stresses will occur as the matric suction increases. As the tensile stress reaches the tensile strength of the soil, a shrinkage crack will initiate in the subgrade.

2.3 Tensile Stresses and Formation of Shrinkage Cracks

It is believed that there are at least two opinions in the literature about the mechanisms involved in the formation of the shrinkage cracks and their propagation to the pavement surface (Crockford and Little 1987; Lytton et al. 2005; Luo and Prozzi 2009; Sumarac 2004). In one of the mechanisms, the soil will shrink within the edge-moisture variation distance in the vertical direction, and the asphalt concrete layer will deflect with the shrinking soil in a cantilever like action, and cause very high tensile stresses resulting from the bending action on the surface of the asphalt layer. Luo and Prozzi (2009) used the Lytton et al. (2005) approach in analyzing the shrinkage strains and the corresponding stresses using an elastic theory as mentioned in the previous section.

In the other mechanism, the shrinkage crack will initiate in the soil if the tensile shrinkage stress exceeds the tensile strength of the soil. After the crack initiation, the propagation of the crack depends on a number of factors, including loading condition, the crack length, and boundary conditions (Crockford and Little 1987). The progression of the initial crack is critical to the development of the longitudinal crack found on the pavement surface (Ayad et al. 1997). Sumarac (2004) investigated this problem utilizing a simpler but practical approach using elastic theory.

Since these high PI soils will shrink in three-dimensions (but not necessarily in equal amounts in each direction) it is very reasonable that both of the failure mechanisms occur at the same time. However, one of those failure mechanisms could dominate the occurrence of the surface longitudinal cracks depending on several factors including the bonding strength between the high PI subgrade layer and the layer above it (as well as the fracture toughness of the material above the shrinking soil), the magnitudes of suction stress that will cause shrinkage cracks and horizontal strains, and the magnitude of volume change in the vertical direction (Lytton et al. 2005; Luo and Prozzi 2008; Puppala et al. 2009). While determination of the initial conditions for formation of the cracks is critical, the analysis of crack propagation in the pavement was also investigated by researchers (Luo and Prozzi 2009; Ayad et al. 1997). Luo and Prozzi (2009) studied the crack propagation problem from the strain energy release point of view using the finite element method. At energy equilibrium, the strain energy release

rate is equal to the surface energy of the generated two crack surfaces. The strain energy release rate (e.g., the surface free energy of the crack surface) is a function of the stress intensity factor (the fracture toughness of the material), which is a constant material property and can be measured in the laboratory. The direct experimental determination of the fracture toughness of a clayey soil is, however, very difficult. Instead, the fracture toughness can be inferred from other material constants, which in turn can be determined from laboratory tests or inferred from known relationships (Ayad et al. 1997). The fracture toughness of different soils and other pavement materials have been measured in the laboratory (Harrison et al. 1994; Crockford and Little 1987). When the stress intensity factor is larger than the fracture toughness of the material, the crack is unstable and will propagate to release energy until the equilibrium is reached. When the stress intensity factor is smaller than the fracture toughness, the crack remains stable. The fracture toughness of the soil should also depend on its current matric suction level. The initiation and propagation of the shrinkage cracks can be evaluated using a finite element analysis.

Long (2006) performed numerical simulations to study the field moisture diffusivity using a conceptual model of moisture diffusion in a cracked soil mass. A rough correlation between field and laboratory measurements of moisture diffusion coefficients has been presented for different crack depth patterns. Shrinkage cracks have significant effects on the soil's diffusivity parameter, and can be modeled in the laboratory under controlled conditions. Recently, Mabirizi and Bulut (2010) conducted drying and wetting tests on different high plasticity clay soils, and have found significant differences in diffusivity between the cracked and intact soils.

This complex stress-strain field in the pavement subgrade layer, resulting from moisture content (suction) changes, requires a comprehensive approach for the analysis of the shrinkage cracking problems in high-plastic subgrade soils. A detailed laboratory testing program is needed to determine the basic index properties and unsaturated parameters of the high PI shrinking soils. Although there are several models available in the literature, the numbers and characteristics of the parameters of the models are complex, and their determination is time consuming and expensive. Simple and

practical approaches are needed to understand and analyze the moisture diffusion process and development of tensile stresses in the soil. A shrinkage crack will initiate in the soil if the tensile shrinkage stress exceeds the tensile strength of the soil.

3. SITE AND SOIL DESCRIPTION

Soil specimens from four sites in Oklahoma that are experiencing drying shrinkage problems were obtained for laboratory soil testing. Oklahoma Department of Transportation (ODOT) conducted the drilling process and sampled thin-walled tube soil specimens for this project. These sites are located in Oklahoma City near Lake Hefner (named as Lake Hefner site), in Norman on Robinson Street (named as Norman site), along Interstate Highway I-35 in Ardmore (named as Ardmore site), and from Idabel (named as Idabel site) in Oklahoma. Both Lake Hefner and Norman sites are bike trails about 12 feet wide constructed using a thin layer of base material with a thin layer of asphalt concrete on top. The bike trail at the Lake Hefner site is located east of Lakeshore Drive in Lakeshore Park, which is in southwest side of Lake Hefner. The bike trail at the Norman site is located north of West Robinson Street at the intersection of West Robinson Street and Woods Avenue. The Ardmore site along I-35 is located between 12th Avenue and Veterans Boulevard. The Idabel site is located west of Idabel on Highway 70. According to ODOT, the sites have been experiencing longitudinal cracks due to drying shrinkage of high plastic subgrade soils for number of years.

The shrinkage cracks in the asphalt material at the Norman site were covered by asphalt emulsion. Therefore, the size of the cracks were not that visible. However, from the nature of the surface treatment and close visual inspection, the size and length of the cracks seemed significant. Figure 3.1 depicts a picture of the sealed cracks at the Norman site. Longitudinal cracks due to drying shrinkage of high plastic subgrade soils were clearly visible at the Lake Hefner site. Figure 3.2 shows the longitudinal cracks along the bike trail at the Lake Hefner site. The cracks were mostly along the shoulder of the pavement. The cracks were from about a few milimeters to about 30 milimeters wide.

Figure 3.1. Longitudinal Drying Shrinkage Problem at Norman Site (Photo taken on November 21, 2012).

Figure 3.2. Longitudinal Drying Shrinkage Problem at Lake Hefner Site (Photo taken on November 21, 2012).

3.1 Soil Sampling

ODOT collected soil specimens using thin-walled tube samplers at four boring holes at the Norman site on October 9, 2012. Thin-walled tube samplers were hydraulically pushed to the depths of 3.8, 17.1, 17.7, and 17.8 feet for obtaining intact specimens. These specimens were collected from the ODOT's main office in Oklahoma City and brought to Oklahoma State University for laboratory testing. Immediately after that a comprehensive visual inspection and description of the specimens was conducted. The results of the visual inspection are provided in Appendix A. Three boring holes were made at the Lake Hefner site on October 11, 2012 to depths of 9.9, 8.7, and 8.5 feet for obtaining thin-walled tube specimens. The thin-walled tube specimens were collected from the ODOT's main office in Oklahoma City and carried to Oklahoma State University for visual inspection and laboratory testing. The results of the visual inspection and soil descriptions are given in Appendix B.

Seven boring holes were made by ODOT at the Ardmore site along the Interstate Highway I-35 for collecting thin-walled tube specimens on January 8, 2013. The thin-walled tubes were hydraulically pushed to the depths of 3.57, 3.45, 6.0, 8.0, 8.0, 8.0, and 8.0 feet for sampling. These specimens were delivered to OSU labs by ODOT for laboratory testing in this study. Immediately after the arrival of the specimens a comprehensive visual inspection and description of the samples were performed. The details of the inspection are provided in Appendix C. Three boring holes were made at the Idabel site. The thin-walled tubes were hydraulically pushed to the depths of 9.0, 9.0 and 8.9 feet for obtaining intact specimens. These specimens were delivered to Oklahoma State University for laboratory testing. Immediately after that a comprehensive visual inspection and description of the specimens was conducted. The results of the visual inspection are described in Appendix D.

3.2 Conditions of Soil Specimens and Their Descriptions

The soil specimens from all the four sites were significantly disturbed and were in very dry conditions with suction values close to 5 pF (4 log kPa). As it is known the wilting point of vegetation is around 4.5 pF (3.5 log kPa). This indicates that the soils were

extremely dry. Due to the very severe drought season in 2012, the specimens were very dry, with various sizes of shrinkage cracks and root fibers. The poor conditions of the specimens have created significant amount of difficulty in setting up the specimens for laboratory testing. One major problem was with the drying diffusion coefficient measurement test setups using the thermocouple psychrometers. Thermocouple psychrometers function properly when the suction in the soil is in between about 3.7 pF (2.7 log kPa) and 4.7 pF (3.7 log kPa). The extremely dry specimens, therefore, were exposed to a wetting process before they can be setup for the drying diffusion coefficient measurements. Since the conditions of the specimens were bad (e.g., significant amount disturbance, cracks, and root fibers), some of the test specimens simply failed during the wetting-drying process. Another problem with the soil samples was the short length of the specimens. The diffusion test requires soil specimens of at least 250-300 mm in length, so that the initial suction condition of the soil can be determined in the proximity of the diffusion test specimen.

In an ideal condition, all the tests need to be performed on the same soil specimens for the proper interpretation of the test results. Due to the significant amount of sample disturbance, this was not possible. Furthermore, in order to reduce the number of tests and determine the soil parameters on the different soil types, the research team grouped the specimens from each site into Soil Types based on their visual inspection (e.g., mostly in terms of color and to some extent the texture). The different soil types identified for the Norman, Lake Hefner, Ardmore and Idabel sites are given in Appendix A, Appendix B, Appendix C and Appendix D, respectively.

4. LABORATORY SOIL TESTS

This chapter discusses the laboratory soil tests conducted at Oklahoma State University. The tests were conducted on the soil specimens collected from the four sites located in the state of Oklahoma named Norman, Lake Hefner, Ardmore, and Idabel. Thin-walled tube specimens were sampled by the Oklahoma Department of Transportation (ODOT) and delivered to OSU for testing. The different tests conducted are the Atterberg limits, water content, hydrometer analysis, sieve analysis, compaction, suction measurements using the filter paper, chilled-mirror psychrometer, and thermocouple psychrometers, and drying diffusion coefficient measurements. In total, 35 drying diffusion coefficient tests were conducted. Water content and total suction measurements were determined for at least every soil specimen set for the drying diffusion coefficient test. All the received soil specimens were stored in a temperature-controlled room in sealed condition in ice-chests. The laboratory determination of water content was conducted using the ASTM D2216 for all the specimens selected for the drying diffusion test. Other tests were performed on every type of soil identified throughout a visual inspection and identification process described in the previous chapter and appendices.

4.1 Atterberg Limits

Liquid limit and plastic limit tests were conducted in accordance with the ASTM D4318. The liquid and plastic limits correspond to different levels of consistencies in fine-grained soils. The values may vary according to the clay mineral type and percentage in the whole soil mixture. For the liquid and plastic limit tests, the soil sample was oven dried at 60^{o}C for 5 hours, and then crushed and air-dried. The sample was further broken into smaller pieces by using a hand rammer and then ground to finer particles using grinding machines. The ground sample was passed through the US sieve #40. The sample passing the sieve was collected and used for obtaining the Atterberg limits.

For conducting the liquid limit test, the samples were mixed with distilled water and placed in a ceramic cup for moisture conditioning for 24 hours. The ceramic cup was covered with plastic wrap to avoid moisture loss. After moisture conditioning, the liquid

limit test was performed according to ASTM D4318. The plastic limit test was conducted on the same soil following the ASTM D4318 testing specifications.

4.2 Hydrometer Analysis

Hydrometer analysis is the test used to determine the grain size distribution of the soil particles passing the US sieve #200. The analysis is based on the Stoke's law which relates the terminal velocity of a falling sphere in a liquid to its diameter. A series of density measurements at known depth of suspension and at known times of settlement gives the percentages of particles finer than the diameters given by Stoke's law. The series of readings reflects the amount of different sizes of particles in the fine-grained soils. The ASTM D422-63 testing method was adopted for sample preparation and testing. A dispersing solution was prepared by mixing 40 grams of sodium hexametaphosphate in 1000 milliliters of distilled water. This solution is required for deflocculation of particles, as the clay particles have tendency to adhere to each other and form larger masses. Fifty grams of soil passing the US sieve #200 is required for the hydrometer analysis. The soil sample is mixed with 125 milliliters of dispersing solution. Finally, distilled water is added to a make a total of 1000 milliliters volume of suspended solution. The suspension is kept undisturbed, and readings are taken at 2, 5, 15, 30, 60, 240, 1440 minutes interval. The combined sieve and hydrometer analyses permitted estimates of the clay fraction of the soil.

4.3 Sieve Analysis

Fine-grained plastic clay particles tend to adhere together when dried, even when subjected to grinding. Therefore, dry sieve analysis of such clays is not usually recommended. To avoid this potential problem, a wet sieve analysis procedure was adopted. The wet sieving was followed according to ASTM D92-95. The sample was soaked in water for 2 hours in order to prevent the finer materials from adhering to the larger particles. The test specimen was then transferred to the sieve #200 for washing. With a small jet of water from a rubber hose, the sample was washed until the water passing through the sieve contains only traces of the specimen. Exercise of care during washing was performed to prevent loss by splashing. Then, the washed residue in the

sieve was dried in the oven at 105±5^{o}C. The dried residue was transferred to coarser sieve for the analysis. The percentage of soil passing was calculated per ASTM D92-95.

4.4 Soil Compaction

Compaction tests were conducted accoring to ASTM D698. The soil sample was taken and oven dried for 24 hours at 140^{o}F (60^{o}C). The sample was grounded and about 2000 grams of the sample was used for the compaction test. The soil sample was mixed with water and allowed to cure per ASTM D698 guidelines. The mold and collar were assembled and secured to the base plate. The soil was compacted in three layers, each layer receiving 25 number of drops from 12 inches. After the compaction, the collar and base plate were removed from the mold. A knife was used to trim the soil at the top. The mass of the compacted specimen and mold was determined and recorded to the nearest gram. The compacted specimen was then removed from the mold using a hydraulic jack. The compaction curve was determined per the guidelines in Li and Sego (2000).

4.5 Soil Total Suction

Soil suction can simply be described as a measure of the ability of a soil to attract and hold water. It is the quantity of moisture energy that can be used to characterize the behavior of unsaturated soils. The filter paper method (as described in Bulut et al. 2001), chilled-mirror psychrometer (as described in Bulut et al. 2002), and thermocouple psychrometers (as described in Bulut and Leong 2008) have been used in determining the total suction characteristics of the soils. Thermocouple psychrometers were used with the CR7 datalogger and data acquisition system by the Wescor and Campbell Scientific. The filter paper method and chilled-mirror device were basically adopted for determining the initial total suction in the soil. On the other hand, thermocouple psychrometers were used for continuous monitoring and recording of total suctions for the unsaturated diffusion coefficient measurements.

4.6 Unsaturated Drying Diffusion Coefficient

The drying diffusion coefficient is measured in the laboratory based on the methodology proposed by Mitchell (1979). Based on the Mitchell's approach, a testing equipment and protocol developed at Oklahoma State University for measuring both the drying and wetting diffusion parameters as described in detail in Mabirizi and Bulut (2010). For the laboratory testing, the thin-walled tube cylindrical soil specimens are sealed along the sides and one end by plastic wrap, aluminum foil, and electrical tape. The other end of the specimen is left open to the laboratory atmosphere to permit the evaporation of the soil moisture in response to the suction gradient between the soil and laboratory atmosphere. Thermocouple psychrometers inserted in the sample measure the soil total suction at different time intervals. By measuring the suction and its corresponding time, the drying diffusion coefficient (α_{dry}) can be calculated. The other input parameters needed in the compuation of the diffusion parameter are the atmospheric suction, initial total suction, evaporation coefficient, length of the specimen, and the location of the thermocouple psychrometer from the closed end.

4.7 Laboratory Test Results for Norman, Lake Hefner, Ardmore and Idabel Sites

As discussed in the previous chapter, the soil specimens obtained from each site (e.g., Norman, Lake Hefner, Ardmore, and Idabel) were visually inspected and classified. Based on this description (e.g., mainly by color and texture), the soil specimens were put into different groups. The main purpose of this approach was to reduce the number of tests, and the problems with the soil disturbance. In this regard, the soil specimens collected from the Norman site were grouped into two soil types. Atterberg limits, compaction tests, sieve and hydrometer analyses tests were conducted on the soil specimens selected from each soil type. Table 4.1 gives the results of Atterberg limits on the soil types for each site and Table 4.2 summarizes the diffusion coefficient, initial total suction, maximum dry unit weight, and optimum moisture content test results on the compacted specimens. The compaction curves and grain size distribution plots for each soil type are provided in Appendix E and Appendix F, respectively.

4.7.1 Norman Site Diffusion Test Results on Shelby Tube Specimens

In total, eight drying diffusion coefficient tests were conducted on the soil specimens collected from the Norman site. Table 4.3 gives the initial water content, initial total suction, and diffusion coefficient parameters. The total suction measurements were conducted using either the filter paper method or the chilled-mirror psychrometer, and in some cases, both methods were employed for measuring the initial suction in the soil. The filter paper method takes at least one week for the suction equilibrium. On the other hand, the chilled-mirror device uses a small soil specimen and measures the suction in less than 10 minutes. However, the chilled-mirror device can only reliably measure the suction values larger than about 3.7 pF (2.7 log kPa). This is a big limitation of this equipment for its wide use in engineering practice. The filter paper method measures practically the whole range of suction, but it is more reliable if the suction values are above 2 pF (1 log kPa). The atmospheric suction in the laboratory environment was around 6 pF (5 log kPa) during the diffusion coefficient measurements. Table 4.3 gives a range of diffusivity parameters for the soils at the Norman site. These values are relatively high as compared to some of the diffusion coefficients given in the literature (Lytton et al. 2005). These high values are attributed to the highly disturbed conditions of the specimens and the presence of cracks and root fibers. The maximum to minimum ratio of the coefficients listed in Table 4.3 is about 42.

Table 4.1. Atterberg Limits Test Results on Different Soil Types of Norman, Lake Hefner, Ardmore and Idabel Sites.

Site	Boring No.	Soil Segment No.	Soil Type	Depth (feet)	Liquid Limit (%)	Plastic Limit (%)	Plasticity Index (%)
Norman	1	1B1	1	2.00-2.69	37	17	20
	2	2C1	2	4.00-4.81	36	19	17
Lake Hefner	1	1B1	2	2.00-2.77	38	23	15
Ardmore	2	2A1	1	0.00-0.90	36	24	12
	2	2B1	2	2.00-3.00	53	27	26
Idabel	4	4B2	1	2.00-2.55	56	33	23
	5	5B1	2	2.00-2.33	67	35	32
	5	5D1	1	6.00-6.50	66	37	29
	6	6B1	2	2.00-2.45	60	37	23

Table 4.2. Drying Diffusion Coefficient Test Results on Compacted Samples.

Pavement Site	Soil Type	Compacted Soil from Mixing Soil Segments	Maximum Dry Unit Weight (pcf)	Optimum Moisture Content (%)	Initial Suction (pF)*	Diffusion Coefficient, α_{dry} (cm^2/min)
Norman	1	1A1, 2A1	112.8	17.5	4.38	2.67×10^{-3}
	2	2F1, 2F2, 2H2	118.0	11.5	3.59	4.80×10^{-3}
Lake Hefner	2	1C2, 2C3, 2D1	99.0	26.0	3.53	0.28×10^{-3}
Ardmore	1	1A1, 1A2, 2A1, 2A2	105.2	14.0	4.03	0.85×10^{-3}
	2	1B2, 2B1, 2B2, 1AA1, 1AA2	102.9	18.3	3.69	0.73×10^{-3}
Idabel	2	4D2, 5D2,5E1, 5E2, 6E1	119.1	26.3	3.86	0.78×10^{-3}

*From the first recorded thermocouple psychrometer reading.

Table 4.3. Norman Site, Summary of Laboratory Diffusion Coefficient Test Results

Boring No.	Soil Segment No.	Soil Type	Depth (feet)	Initial Water Content (%)	Initial Total Suction (pF)	Diffusion Coefficient, α_{dry} (cm^2/min)
1	1A3	1	1.04-1.98	9.39	4.85	1.92×10^{-3}
2	2B1	1	2.11-2.88	8.75	5.24	0.26×10^{-3}
2	2C2	2	4.81-5.42	-	4.69	0.70×10^{-3}
2	2H2	2	14.29-15.34	17.9	2.00	0.13×10^{-3}
3	3B2	1	2.90-3.75	10.3	4.53	1.03×10^{-3}
3	3C2	2	4.83-5.90	10.2	4.03	5.40×10^{-3}
4	4A1	1	0.00-0.87	11.9	4.36	1.01×10^{-3}
4	4D2	2	7.17-7.77	15.07	3.69	2.60×10^{-3}

4.7.2 Lake Hefner Site Diffusion Test Results on Shelby Tube Specimens

In total, five drying diffusion coefficient tests were conducted on the soil specimens collected from the Lake Hefner site. Table 4.4 gives the initial water content, initial total suction, and diffusion coefficient parameters. As described in the section above, the filter paper method and chilled-mirror technique were used in measuring the initial total suction in the soil specimens tested for the diffusion coefficient. As compared to the diffusivity parameters for the Norman site, the coefficients for the Lake Hefner site returned slightly larger values indicating that the unsaturated soil moisture will travel faster at the Lake Hefner site than the Norman site. The difference between the maximum and minimum diffusivity parameters at the Lake Hefner site was 2.5, which is very small.

Table 4.4. Lake Hefner Site, Summary of Laboratory Diffusion Coefficient Test Results

Boring No.	Soil Segment No.	Soil Type	Depth (feet)	Initial Water Content (%)	Initial Total Suction (pF)	Diffusion Coefficient, α_{dry} (cm^2/min)
1	1A1	2	0.00-0.80	17.44	3.01	4.00×10^{-3}
2	2C1	2	4.00-4.87	20.2	3.95	5.30×10^{-3}
2	2D2	2	6.98-7.96	16.5	3.30	5.35×10^{-3}
3	3A2	2	0.80-1.50	17.7	3.29	2.20×10^{-3}
3	3C2	2	4.50-5.45	19.8	4.01	3.20×10^{-3}

4.7.3 Ardmore Site Diffusion Test Results on Shelby Tube Specimens

In total, ten drying diffusion coefficient tests were conducted on the soil specimens collected from the Ardmore site. Table 4.5 gives the initial water content, initial total suction, and diffusion coefficient parameters. Depending on the dryness of the soil specimens, either the filter paper method or the chilled-mirror equipment was employed for measuring the initial total suction in the soil. The diffusivity values range from 5.4×10^{-4} cm^2/min to 9.3×10^{-3} cm^2/min for the soils at the Ardmore site. The ratio between the maximum and minimum coefficients was 17. The unsaturated soil diffusion coefficients for the Ardmore site are in the same range as the coefficients for the Norman site. As described previously, the soil specimens from the Ardmore site were also highly disturbed with significant amount of shrinkage cracks and root fibers.

Table 4.5. Ardmore Site, Summary of Laboratory Diffusion Coefficient Test Results

Boring No.	Soil Segment No.	Soil Type	Depth (feet)	Initial Water Content (%)	Initial Total Suction (pF)	Diffusion Coefficient, α_{dry} (cm^2/min)
1	1B1	2	2.00-2.80	14.3	4.71	1.98×10^{-3}
3	3C2	3	4.90-6.00	20.8	4.10	6.11×10^{-3}
4	1BB2	2	2.50-3.40	18.6	4.55	4.25×10^{-3}
4	1CC1	2	4.00-4.88	18.7	4.33	9.30×10^{-3}
5	2BB2	2	2.90-4.00	19.4	3.58	0.65×10^{-3}
5	2CC2	2	4.86-5.86	17.2	4.77	0.78×10^{-3}
6	3AA2	2	0.10-1.10	25.6	3.98	2.06×10^{-3}
6	3DD1	2	6.00-6.50	21.4	4.22	0.97×10^{-3}
7	4AA2	2	0.95-2.00	24.4	3.45	0.54×10^{-3}
7	4DD3	2	6.85-7.50	12.3	5.26	0.59×10^{-3}

4.7.4 Idabel Site Diffusion Test Results on Shelby Tube Specimens

In total, six drying diffusion coefficient tests were conducted on the soil specimens collected from the Idabel site. Table 4.6 gives the initial water content, initial total suction, and diffusion coefficient parameters. As described in the section above, either the filter paper method or the chilled-mirror equipment was employed for measuring the initial total suction in the soil. The diffusivity values range from 5.4×10^{-4} cm^2/min to 5.5×10^{-3} cm^2/min for the soils at the Idabel site. The ratio between the maximum and minimum coefficients was 10. The unsaturated soil diffusion coefficients for the Idabel site are close to the coefficients for the Ardmore site. Also, the soil specimens from the Idabel site were also highly disturbed with significant amount of shrinkage cracks and root fibers.

Table 4.6. Idabel Site, Summary of Laboratory Diffusion Coefficient Test Results

Boring No.	Soil Segment No.	Soil Type	Depth (feet)	Initial Water Content (%)	Initial Total Suction (pF)	Diffusion Coefficient, α_{dry} (cm^2/min)
4	4A2	1	0.45-1.13	30.9	2.87	1.57×10^{-3}
4	4C2	1	4.35-4.95	27.7	2.71	5.47×10^{-3}
4	4D2	1	6.30-6.80	24.1	3.86	7.21×10^{-3}
5	5A2	1	0.35-1.00	28.8	3.71	5.43×10^{-4}
5	5B2	2	2.30-3.05	32.9	3.30	7.21×10^{-4}
6	6D1	1	6.00-6.73	32.4	3.06	5.53×10^{-3}

The details of all the diffusion test results, including the input parameters and the relationship between the measured suction values and theoretical suction predictions, are summarized in Appendix G, H, I and J.

4.8 Suction Compression Index

The change of soil volume is governed by mechanical stress in classical soil mechanics. However, the influence of suction should be considered in unsaturated soils since the volume of soil increases in wetting cycle (e.g., swelling) and decreases in drying cycle (e.g., shrinking). Lytton (1994) proposed the following equation to calculate total volume changes in unsaturated expansive soils:

$$\Delta V/V=-\gamma_h (\log h_f/h_i) -\gamma_\sigma (\log \sigma_f/\sigma_i) -\gamma_\pi \log (\pi_f/\pi_i) \quad (4.1)$$

where, $\Delta V/V$ is the volumetric strain, h_f and h_i are the final and initial matric suctions, σ_f and σ_i are the final and initial mean principle stresses, π_f and π_i are the final and initial osmotic suctions, and γ_h, γ_σ, and γ_π are the volume compression indices for matric suction, mean principle stress, and osmotic suction, respectively.

In most cases the third term (osmotic suction component) in Equation 4.1 can be ignored where the effects of the solutes on volume change are negligible (Lytton et al. 2005). For pavements, the volume change caused by the mechanical stress component can also be ignored for practical purposes (Luo and Prozzi 2007). For near surface soils that are under the effects of drying-wetting cycles, the matric suction component in Equation 4.1 is the main contributor of volume changes in expansive soils. The main soil parameter needed for the matric suction part of Equation 4.1 is the volumetric suction compression index, γ_h. This parameter is calculated for the soils investigated in this study following the methodology given in Covar and Lytton (2001). The basic index properties needed for the calculation of the γ_h parameter are the liquid limit, plastic limit, plasticity index, percent passing 2 micron size, and percent passing sieve No. 200. These soil properties for the Norman, Lake Hefner, Ardmore, and Idabel site soils have been determined and presented in the previous chapter. For the calculation of the γ_h coefficient, Covar and Lytton (2001) defines the activity ratio (Ac) as follows:

$$A_c = PI\ (\%)/f_c\ (\%) \qquad (4.2)$$

where, PI is the plasticity index in percent and f_c is the fine clay content defined as the ratio of the soil finer than 2 micron size over the soil passing sieve No. 200.

Covar and Lytton (2001) evaluated 6500 soil data from the Soil Survey Laboratory (SSL) of the National Soil Survey Center, and divided the soils into 8 separate data groups by their liquid limit and plastic index values as shown in Figure 4.1. The suction compression index of the soil with 100 percent fine clay content, γ_o, can be found from the tables developed by Covar and Lytton (2001). The actual compression index is then calculated using the following relationship:

$$\gamma_h = \gamma_0 * f_c \qquad (4.3)$$

For instance, Figure 4.2 gives the suction compression index for 100% fine clay. Table 4.7 gives the suction compression index values of the soils obtained from the Norman, Lake Hefner, Ardmore, and Idabel sites. The calculated γ_h parameters are employed in the next section for predicting tensile stresses in the subgrade soils.

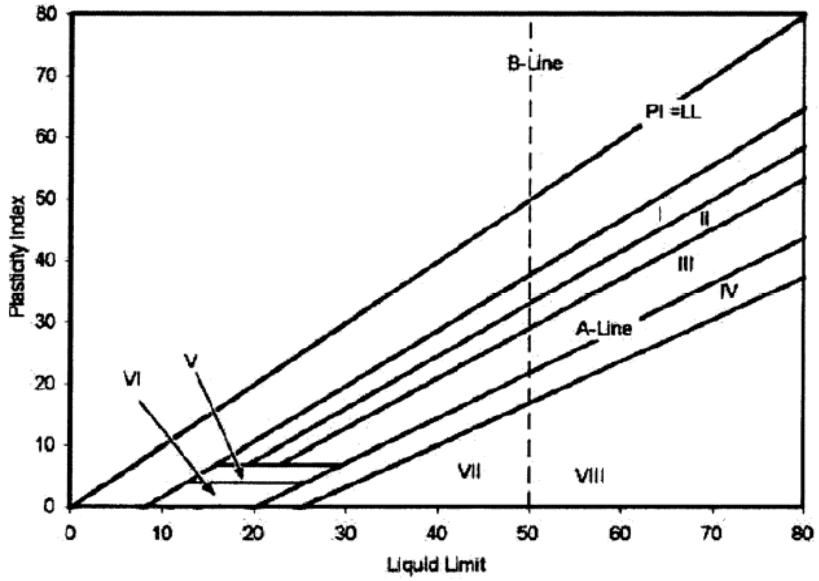

Figure 4.1. Soil Regions for Suction Compression Index (Covar and Lytton 2001).

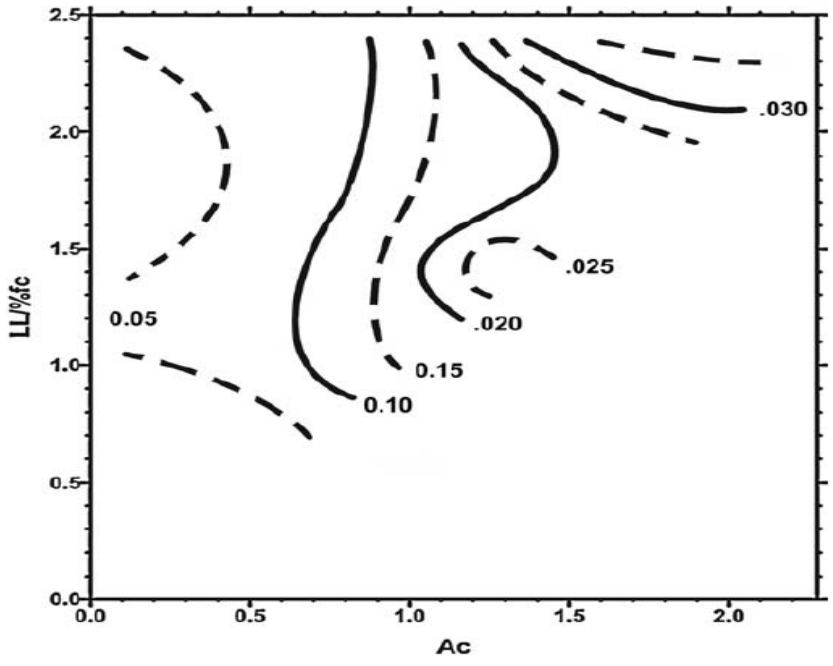

Figure 4.2. Soil Region II for Determining γ_0 (Covar and Lytton 2001).

Table 4.7 Suction Compression Index Values

Site	Soil Segment	Liquid limit (%)	Plastic index (%)	%-2 micron (%)	%-No. 200 sieve (%)	Ac	Zone	γ_0	γ_h
Norman	1B1(1)	36.5	19.8	30.0	87.0	0.57	II	0.09	0.03
	2C1(2)	36.2	17.7	24.0	82.0	0.60	III	0.10	0.03
Lake Hefner	1B1LH(2)	37.6	14.2	20.0	63.3	0.45	III	0.07	0.02
Ardmore	2A1(1)	36.0	12.4	12.0	42.9	0.44	IV	0.08	0.02
	2B1(2)	52.6	25.6	21.0	51.3	0.63	III	0.10	0.04
Idabel	4B2	56.0	23.0	48.0	66.3	0.32	IV	0.05	0.04
	5B1	67.0	32.0	48.0	66.3	0.44	IV	0.07	0.05
	5D1	66.0	29.0	48.0	66.3	0.40	IV	0.06	0.05
	6B1	60.0	23.0	48.0	66.3	0.32	IV	0.05	0.04

5. SUCTION AND TENSILE STRESS PROFILES IN SUBGRADE SOILS

Simple and practical methods are needed to analyze and model the drying shrinkage problems in pavement subgrades. These methods must also consider the principles of unsaturated soil mechanics as it is well-established that the suction change is one of the main causes of the problem. Introduction of simple analytical models for predicting the suction and tensile stresses in the soil has been an important component of this study. The model parameters for these methods must be relatively simple to obtain from the laboratory tests or from the existing literature.

5.1 Suction Profiles by Mitchell's Model

The effect of low relative humidity on the ground surface (e.g., drying soil) on the state of suction in the soil can be determined by means of obtaining a solution of the diffusion equation for a soil profile subjected to a constant state of suction at the surface. The governing equation describing the distribution of suction in the soil profile with time is given by the following diffusion equation (Lytton et al. 2005):

$$\partial u/\partial t = \alpha \, (\partial^2 u)/(\partial x^2) \qquad (5.1)$$

where, u is the suction, t is the time, x is the coordinate, and α is the diffusion coefficient. Mitchell (1979) solved Equation 5.1 for some boundary conditions and obtained the following equation that can be used in predicting suction profiles in subgrade soils:

$$u = u_0 + (u_f - u_0)\,(1\text{-erf}\,(x/(2\sqrt{\alpha t})) \qquad (5.2)$$

where, u is the suction as a function of depth and time, u_o is the initial equilibrium suction, u_f is the final suction, x is the coordinate, α is the diffusion coefficient, and t is the time. The term "erf" is a mathematical term and is known as error function. The error function is readily available in spreadsheets. Laboratory drying diffusion coefficient tests were conducted on the thin-walled tube soil specimens obtained from all the four sites investigated in this study. The results were reported in the previous chapter. The maximum, minimum, and average of those values are given in Table 5.1.

Table 5.1. Ranges of Diffusion Coefficient Values

Location	Minimum (cm^2/sec)	Maximum (cm^2/sec)	Average (cm^2/sec)
Norman	0.22×10^{-5}	9.0×10^{-5}	2.7×10^{-5}
Lake Hefner	3.7×10^{-5}	8.9×10^{-5}	6.7×10^{-5}
Ardmore	0.9×10^{-5}	16.0×10^{-5}	4.5×10^{-5}
Idabel	0.91×10^{-5}	12.0×10^{-5}	5.8×10^{-5}

5.1.1 Parametric Study

A parametric study was undertaken to evaluate Equation 5.2 for predicting suction profiles in the subgrade soils. The main parameters involved in Equation 5.2 are the diffusion coefficient, time, final, and initial suction values. It is noted that the final suction boundary condition is specified on the ground surface, and initial (equilibrium) suction profile is considered to be constant with depth within the subgrade. In the analysis, the initial suction profile is assumed to be 3.5 pF (2.5 log kPa). The other parameters are varied over minimum and maximum ranges as shown in Table 5.2.

Table 5.2. Variables with Their Ranges of Change in Suction Analysis

Variable	Minimum	Maximum	Unit
Final surface suction	3.5	4.5	pF
Drying time	1	6	month
Diffusivity coefficient	1.0×10^{-7}	1.0×10^{-3}	cm^2/sec

Table 5.3 gives the suction profile using Equation 5.2 by varying surface suction in 0.2 pF increments while considering an average constant diffusion coefficient (5.0×10^{-5} cm^2/sec) and three months of drying period. Figure 5.1 depicts the suction profiles using the data in Table 5.3. Figure 5.1 shows the effect of various surface suctions on the suction profile as they form over a period of three months under an average constant

diffusivity value. Figure 5.1 also indicates that the depth to constant suction is relatively shallow and it is at around 0.80 m. It must be noted that the level of the diffusivity value significantly controls the constant suction depth over a fixed drying period.

Table 5.4 and Figure 5.2 depict the effects of various drying periods on the suction profiles at constant surface suction of 4.5 pF (3.5 log kPa) and diffusivity coefficient of 5.0×10^{-5} cm^2/sec. As the surface of the subgrade is exposed to a high suction value (4.5 pF which is close to the wilting point of vegetation), the suction envelopes expand laterally with increasing times. At six months, the depth to constant suction increases from about 0.80 m at three months to about 1.00 m at six months.

Table 5.3. Suction Distribution vs Depth at Different Final Surface Suctions

Depth (m)	Final surface suction (Diffusive coefficient $5.0 \times 10^{-5} \mathrm{cm}^2/\mathrm{sec}$, and drying time 3 months)				
	3.7 pF	3.9 pF	4.1 pF	4.3 pF	4.5 pF
0.00	3.70	3.90	4.10	4.30	4.50
0.10	3.64	3.79	3.93	4.08	4.22
0.20	3.59	3.69	3.78	3.88	3.97
0.30	3.56	3.61	3.67	3.73	3.78
0.40	3.53	3.56	3.59	3.62	3.65
0.50	3.51	3.53	3.54	3.56	3.57
0.60	3.51	3.51	3.52	3.52	3.53
0.70	3.50	3.50	3.51	3.51	3.51
0.80	3.50	3.50	3.50	3.50	3.50

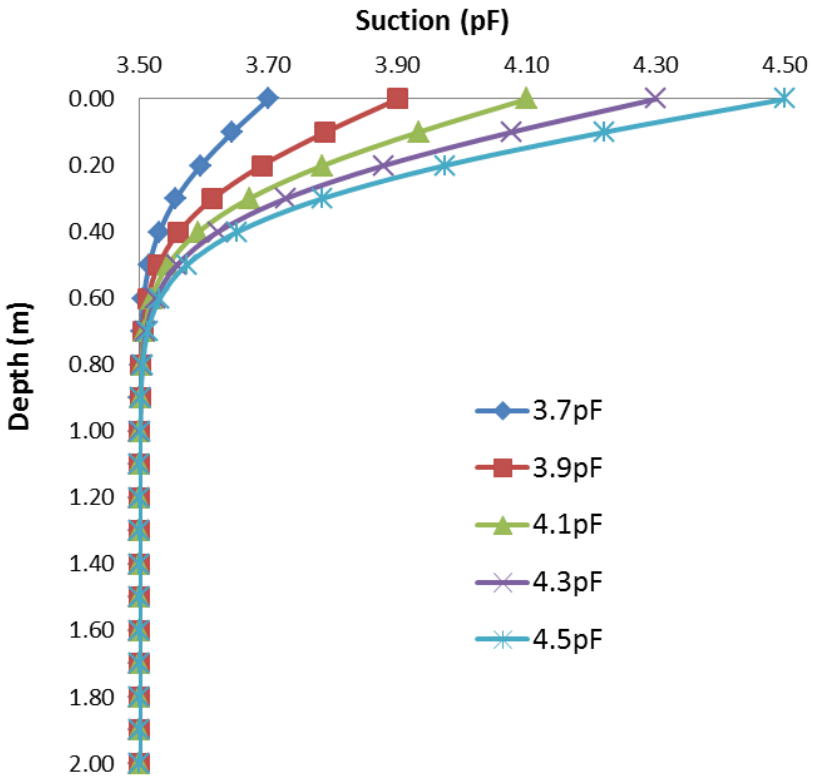

Figure 5.1. Suction Distributions with Depth at Different Final Suctions

Table 5.4. Suction Distribution vs Depth at Different Drying Times

Depth (m)	Drying time (Diffusive coefficient $5.0 \times 10^{-5} \mathrm{cm}^2/\mathrm{sec}$, and final surface suction 4.5 pF)					
	1 month	2 months	3 months	4 months	5 months	6 months
0.00	4.50	4.50	4.50	4.50	4.50	4.50
0.10	4.03	4.16	4.22	4.26	4.28	4.30
0.20	3.71	3.88	3.97	4.03	4.08	4.11
0.30	3.56	3.69	3.78	3.85	3.90	3.95
0.40	3.51	3.58	3.65	3.71	3.77	3.81
0.50	3.50	3.53	3.57	3.62	3.66	3.71
0.60	3.50	3.51	3.53	3.56	3.60	3.63
0.70	3.50	3.50	3.51	3.53	3.55	3.58
0.80	3.50	3.50	3.50	3.51	3.53	3.54
0.90	3.50	3.50	3.50	3.51	3.51	3.52
1.00	3.50	3.50	3.50	3.50	3.51	3.51
1.10	3.50	3.50	3.50	3.50	3.50	3.51
1.20	3.50	3.50	3.50	3.50	3.50	3.50

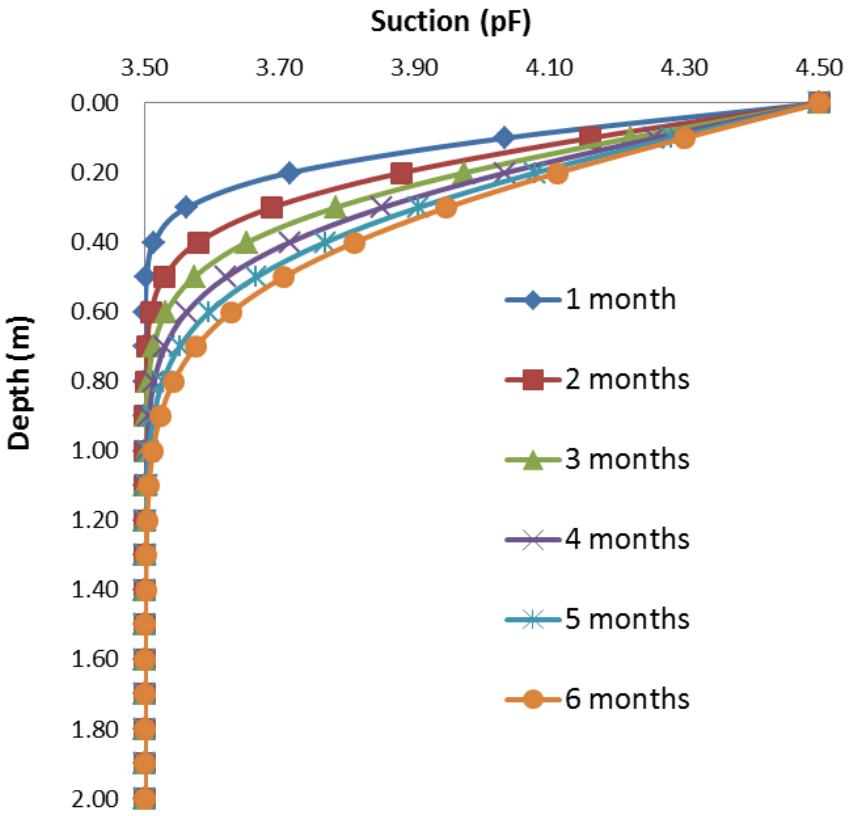

Figure 5.2. Suction Distributions with Depth at Different Drying Times

As part of the parametric study, the effects of the diffusivity parameter in predicting the suction profile using Equation 5.2 are undertaken for a constant suction boundary condition on the surface of the subgrade during a drying period of 3 months. The diffusivity parameter was changed from a small value (1.0×10^{-7} cm^2/sec) representing a tight soil with no cracks and to a large value (1.0×10^{-3} cm^2/sec) representing a loose soil with cracks. Table 5.5 and Figure 5.3 give the suction envelopes showing the effects of diffusivity.

Table 5.5. Suction Distribution vs Depth at Different Diffusive Coefficients

Depth (m)	Diffusive coefficient (Final surface suction 4.5pF, and drying time 3 months)				
	1.0×10^{-7}	1.0×10^{-6}	1.0×10^{-5}	1.0×10^{-4}	1.0×10^{-3}
0.00	4.50	4.50	4.50	4.50	4.50
0.10	3.50	3.51	3.92	4.30	4.44
0.20	3.50	3.50	3.61	4.11	4.37
0.30	3.50	3.50	3.52	3.95	4.31
0.40	3.50	3.50	3.50	3.81	4.25
0.50	3.50	3.50	3.50	3.71	4.19
0.60	3.50	3.50	3.50	3.63	4.13
0.70	3.50	3.50	3.50	3.58	4.07
0.80	3.50	3.50	3.50	3.54	4.02
0.90	3.50	3.50	3.50	3.52	3.97
1.00	3.50	3.50	3.50	3.51	3.92
1.10	3.50	3.50	3.50	3.51	3.88
1.20	3.50	3.50	3.50	3.50	3.84
1.30	3.50	3.50	3.50	3.50	3.80
1.40	3.50	3.50	3.50	3.50	3.76
1.50	3.50	3.50	3.50	3.50	3.73
1.60	3.50	3.50	3.50	3.50	3.70
1.70	3.50	3.50	3.50	3.50	3.67
1.80	3.50	3.50	3.50	3.50	3.65
1.90	3.50	3.50	3.50	3.50	3.63
2.00	3.50	3.50	3.50	3.50	3.61

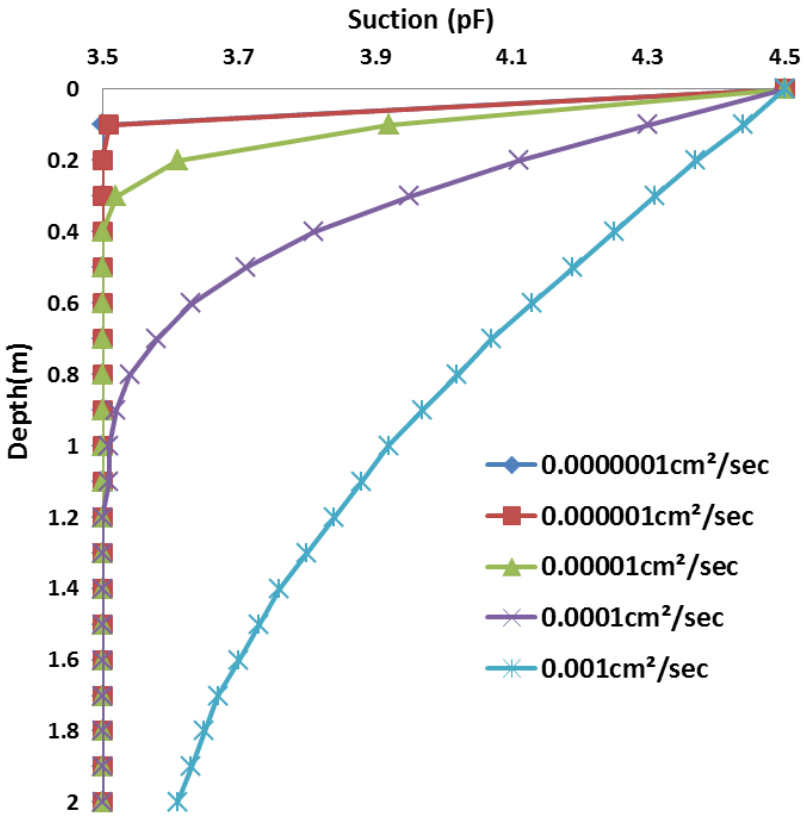

Figure 5.3. Suction Distributions with Depth at Different Diffusion Coefficients.

As it is shown in Figure 5.3, the diffusivity coefficient has the greatest influence on the suction distribution in the soil profile. The depth to constant suction can exceed 2.0 m for a high diffusivity coefficient of 1×10^{-3} cm^2/sec indicating either a very loose soil or cracked soil or both.

5.2 Suction Profiles by Abaqus Software

In this study, the finite element computer program was used to verify the suction profile prediction model by Mitchell (e.g., Equation 5.2). In the comparison analysis, the surface suction was set to a constant value of 4.5 pF, diffusion coefficient of 5.0×10^{-5} cm^2/sec, and drying period of 3 months. Both analyses results are given Table 5.6 and Figure 5.4. The results indicate that the analytical method given by Mitchell (1979) is quite reasonable as compared to the finite element analysis using Abaqus.

Table 5.6. Comparison of Suction Profiles between Mitchell Model and Abaqus Software

Depth (m)	Mitchell Model (pF) (Equation 5.2)	Abaqus Results (pF)
0.00	4.50	4.50
0.10	4.22	4.11
0.20	3.97	3.87
0.30	3.78	3.72
0.40	3.65	3.63
0.50	3.57	3.58
0.60	3.53	3.55
0.70	3.51	3.53
0.80	3.50	3.51
0.90	3.50	3.50
1.00	3.50	3.50

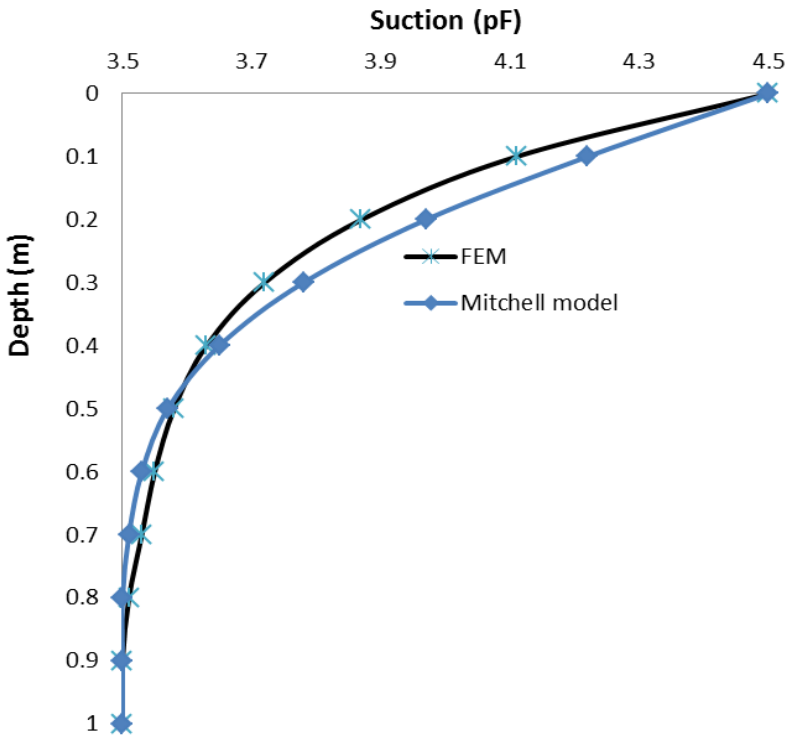

Figure 5.4. Comparison of Suction Profiles between Mitchell Model and Abaqus Software

5.3 Tensile Strength of Clay Soils

Literature presents various fitting and/or prediction based equations based on soil testing and some assumptions. The correlations have been established between soil parameters like clay content (CL), liquid limit (LL), plasticity index (PI), cation exchange capacity (CEC), water content (WC), and suction (u). In this section, some of those equations are used to predict the tensile strength of the soils that have been collected from the four sites (Norman, Lake Hefner, Ardmore, and Idabel) investigated in this study.

Barzegar et al. (1995) showed that clay content and type played a key role in determining tensile strength. In their study, the soil samples were obtained from eight different locations across Australia, and the soils were air-dried, sieved through 1-mm screen, and mixed thoroughly before preparing the specimens for testing using Brazilian splitting test method. Tensile strength tests were performed after the specimens were air-dried for 3 days, and also oven-dried. Based on the laboratory testing results on the soil samples with different clay contents and mineralogy, the following regression equations were obtained:

$$\sigma_t = 632.10 + 38.23CL \quad (5.3)$$

$$\sigma_t = -125.21 + 21.10CEC \quad (5.4)$$

where, σ_t is the tensile strength, CL is the clay content in percent, and CEC is the cation exchange capacity.

Zeh and Witt (2005) tested a medium plastic clay (PI = 23.5%, clay content = 41.1%, liquid limit = 44.9%, plastic limit = 21.4%, internal friction angle = 25^o) for its tensile strength. The clay content is based on 2 micron size. Soil samples were prepared in a standard Proctor mold at 97 % optimum water content. The specimens then were dried or wetted slowly to target water contents. According to the test results, a model between suction and tensile strength was proposed and analytic calculations from capillary theory were used to verify the model:

$$\sigma_t = 10.349 + 331.214\exp\{-0.5[\ln(u/15388.92)/2.187]^2\} \quad (5.5)$$

where, σ_t is the tensile strength and u is the matric suction. Win (2006) conducted a series of experiments to determine the effect of liquid limit, plasticity index and clay content on the tensile strength of soils in Australia. The soil samples tested were sandy clay, silty clay and silty sand whose liquid limits were from 25% to 40%, plasticity indices were from 8% to 18% and clay contents were from 15.9% to 35.5%. The tensile strength tests were performed at 95%-99% Proctor compaction. The following relationships were obtained from the regression analysis:

$$\sigma_t = 1.2748LL - 4.827 \quad (5.6)$$

$$\sigma_t = 2.1446PI + 9.3421 \quad (5.7)$$

$$\sigma_t = 1.15CL + 9.0813 \quad (5.8)$$

where, σ_t is the tensile strength, LL is the liquid limit, PI is the plasticity index, and CL is the clay content of the soil in percent based on 2 micron size.

Venkataramana et al. (2009) found out that tensile strength of soils varied greatly from one model to another based on a comprehensive literature review. They considered that the wide range of tensile strengths found in the literature were due to different clay contents, clay types and water contents. Venkataramana et al. (2009) tested CH and CL soils with the clay contents around 50%, liquid limit around 60%, and plasticity index around 35%. The soils passing 425µm sieve size were mixed with the desired amount of water, and the tensile strength tests were conducted using a triaxial testing device and the suction measurements were performed with the help of WP4 chilled mirror psychrometer. Based on the test results, they have proposed the following equation for predicting the tensile strength of the soil:

$$\sigma_t = 0.001CL^{1.5}\,CEC^{0.5}\,u^{0.5} \quad (5.9)$$

Where, σ_t is the tensile strength, CL is the clay content in percent based on 2 micron size, CEC is the cation exchange capacity, and u is the matric suction of the soil. In

addition to the tensile strength equations that have been summarized above, Fang and Chen (1971) proposed the following relationship:

$$\sigma_t = 31.44 + 1.24PI - 0.01761PI^2 + 0.00011PI^3 \quad (5.10)$$

Where, σ_t is the tensile strength and PI is the plasticity index. Greene et al. (2002) proposed an equation in terms of the cation exchange capacity as follows:

$$\sigma_t = -39 + 16.7CEC \quad (5.11)$$

Where, σ_t is the tensile strength and CEC is the cation exchange capacity. These nine equations (e.g., Equation 5.3 through Equation 5.11) have been evaluated using the test results obtained on the Norman, Lake Hefner, Ardmore, and Idabel site soils as given in Table 5.7. For the suction-based models, a 3.5 pF suction was assumed for the soils as shown in Table 5.7. The calculated tensile strength values are summarized in Table 5.8.

Table 5.7. Parameters Used to Calculate Tensile Strength in Four Locations

Location	Clay content (CL) %	Plastic index (PI)%	Liquid limit (LL)%	CEC meq/100g	Suction (u=3.5pF) kPa
Norman	84.5	18.8	36.3	7.0	316
Lake Hefner	63.3	14.2	37.6	7.0	316
Ardmore	47.1	19.0	44.3	7.0	316
Idabel	66.3	26.8	62.2	7.0	316

Table 5.8. Tensile Strength of the Soils at the Four Sites

Location	Norman	Lake Hefner	Ardmore	Idabel
	(kPa)			
Equation 5.3*	3862	3052	2432	3166
Equation 5.4	22	22	22	22
Equation 5.5	79	79	79	79
Equation 5.6	41	43	52	74
Equation 5.7	50	40	50	67
Equation 5.8	106	82	63	85
Equation 5.9	59	39	25	41
Equation 5.10	49	46	49	54
Equation 5.11	78	78	78	78
Average	61 kPa	54 kPa	52 kPa	63 kPa

*The average values given in the table exclude the values predicted by Equation 5.3.

Obviously, the tensile strength values predicted from Equation 5.3 are much greater than the values predicted from the rest of the equations. The main reason behind the major difference is that the tensile strength predicted by Equation 5.3 is based on the completely dry soil specimens (Barzegar et al. 1995). The tensile strength values predicted from the rest of the equations (as given in Table 5.8) range from 22 kPa to 106 kPa. The average tensile strength for the four sites investigated in this study varies from 52 kPa to 63 kPa. The average tensile strength is the highest for the Idabel site and the lowest for the Ardmore site.

5.4 Tensile Stress Distribution in Subgrade Soils Based on a New Model

Tensile stresses in subgrade soils develop in response to the suction profiles in the soil. Sumarac (2004) presented an analytical approach for shrinkage crack analysis using a water content change approach. In the current study, the Sumarac (2004) water content

based model was modified for the suction stress state in unsaturated soils. The modified equation is given as:

$$\sigma_y = [(E_{\gamma h})/((1-2\nu)(1+\nu))](u_f - u_0)\times(1-\text{erf } x/(2\sqrt{\alpha t})) \quad (5.12)$$

where, σ_y is the tensile stress in horizontal direction, E is the modulus of elasticity of the soil, ν is the Poisson's ratio of the soil, γ_h is the suction compression index (as defined in Lytton et al. 2004), u_f is the final matric suction at the ground surface, u_o is the initial matric (equilibrium) suction in the soil profile, x is the vertical coordinate, α is the diffusion coefficient, and t is the time. Also, the term "erf" is the error function. Equation 5.12 was derived using the analytical equations given in Mitchell (1979) for suction changes and Sumarac (2004) for tensile stresses based on water content variations using the plane strain assumption. In the derivation, it was also assumed that the volumetric strain is related to suction change by the suction compression index given in Lytton et al. (2004).

5.4.1 Parametric Study

A parametric study was conducted for Equation 5.12 considering wide ranges of soil data and suction boundary conditions as given in Table 5.9. In the analysis, the Poisson's ratio of the soil was assumed to be 0.3.

Furthermore, rather than analyzing the effects of each parameter in Equation 5.12 independently, some of the parameters were combined to reduce the number variations in the parametric study. Therefore, in order to simplify analysis, the first term in Equation 5.12 is taken as a single factor k:

$$K = (E_{\gamma h})/((1-2\nu)*(1+\nu)) \quad (5.13)$$

The minimum and maximum values of k can be obtained by substituting the involved variable ranges as follows.

Table 5.9. Variables with Their Range of Change in Tensile Stress Analysis

Variable	Minimum	Maximum	Unit
Final surface suction	3.5	4.5	pF
Drying time	1	6	month
Diffusion coefficient	1.0×10^{-7}	1.0×10^{-3}	cm^2/sec
Elastic modulus	3000	20000	kPa
Suction compression index	0.01	0.06	/

$k_{min} = (E_{\gamma h})/((1-2v)*(1+v)) = (3000 \times 0.01)/((1-2*0.3)(1+0.3)) = 58$ kPa/pF

$k_{min} = (E_{\gamma h})/((1-2v)*(1+v)) = (20000 \times 0.06)/((1-2*0.3)(1+0.3)) = 2308$ kPa/pF

The values of k used in the analyses are 50 kPa/pF, 100 kPa/pF, 250 kPa/pF, 500 kPa/pF, 1000 kPa/pF, and 2300 kPa/pF.

Similarly, the αt term in Equation 5.12 is considered a single term as follows:

$$m = \alpha t \qquad (5.14)$$

The minimum and maximum values of the term m are calculated as follows.

$m_{min} = 1.0*(10^{-7}\ cm^2)/sec*1$ month or $(1*30*24*3600)sec = 0.2592cm^2$

$m_{max} = 1.0*(10^{-3}\ cm^2)/sec*6$ month or $(6*30*24*3600)sec = 15552cm^2$

The values of the m used in the analyses are 0.25 cm^2, 2.5cm^2, 25cm^2, 250cm^2, 25000cm^2, 16000cm^2. Tables 5.10, 5.11, 5.12 and the corresponding Figures 5.5, 5.6, 5.7 obtained using the data listed in Tables 5.10, 5.11, and 5.12 depict the tensile stresses with different final surface suctions, k-values and m-values.

Table 5.10. Tensile stress (kPa) Distribution vs Depth at Different Final Surface Suctions

Depth (m)	Final surface suction ($k = 300\text{kPa/pF}$, $m = 250\text{cm}^2$)				
	3.7pF	3.9pF	4.1pF	4.3pF	4.5pF
0.00	60	120	180	240	300
0.10	39	79	118	157	196
0.20	22	45	67	89	111
0.30	11	22	32	43	54
0.40	4	9	13	18	22
0.50	2	3	5	6	8
0.60	0	1	1	2	2
0.70	0	0	0	1	1
0.80	0	0	0	0	0

Table 5.11. Tensile Stress (kPa) Distribution vs Depth at Different k Values

Depth (m)	k value (kPa/pF) (Final surface suction 4.5pF, and $m = 250\text{cm}^2$)					
	50	100	250	500	1000	2300
0.00	50	100	250	500	1000	2300
0.10	33	65	164	327	654	1505
0.20	19	37	93	186	371	854
0.30	9	18	45	90	180	414
0.40	4	7	18	37	73	168
0.50	1	3	6	13	25	58
0.60	0	1	2	4	8	18
0.70	0	0	1	1	2	5
0.80	0	0	0	0	1	1
0.90	0	0	0	0	0	0

Table 5.12. Tensile Stress (kPa) Distribution vs Depth at Different m Values

Depth (m)	m value (cm^2) (Final surface suction 4.5pF, and $k = 300 cm^2$)					
	0.25	25	150	500	2500	16000
0.00	300	300	300	300	300	300
0.10	0	47	169	225	266	287
0.20	0	2	75	158	233	273
0.30	0	0	25	103	201	260
0.40	0	0	6	62	171	247
0.50	0	0	1	34	144	234
0.60	0	0	0	17	119	221
0.70	0	0	0	8	97	209
0.80	0	0	0	4	78	196
0.90	0	0	0	1	61	184
1.00	0	0	0	1	47	173
1.10	0	0	0	0	36	161
1.20	0	0	0	0	27	151
1.30	0	0	0	0	20	140
1.40	0	0	0	0	14	130
1.50	0	0	0	0	10	121
1.60	0	0	0	0	7	111
1.70	0	0	0	0	5	103
1.80	0	0	0	0	3	94
1.90	0	0	0	0	2	87
2.00	0	0	0	0	2	79

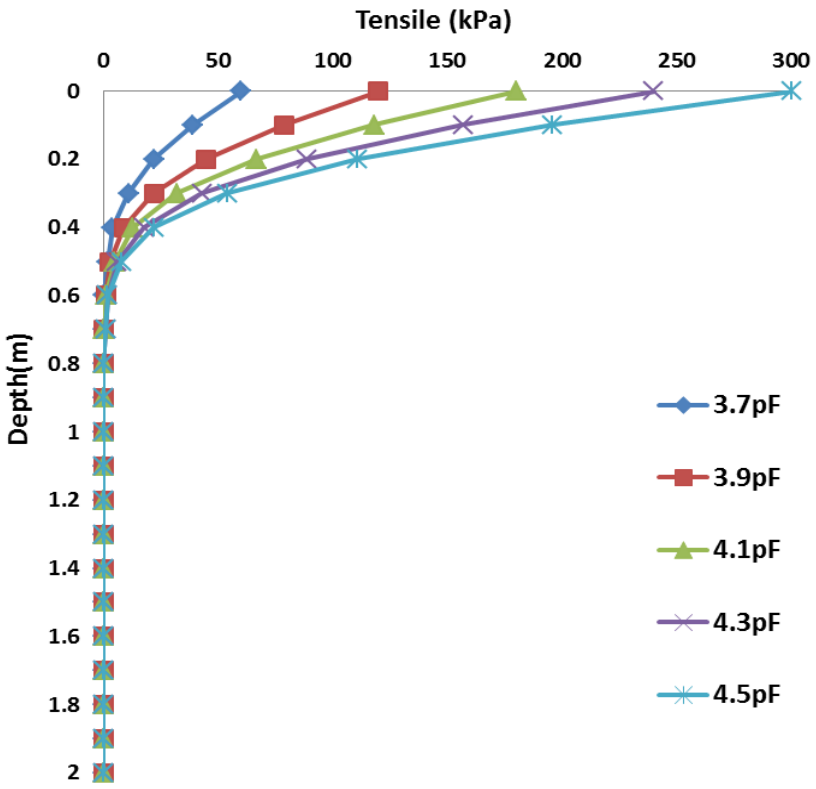

Figure 5.5. Tensile Stress Distribution along Depth at Different Final Surface Suction

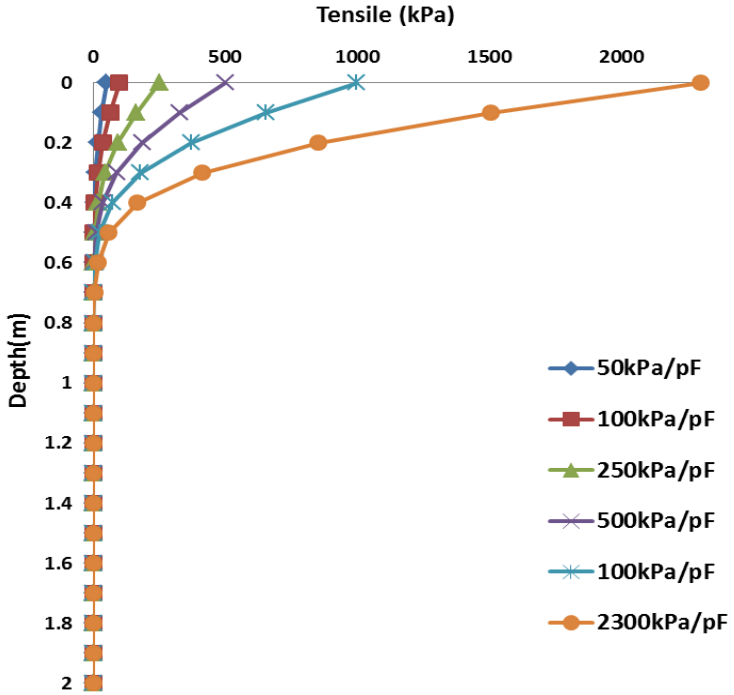

Figure 5.6. Tensile Stress Distribution along Depth at Different k Values

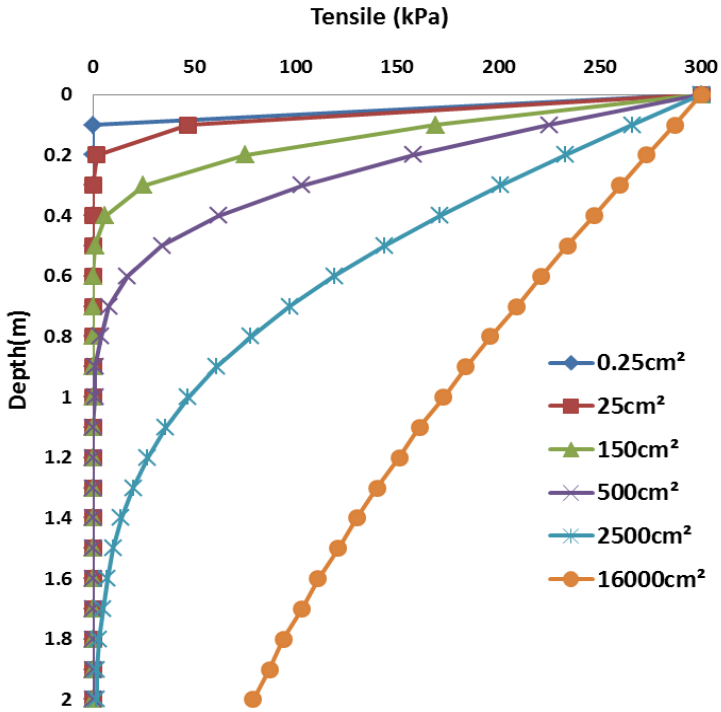

Figure 5.7. Tensile Stress Distribution along Depth at Different m Values

In this parametric analysis, the introduction of the k and m parameters simplifies the analysis. For instance, as given in Table 5.9, the k value of 300 kPa/pF has the same meaning of elastic modulus equal to 7800 kPa and suction compression index equal to 0.02. Similarly, the m value of 250 cm^2 has the same meaning of the diffusion coefficient equal to 5×10^{-5} cm^2/sec and the drying time equal to 2 months. In other words, this parametric analysis gives the trends of the different parameters in Equation 5.12. For example, as given in Table 5.10 and Figure 5.5, the tensile stresses in the soil vary from 60 kPa to 300 kPa when final surface suction increases from 3.7 pF (2.7 log kPa) to 4.5 pF (3.5 log kPa) at fixed k and m values of 300 and 250, respectively. If the average tensile strength values in Table 5.8 are considered, the soil at a suction value of 3.7 pF is at the verge of cracking due to the development of tensile stresses in the soil as a result of drying.

As it can be seen in Table 5.11 and Figure 5.6, the tensile stresses increase from 50 kPa to 2300 kPa when the k-value increases from 50 kPa/pF to 2300 kPa/pF at a constant surface suction of 4.5 pF and the m-value equal to 250 cm^2. Also, from Table

5.12 and Figure 5.7, it can be seen that the tensile stresses increase significantly with depth when the m-value increases. It should be noted again that very wide combinations of the parameters in Equation 5.12 are considered in the analysis. Furthermore, the analysis based on Equation 5.12 does not have an upper bound in terms of the predicted stresses. In other words, Equation 5.12 only predicts the behavior of the parameters involved and the changes in tensile stresses in the soil. In many cases, those predicted (calculated) tensile stresses will not realize in the soil because the soil will simply crack when the tensile stress reaches the tensile strength of the soil.

5.5 Tensile Stress Distribution in Subgrade Soils Based on Abaqus Software

In the previous section, a new model (e.g., Equation 5.12) was introduced in terms of the suction compression index and suction for predicting tensile stresses in subgrade soils. The input parameters for this model can be obtained from basic soil index properties and climatic boundary conditions of the site under investigation. In this section, a comparison study is presented between the results from Equation 5.12 and finite element software Abaqus. For the analysis, the initial suction is assumed to be 3.5 pF, final surface suction 4.5 pF, diffusion coefficient
5.0×10^{-5} cm^2/sec, drying period of 3 months, Poisson's ratio 0.3, elastic modulus of the soil 5,000 kPa, and suction compression index 0.02. The results are presented in Table 5.13 and Figure 5.8

The comparison study conducted using the given material properties and boundary conditions indicate that the new model makes reasonable predictions at greater depths as compared the results obtained from Abaqus. It is believed that the large differences close to the ground surface are from the displacement boundary conditions imposed in the Abaqus analysis. A more comprehensive study and calibration of the model are needed for realistic comparison of the two analyses methods.

Table 5.13. Comparison of Tensile stress Profiles between New model and Abaqus Software

Depth (m)	New Model (Equation 5.12)	Abaqus Analysis
	(kPa)	
0.00	192	136
0.10	138	105
0.20	90	61
0.30	54	38
0.40	29	24
0.50	13	15
0.60	6	8
0.70	2	5
0.80	0	3
0.90	0	2
1.00	0	1

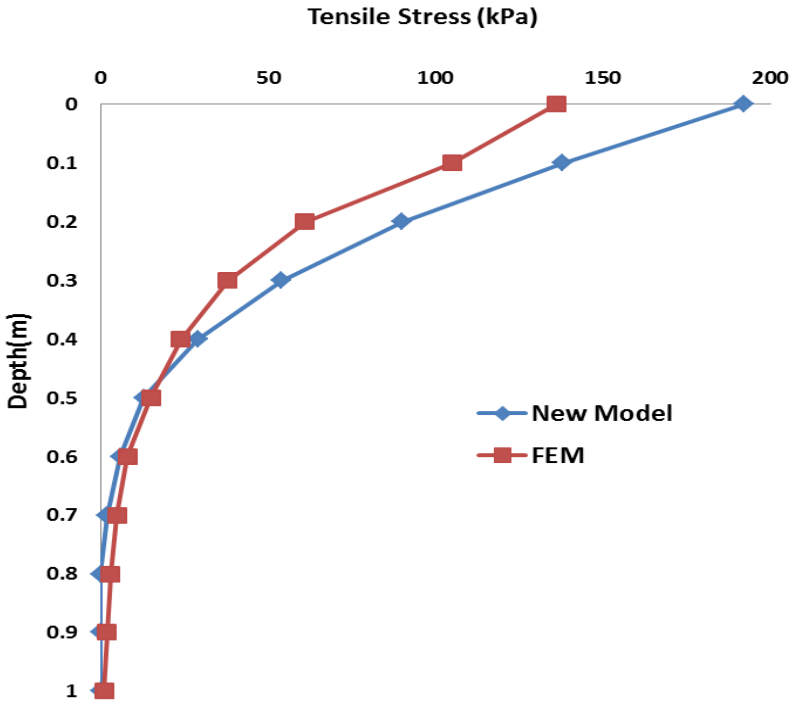

Figure 5.8. Comparison of Tensile Stress Profiles between New Model and Abaqus Software

6. EFFECTS OF HORIZONTAL MOISTURE BARRIERS ON SUCTION, TENSILE STRESS AND DEFORMATION PROFILES OF SUBGRADE SOILS

The analytical models (e.g., Equation 5.2 and Equation 5.12) presented in the previous sections for the suction and tensile stresses in the subgrade soil profiles consider that the subgrade material is exposed to the atmosphere at the ground surface, and the effects of the impermeable asphalt or concrete pavement layer on the surface are not taken into account. This effect is with regard to the boundary conditions and could be important when the state of suction change and tensile stress change right at the vicinity of the pavement edge are considered. Therefore, a finite element method software package (Abaqus) was employed for the analysis of suction and tensile stress changes under different boundary conditions.

For the finite element method modeling, the heat diffusion equation for the suction and linear elasticity for the tensile stress computations was employed. In terms of the governing differential equations between Equation 5.1 for the suction distribution and heat diffusion equation in Abaqus, both equations are the same, and the only difference is that the suction (u) is replaced with temperature and unsaturated moisture diffusivity (α) is replaced with the heat diffusivity. For the linear elastic tensile stress model, the plane strain condition was assumed.

6.1 The Finite Element Method Model Geometry and Boundary Conditions

The model geometry includes three parts: pavement slab, subgrade layer, and horizontal moisture barrier. The properties of these sections are given in Table 6.1. The model geometry is shown in Figure 6.1. There are four main boundaries in the model as shown in Figure 6.1. The AB side is the bottom of the subgrade and regarded as fixed for displacements, and also no suction change along this boundary. The sides AD and BC are the vertical boundaries at the left and right side of the pavement shoulders. These sides can move freely in terms of displacements, and suction change can also take place along those boundaries. The surface boundary CD can have free displacements, and is exposed to the different values of constant suctions depending on the case under investigation.

Table 6.1. FEM Model Parameters

Pavement slab: Elastic modulus = 2500MPa, Poisson's ratio = 0.33, Thickness = 0.3 m, Length = 7.2 m, Diffusion coefficient = 0.00 cm^2/sec (impermeable slab).
Subgrade: Poisson's ratio = 0.30, Length = 12 m, Depth = 6 m, Suction compression index = 0.04, Elastic modulus = 10 MPa, Diffusion coefficient = $1.6 \times 10^{-4} \mathrm{cm}^2/\mathrm{sec}$, Drying time = 3 months, Final surface suction = 4.5 pF
Horizontal moisture barrier: Length = 0.5 m, 1.0 m, and 1.5 m Diffusion coefficient =0.00cm^2/sec (impermeable layer).

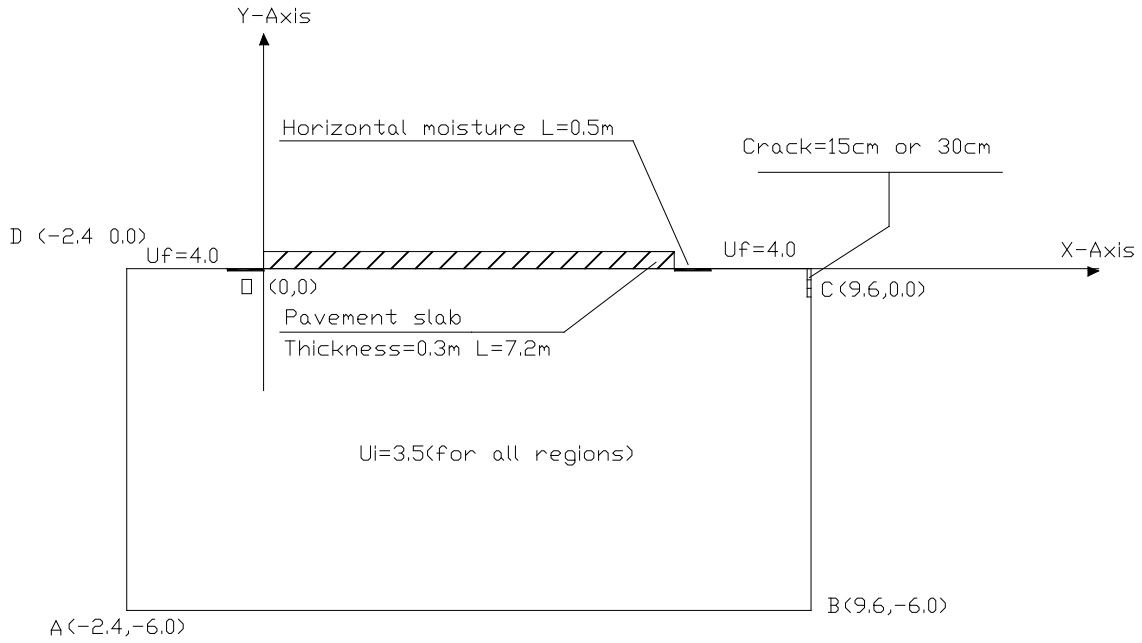

Figure 6.1. Finite Element Method Model Geometry and Boundary Conditions

The origin of coordinate system is located at the left edge of the pavement slab as shown in Figure 6.1. The positive x- and y-coordinates are also shown. The finite element model geometry was discretized using 4-node quadrilateral elements with element size 0.3 m by 0.3 m. The discretized finite element mesh is given in Figure 6.2.

Figure 6.2. Finite Element Mesh

6.2 Influence of Displacement Boundary Conditions on Tensile Stresses in Subgrade Soils

It is assumed that the displacement boundary conditions only affect the tensile stress distribution in the subgrade soil, and has no effect on the suction distribution. Two cases of displacement boundary conditions have been considered in the analysis. In Case 1, both AD and BC boundaries can move freely, and in Case 2, both AD and BC boundaries are fixed in the horizontal direction (Figure 6.1). In both cases, the bottom boundary is fixed, and the top surface boundary is free.

Horizontal tensile stresses along the x- and y-axis have been computed using Abaqus software. Table 6.2, Figure 6.3, and Figure 6.4 summarize the tensile stress values. Tensile stresses (e.g., the positive values in Table 6.2, Figure 6.4) computed based on the Case 1 boundary conditions are lower than those from Case 2 along both x- and y-directions. These stresses are comparatively higher than the stresses obtained using the analytical approach given in the previous section. The main difference is attributed to the displacement boundary conditions. In addition, in the analysis, the pavement slab acts only as an impermeable boundary layer, and no structural interaction between the slab and the subgrade soil (e.g., free, no-constraint, boundary between the slab and soil).

Table 6.2. Horizontal tensile stress distributions along x- and y-directions

Horizontal tensile stress along x-axis (kPa)			Horizontal tensile stress along y-axis (kPa)		
Horizontal Distance (m)	Case 1	Case 2	Vertical Distance (m)	Case 1	Case 2
-1.5	140	313	0.0	133	224
-1.2	154	303	0.3	68	154
-0.9	160	290	0.6	-14	56
-0.6	158	273	0.9	-37	17
-0.3	149	251	1.2	-37	3
0	133	224	1.5	-30	-2
0.3	112	193	1.8	-21	-4
0.6	89	162	2.1	-13	-4
0.9	68	133	/	/	/
1.2	51	111	/	/	/
1.5	39	94	/	/	/

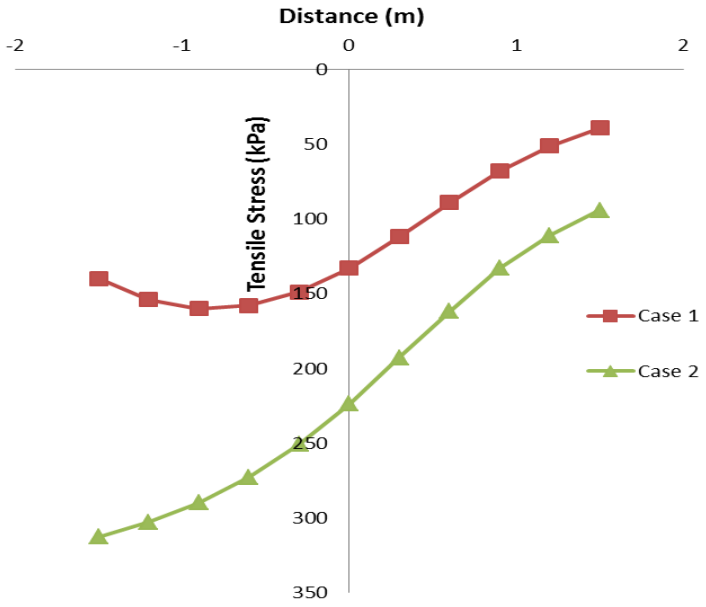

Figure 6.3. Horizontal Tensile Stress Distribution along X-axis for Case 1 and Case 2

Displacement Boundary Conditions

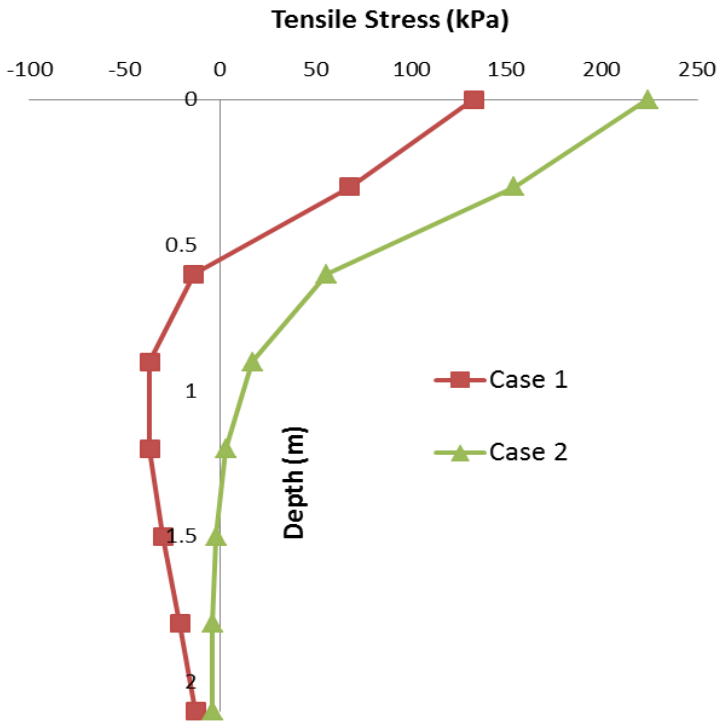

Figure 6.4. Horizontal Tensile Stress Distribution along Y-axis for Case 1 and Case 2 Displacement Boundary Conditions

6.3 Effects of Horizontal Moisture Barrier on Suction, Stress and Displacements

The change in moisture content results in an increase or decrease of suction in the subgrade soils. Correspondingly, tensile stresses also change in the subgrade. One of the effective ways of stabilizing the changes in moisture content of the subgrade soils is the use of horizontal moisture barriers along the shoulders of pavements.

In order to investigate the effects of horizontal moisture barriers on suction, tensile stress, and displacement, the following four cases are considered. The location of the moisture barrier is shown in Figure 6.1. The moisture barrier extends from the edge of the pavement slab and it is assumed that it is fully bonded to the slab. In other words, there is no moisture leakage between the slab and the barrier.

Case 1: No moisture barrier

Case 2: 0.5 m long moisture barrier

Case 3: 1.0 m long moisture barrier

Case 4: 1.5 m long moisture barrier

6.3.1 The Effect of Moisture Barrier on Suction Distribution

Table 6.3 and Figure 6.5 give the suction distribution in vertical direction starting from origin as shown in Figure 6.1 for the four cases analyzed. The effect of the horizontal moisture and its length on the reduction of the suction change is significant. Figure 6.6 and Figure 6.7 also show how the suction contours are pushed away from the edge of the pavement for the case of no moisture barrier and 1.5 m long horizontal moisture barrier. In Figures 6.6 and 6.7, the red color designates high suction (4.5 pF) and the blue color shows the low suction (3.5 pF) regions. Suction increase is 1.0 pF at the point of origin (Figure 6.1) for Case 1, and is 0.11 pF, 0.02 pF and 0.00 pF for Case 2, 3, and 4, respectively.

Table 6.3. Suction (pF) distribution in y-direction

Depth (m)	Case1	Case 2	Case 3	Case 4
0.0	4.50	3.61	3.52	3.50
0.3	3.81	3.59	3.52	3.50
0.6	3.63	3.53	3.51	3.50
0.9	3.55	3.52	3.51	3.50
1.2	3.53	3.51	3.50	3.50
1.5	3.51	3.51	3.50	3.50
1.8	3.50	3.50	3.50	3.50

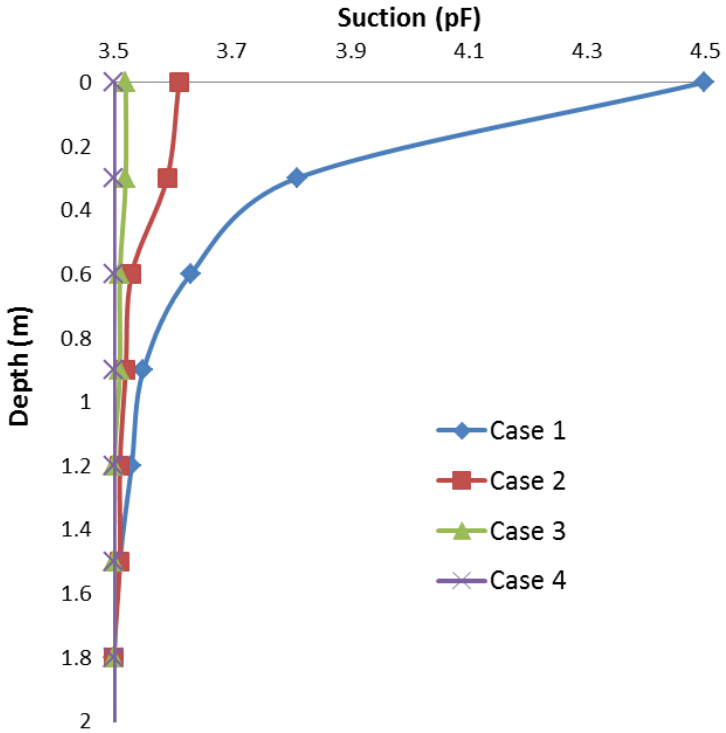

Figure 6.5. Vertical Suction Distribution for Different Moisture Barrier Conditions

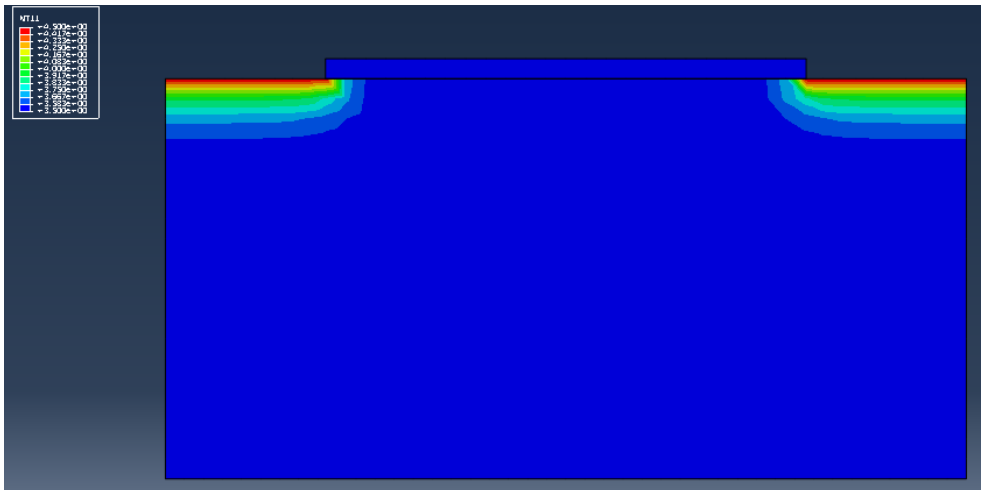

Figure 6.6 Suction Distribution for Case 1 (No Horizontal Moisture Barrier)

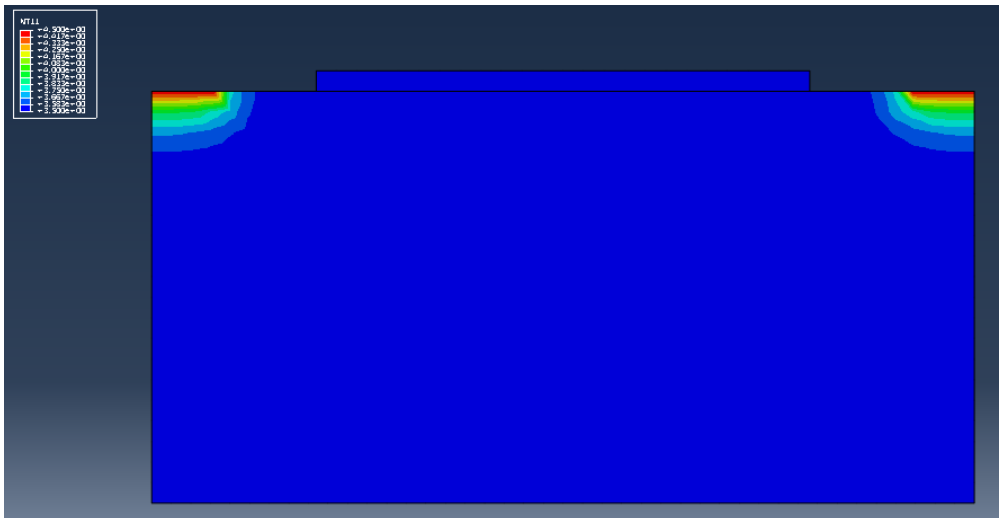

Figure 6.7. Suction Distribution for Case 4 (1.5 m Long Horizontal Moisture Barrier)

6.3.2 The Effect of Moisture Barrier on Tensile Stress Distribution

Tensile stresses can be determined using finite element method after initial and final suction distributions are obtained. Using the software package Abaqus the corresponding tensile stresses are computed for the four cases of moisture barrier conditions mentioned above. Table 6.4 and Figure 6.8 give the horizontal tensile stress values with depth from the origin of the coordinate system given in Figure 6.1. As given in Table 6.4, horizontal tensile stress values decrease from 133 kPa to 18 kPa as the length of the horizontal moisture barrier increases from 0 (no moisture barrier) to 1.5 m long moisture barrier.

6.3.2.1 No-Constraint (Free) Interface Boundary Between the Slab and Soil

Figure 6.9 and Figure 6.10 show in color contours the distribution of the stresses for the no moisture barrier (Case 1) and for a 1.5 m long moisture barrier (Case 4), respectively. These stresses develop within the subgrade soil only as the interface between the pavement slab and soil is free. In other words, the pavement slab acts only as an impermeable layer and there is no interface interaction between the pavement layer and subgrade. A close observation of Figure 6.9 and Figure 6.10 indicate that the

red zone (high tensile stresses zone) moves away from the pavement slab with the consideration of the moisture barrier.

Table 6.4. Tensile stress (kPa) Distribution in Y-direction (No-Constraint Boundary)

Depth (m)	Case1	Case 2	Case 3	Case 4
0.0	133	83	42	18
0.3	68	46	27	13
0.6	-14	-5	2	2
0.9	-37	-23	-11	-4
1.2	-37	-25	-15	-7
1.5	-30	-21	-13	-7
1.8	-21	-15	-10	-5
2.1	-13	-10	-6	-4

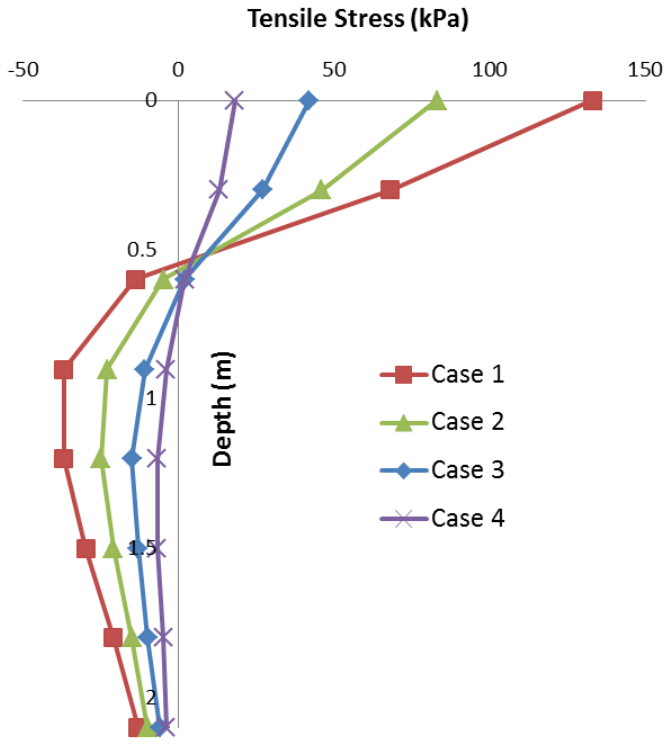

Figure 6.8. Tensile Stress Distribution in Y-direction for Different Lengths of Moisture Barriers

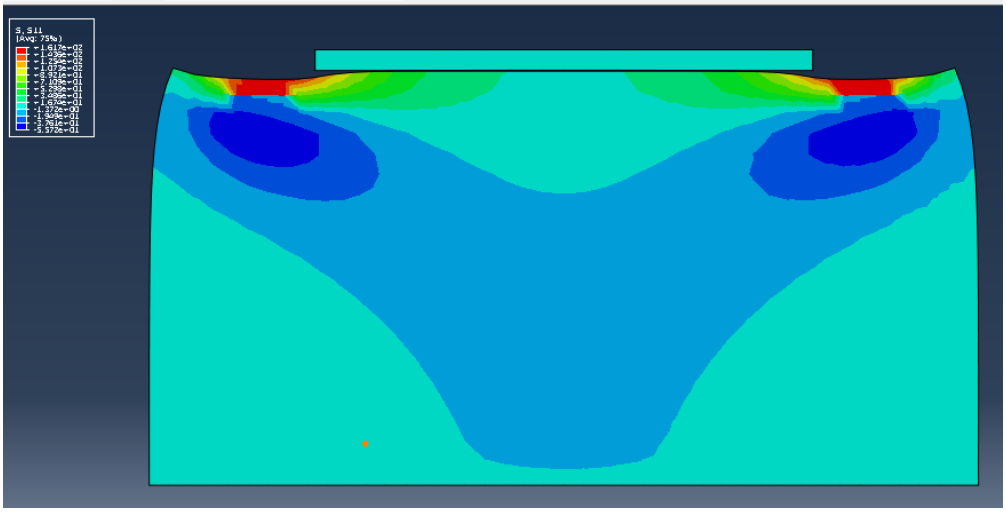

Figure 6.9. Tensile Stress Distribution for Case 1 (No Horizontal Moisture Barrier)

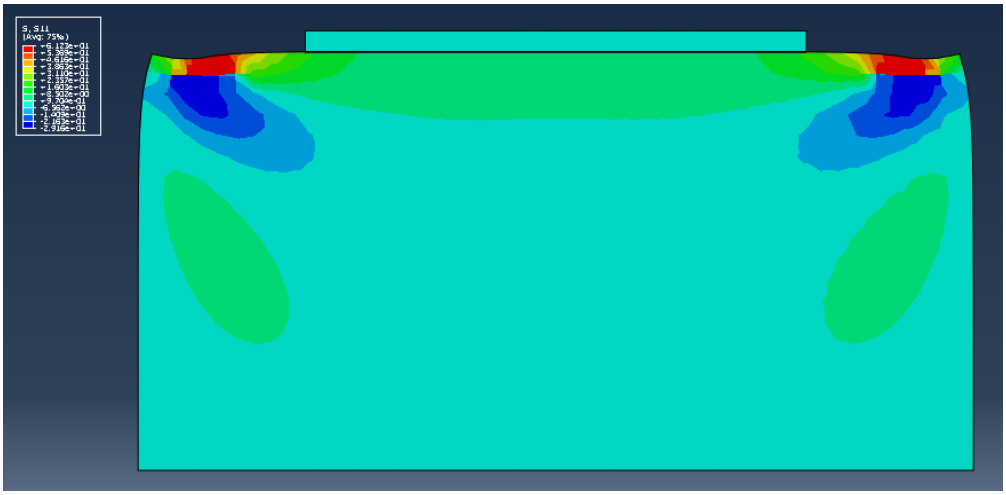

Figure 6.10. Tensile Stress Distribution for Case 4 (1.5m Long Horizontal Moisture Barrier)

6.3.2.2 Fully-Constraint (Bonded) Interface Boundary Between the Slab and Soil

Table 6.5, Figure 6.11, and Figure 6.12 depict the effects of fully-constrained (bonded) interface condition between the pavement slab and subgrade soil for different lengths of horizontal moisture barriers. In the fully-constrained interface modeling, it is assumed

that the pavement slab has the same vertical and horizontal displacement as the surface of the subgrade. Therefore, for the fully-bonded interface, there is transfer of stresses from the soil to the slab, and potential high stress concentrations develop within the bottom of the slab in the edge-moisture variation region as shown in Figure 6.12, indicating the reflective cracking potential from the subgrade.

Table 6.5. Tensile stress (kPa) Distribution in Pavement Slab in X-direction (Fully-Constrained Boundary)

Distance (m)	Length 1	Length 2	Length 3	Length 4
0.0	7	120	90	50
0.3	51	413	301	193
0.6	362	445	343	226
0.9	599	430	343	231
1.2	747	405	329	224
1.5	825	382	312	213
1.8	855	364	296	203
2.1	850	320	280	193

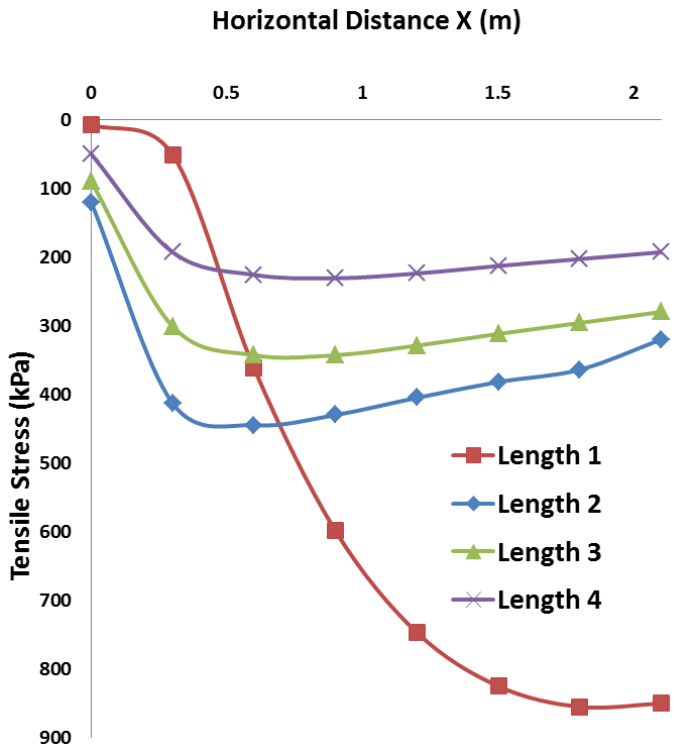

Figure 6.11. Tensile Stress Distribution along X-direction (Fully-Constrained Boundary)

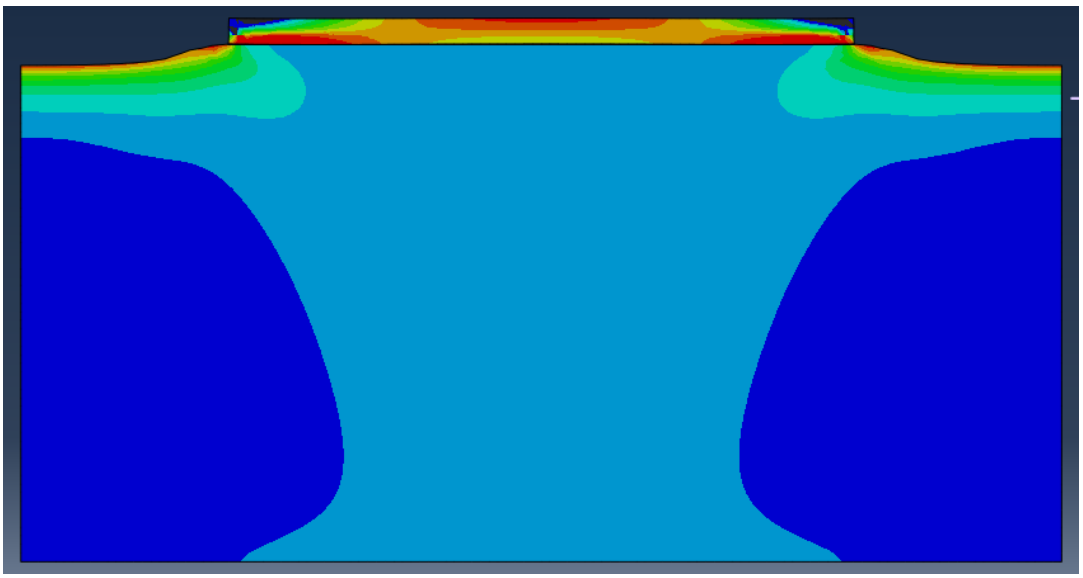

Figure 6.12. Tensile Stress Distribution with 0.5 m Long Horizontal Moisture Barrier (Fully-Constrained Boundary)

6.3.2.3 Semi-Constraint (Partial Bonding) Interface Boundary Between the Slab and Soil

Table 6.6, Figure 6.13, and Figure 6.14 depict the effects of semi-constrained (partial bonding) interface condition between the pavement slab and subgrade soil for different lengths of horizontal moisture barriers. In the Abaqus software modeling, the semi-constrained interface is known as finite displacement between the pavement slab and subgrade with more than 25% relative horizontal movement, while the pavement slab has the same vertical displacement as the subgrade soil. For the semi-bonded interface, there is transfer of stresses from the soil to the slab, but to a lesser degree as compared to the fully-constrained boundary as described above. Since a relative horizontal displacement is allowed in this case, the transfer of horizontal stresses from the subgrade to the slab are limited, and the behavior of the slab is dominated by the vertical shrinkage displacements in the edge-moisture variation distance. This, in turn, results in the development of high potential tensile stress concentrations at the top of the slab within the edge-moisture variation distance as shown in Figure 6.14.

Table 6.6. Tensile stress (kPa) Distribution in Pavement Slab in X-direction (Semi-Constrained Boundary)

Distance (m)	Length 1	Length 2	Length 3	Length 4
0.0	22	8	2	1
0.3	389	121	37	20
0.6	722	224	71	40
0.9	890	276	88	52
1.2	931	289	92	57
1.5	891	276	87	56
1.8	810	250	76	52
2.1	714	218	62	46

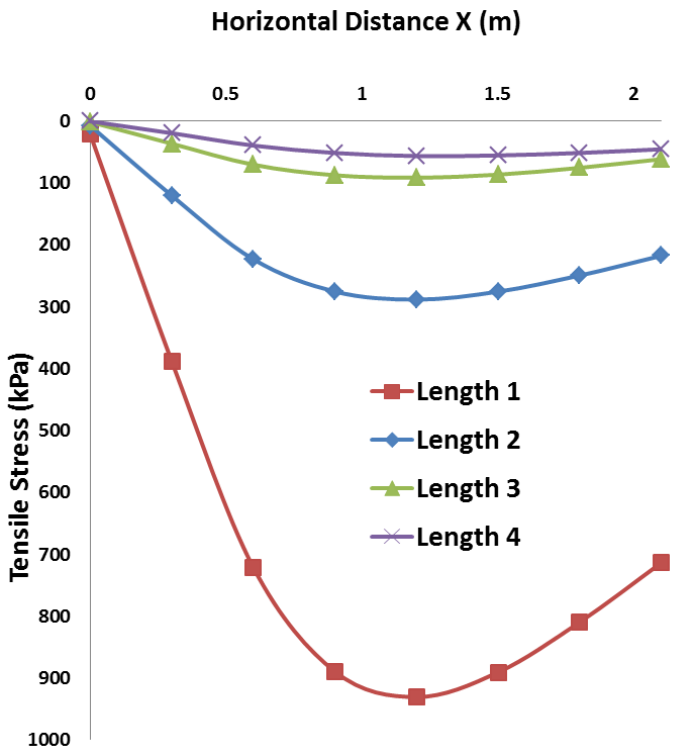

Figure 6.13. Tensile Stress Distribution along X-direction (Fully-Constrained Boundary)

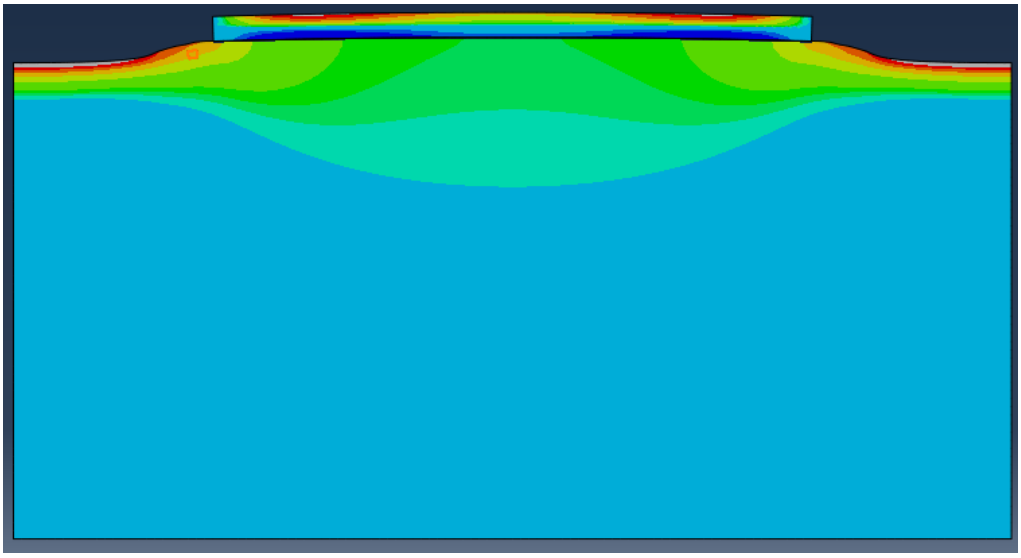

Figure 6.14. Tensile Stress Distribution with 0.5 m Long Horizontal Moisture Barrier (Fully-Constrained Boundary)

6.3.3 The Effect of Moisture Barrier on Subgrade Soil Deformations

For the moisture barrier cases investigated in this study, the elastic deformations of the subgrade soil are computed using Abaqus software. Table 6.7 and Figure 6.15 depict the vertical displacements below the ground surface at the edge of the pavement. In spite of the simple elastic analysis in the finite element model, the displacements are not unreasonable for these soils. Similar to the effects of the barriers on the suction and stress distributions as given in the previous sections, there is significant reduction in vertical displacements. Figure 6.16 shows the displacement contours in color for the case of no moisture barriers.

Table 6.7. Settlement Distribution (cm) in Y direction

Depth (m)	Case1	Case 2	Case 3	Case 4
0.0	2.1	0.7	0.2	0.1
0.3	0.9	0.4	0.1	0.0
0.6	0.6	0.3	0.1	0.0
0.9	0.4	0.2	0.0	0.0
1.2	0.4	0.2	0.0	0.0
1.5	0.3	0.2	0.0	0.0
1.8	0.3	0.2	0.0	0.0
2.1	0.2	0.2	0.0	0.0

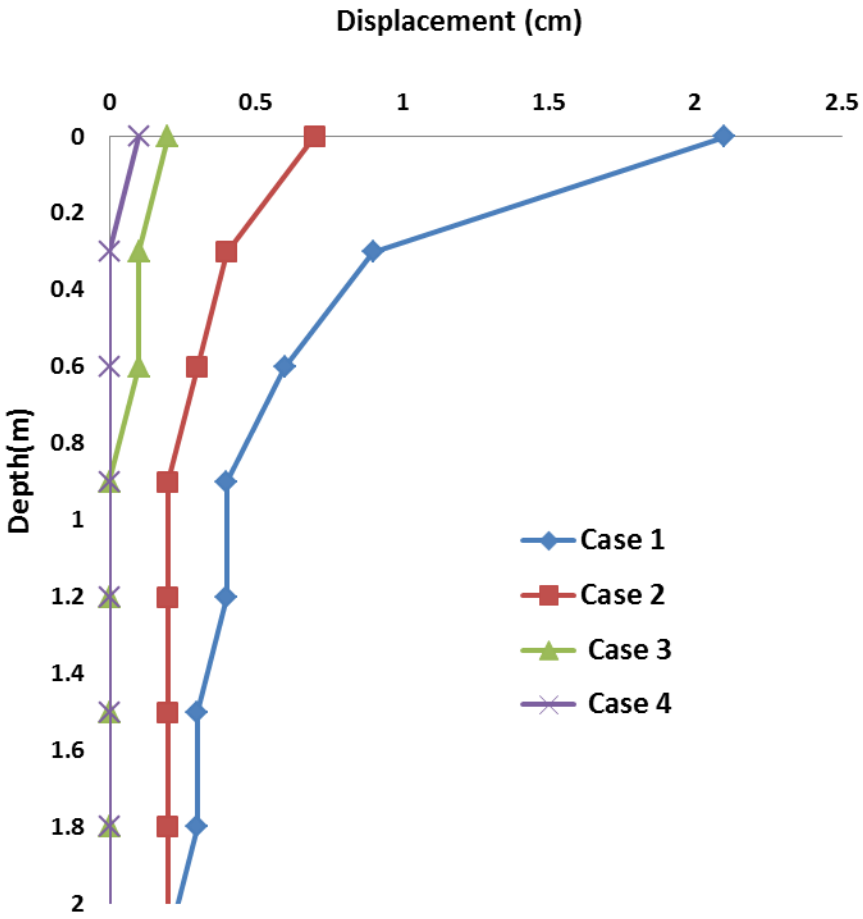

Figure 6.15. Displacement Profiles for Different Lengths of Moisture Barriers

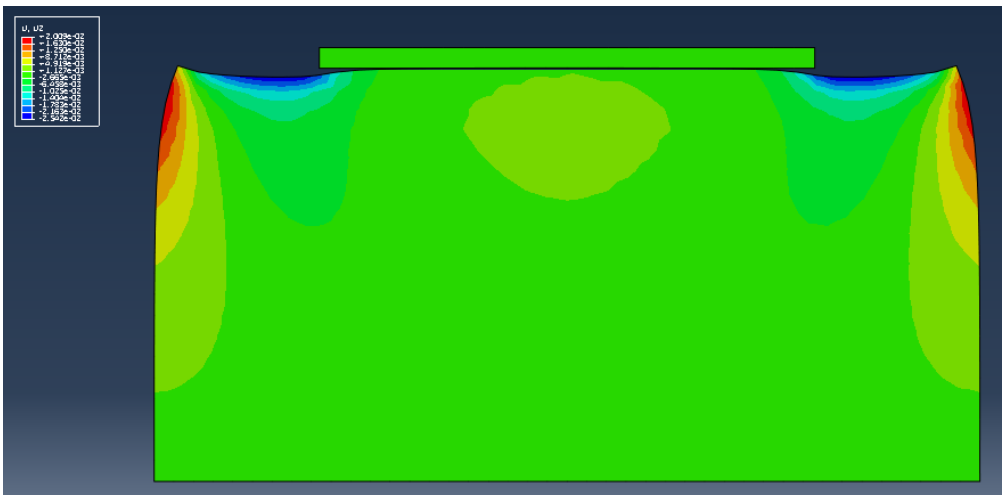

Figure 6.16. Displacement Profile for Case 1 (No Horizontal Moisture Barrier)

7. CONCLUSIONS AND RECOMMENDATIONS

This study investigated drying shrinkage problems in pavement subgrade soils using the principles of unsaturated soil mechanics. Soil specimens were obtained from four different sites in Oklahoma and subjected numerous laboratory tests for obtaining soil input parameters for analyzing and modeling the drying shrinkage problem. In many cases, the average of the test results of each parameter are used in the analytical and numerical analyses of the problem. The main reason behind this approach was that the soil specimens obtained from the four sites in Oklahoma were highly disturbed and in very dry conditions due to the extremely dry summer of 2012. These conditions prevented the research team from investigating each site individually in detail. However, the average results of the some of the soil parameters and wide ranges of the climatic effects in terms of the surface suction boundary conditions still enabled the research team to conduct a unique analysis of the problem. In these analyses, the surface and subsurface suction boundary conditions were selected representative of the climatic and soil condtions in Oklahoma.

In many cases, this type of cracking initiates in the drying subgrade soil and reflects from the highly plastic subgrade through the pavement structure. The relatively impermeable pavement surface has a significant impact on the formation of the non-uniform moisture profiles. The mechanism of crack development, therefore, is rooted in the moisture (suction) variation in the shrinking high PI subgrade soil. The gradients of moisture variation, together with the soil volume change characteristics, determine the tensile stress distribution and shrinkage crack initiation.

This study introduced simple and practical models that can be used in analyzing the suction and tensile stress distributions within the subgrade soil. The model parameters were obtained from the laboratory tests and climatic conditions of Oklahoma. The results from these simple models were compared with the results obtained from the commercially available software package Abaqus. The comparison of the suction profiles from the Mitchell model and Abaqus program were very close to each other. However, there were some differences between the predicted horizontal tensile

stresses between the new model that was introduced in this study and the results from Abaqus. The major differences between the tensile stresses were at shallower depths near the ground surface, and those differences were attributed to the displacement boundary conditions considered in the finite element method modeling using Abaqus. Furthermore, the comparison analysis was only based on limited range of soil and climatic boundary conditions.

In the study, a significant number of available tensile strength prediction models from the literature were evaluated and used in predicting the tensile strength of the soils tested in this study. The predicted tensile strength values were within the ranges of the predicted tensile stresses determined using the new model and Abaqus software, when the equilibrium suction level of 3.5 pF (2.5 log kPa) was considered in the analysis.

In this study, the effects of horizontal moisture barrier on the suction and tensile stress distribution within the subgrade soil at the edge of the pavement were investigated using the finite element method with Abaqus computer program. Different lengths of moisture barrriers were modeled in the analysis. The horizontal moisture barrier can greatly control the distribution pattern of suction and keep the moisture variations underneath the pavement to a minimum. The lengths of the horizontal moisture barriers can be optimized using the analytical and numerical approach taken in this study.

The results of this study can lead to some recommendations that could be considered for the verification and calibration of the approaches taken in this report with respect to the following items: a) a comprehensive field monitoring of suction (and possibly displacement) variations of the soil profile at the edge of the pavement; b) measuring the tensile strength of the typical Oklahoma subgrade soils considering varios soil parameters and suction boundary conditions. The laboratory scale tests should be carefully designed such that the boundary effects are eliminated (or reduced) as much as possible.

REFERENCES

Ayad, R., J.M. Konrad, and M. Soulie (1997). Desiccation of a Sensitive Clay: Application of the Model CRACK. Canadian Geotechnical Journal, V 34, pp. 943-951.

Barzegar, A. R., J. M. Oades, P. Rengasamy and R. S. Murray (1995). Tensile Strength of Dry, Remoulded Soils as Affected by Properties of the Clay Fraction. Geoderma, Vol. 65, pp.93–108.

Bulut, R. and E. C. Leong (2008). Indirect Measurement of Suction. Special Issue on Laboratory and Field Testing of Unsaturated Soils. Journal of Geotechnical and Geological Engineering, Vol. 26, No. 6, pp. 633-644.

Bulut R., R.L. Lytton, W.K. Wray (2001). Soil Suction Measurements by Filter Paper. ASCE Geotechnical Special Publication No. 115, pp. 243–261.

Bulut R., S.M. Hineidi, and B. Bailey (2002). Suction Measurements—Filter Paper and Chilled Mirror Psychrometer. Proceedings of the Texas Section American Society of Civil Engineers, Fall Meeting, Waco, October 2-5, 2002, CD-ROM.

Covar, A.P. and R.L. Lytton (2001). Estimating Soil Swelling Behavior Using Soil Classification Properties. ASCE Geotechnical Special Technical Publication No. 115

Crockford, W. W. and D.N. Little (1987). Tensile Fracture and Fatigue of Cement-Stabilized Soil. Journal of Transportation Engineering, Vol. 113, No. 5, American Society of Civil Engineers (ASCE), pp. 520-537.

Fang, H. Y., and W. F. Chen (1971). New Method for Determination of Tensile Strength of Soils. Highway. Res. Rec., 375, pp.62–68.

Fredlund, D.G. and Morgenstern, N.R. (1977). Stress State Variables for Unsaturated Soils. Journal of Geotechnical Engineering, Vo. 103, pp. 447–466.

Greene, S. B. R., A. R. Egglenton and P. Rengasamy (2002). Relationships between Clay Mineralogy and the Hard Setting Properties of the Soil in the Carnarvon Horticultural District of Western Australia. Appl. Clay Sci., Vo. 20, pp. 211–223.

Harison, J. A., B.O. Hardin, and K. Mahboub (1994). Fracture Toughness of Compacted Cohesive Soils Using Ring Test. Journal of Geotechnical Engineering, Vol. 120, No. 5, pp. 872-891.

Jayatilaka, R., D.A. Gay, R.L. Lytton, and W.K. Wray (1993). Effectiveness of Controlling Pavement Roughness due to Expansive Clays with Vertical Moisture Barriers. FHWA/TX-92/1165-2F Research Report, Texas Transportation Institute, College Station, Texas.

Kodikara, J.K., S.L. Barbour, and D.G. Fredlund (2002). Structure Development in Surficial Heavy Clay Soils: A Synthesis of Mechanisms. Australian Geomechanics, Vol. 37, No. 3, pp. 25–40.

Konrad, J.-M., and R. Ayad (1997). Desiccation of a Sensitive Clay: Field Experimental Observations. Canadian Geotechnical Journal, Vol. 34, pp. 929-943.

Li, H. and D.C. Sego (2000). Equation for Complete Compaction Curve of Fine-Grained Soils and Its Application. Constructing and Controlling Compaction of Earth Fills, ASTM STP 1384.

Long, X. (2006). Prediction of Shear Strength and Vertical Movement due to Moisture Diffusion through Expansive Soils. Ph.D. Dissertation. Texas A&M University, College Station, Texas.

Luo, R. (2007). Minimizing Longitudinal Pavement Cracking due to Subgrade Shrinkage. Ph.D. Dissertation. University of Texas-Austin, Texas.

Luo, R. and J.A. Prozzi (2009). Combining Geogrid Reinforcement and Lime Treatment to Control Dry Land Longitudinal Cracking. Transportation Research Record: Journal of the Transportation Research Board, Volume 2104, pp. 88-96.

Luo, R. and J.A. Prozzi (2008). Development of Longitudinal Cracks on Pavement over Shrinking Subgrade. Transportation Research Board 87th Annual Meeting, Paper #08-1034, CD-ROM.

Lytton, R. L., C. Aubeny, and R. Bulut (2005). Design Procedure for Pavements on Expansive Soils, Research Report FHWA/TX-05/0-4518-1, Vol. 1, Texas Transportation Institute, Texas A&M University, College Station, Texas.

Lytton, R.L. (1994). Prediction of movement in expansive clay. Vertical and Horizontal Deformations of Foundations and Embankments, Publication No. 40, Yeung, A.T., and Felio, G.Y. ed. ASCE, New York, NY, Vol. 2, pp. 1827-1845 1994.

Mabirizi, D. and R. Bulut (2010). A Unified Testing Method for Measuring Unsaturated Soil Drying and Wetting Diffusion Coefficients in Laboratory, Transportation Research Record: Journal of the Transportation Research Board, No. 2170, Transportation Research Board of the National Academies, Washington, D.C., pp. 109-118.

McKeen, R.G. (1981). Design of Airport Pavements on Expansive Soils. Report No. DOT/FAA-RD-81-25, Federal Aviation Administration, Washington, D.C.

Mitchell, P. W. (1979). The structural analysis of footings on expansive soil. Kenneth W.G. Smith and Associates Research Report No. 1, pp. 1-159, Newton, South Australia.

Nevels, J.B. (2006). An Evaluation of Horizontal Membrane Barriers in Controlling Longitudinal Cracking. ASCE Special Publication No. 147, pp. 269-280.

Nuhfer, E.B., R.J. Proctor, and N. Moser (1993). The Citizen's Guide to Geologic Hazards. AIPG Press: Arvada, CO; p 134.

Puppala, A.J., T. Manosuthhikji, L. Hoyos, and S. Nazarian (2009). Moisture and Suction in Clay Subgrades Prior to Initiation of Pavement Cracking, TRB 88th Annual Meeting Compendium of Papers DVD, Transportation Research Board Annual Meeting 2009 Paper #09-1522, 13p.

Zeh, R. M., and K. J. Witt (2005a). Suction-Controlled Tensile Strength of Compacted Clays." Proc.,16th Int. Conf. Soil Mech. Geotech. Eng., Vol. 4, Osaka, Japan, pp.2347–2352.

Sabnis, A., I. Abdallah, S. Nazarian, and A.J. Puppala (2010). Development of Shrinkage Model for Clays Based on Moisture Variation. Experimental and Applied Modeling of Unsaturated Soils, Proceedings of Sessions of GeoShanghai 2010 International Conference, June 3-5, Shanghai, pp. 166-172.

Sumarac, D. (2004). Moisture Diffusion Induced Soil Cracking. The First International Conference on Computational Mechanics (CM'04), Belgrade, Serbia and Montenegro, November 15-17, 2004, pp. 1-13.

Thornthwaite, C.W. (1948). An Approach Toward a Rational Classification of Climate. Geographical Review, Vol. 38, pp. 55-94.

Thornthwaite, C.W. and J.R. Mather (1955). The Water Balance. *Publication of Climatology*, Laboratory of Climatology, Vol. 8, No. 1, 104 p.

Venkataramana, K., Rao, B. H., and Singh, D. N. (2009). A Critical Review of the Methodologies Employed for Determination of Tensile Strength of the Fine-Grained Soils. Journal Testing Evaluation, Vo. 37, pp.115–121.

Witczak, M.W., C.E. Zapata, and W.N. Houston (2006). Models Incorporated into the Current Enhanced Integrated Climatic Model for Used in Version 1.0 of the ME-PDG. NCHRP 9-23 Project Report, Arizona State University, Tempe, Arizona.

Win, S. S. (2006). Tensile Strength of Compacted Soils Subject to Wetting and Drying. M.S. thesis, Univ. of New South Wales, Sydney, Australia.

Wray, W.K. and K.T. Meyer (2004). Expansive Clay Soil… A Widespread and Costly GeoHazard. GeoStrata, ASCE GeoInstitute. Vol. 5, No. 4, October, 2004. pg. 24-25, 27-28.

APPENDICES

APPENDIX A

Table A1. Norman Site, Boring 1, Soil Description Based on Visual Inspection

Shelby Tube	Soil Segment	Depth (feet)	Soil Description	Soil Type
1A	1A1	0 to 0.83	Light to dark brown, root fibers close to surface, significant amount of sample disturbance and cracking. Only in 1B1 and 1B2, there are some iron stains.	Type 1
	1A2	0.83 to 1.04		
	1A3	1.04 to 1.98		
1B	1B1	2.0 to 2.69		
	1B2	2.69 to 3.32		

Table A2. Norman Site, Boring 2, Soil Description Based on Visual Inspection

Shelby Tube	Soil Segment	Depth (feet)	Soil Description	Soil Type
2A	2A1	0 to 0.75	Light brown 2A1 to dark brown 2A5, root fibers close to the surface. Only in 2A1, significant deep cross-sectional crack almost dividing it into two halves. Only in 2A1 and 2A2, there are some iron stains.	Type 1
	2A2	0.75 to 1.07		
	2A3	1.07 to 1.37		
	2A4	1.37 to 1.71		
	2A5	1.71 to 1.90		
2B	2B1	2.11 to 2.88	Light brown, significant disturbance, few small white aggregates.	Type 1
	2B2	2.88 to 3.19		
	2B3	3.19 to 3.5		
2C	2C1	4.0 to 4.81	Red in color, some disturbance.	Type 2
	2C2	4.81 to 5.42		
2D	2D1	6.0 to 6.63		
	2D2	6.63 to 7.16		
	2D3	7.16 to 8		
2E	2E1	8.0 to 9.02	Red in color, partial disturbance, hair cracks in the undisturbed part.	
	2E2	9.02 to 10	Red in color, minimal disturbance.	
2F	2F1	10.0 to 10.55	Red in color, almost no disturbance, moist. For 2F1 only, surface along the length of the specimen is darker in color than the bottom end. For 2F2 only, the specimen has been broken into two pieces while unwrapping. For 2H3 only, specimen already broken into 2 pieces.	
	2F2	10.55 to 11.35		
	2F3	11.35 to 11.95		
2G	2G1	12.0 to 12.72		Type 2
	2G2	12.72 to 13.34		
	2G3	13.34 to 14		
2H	2H1	14.0 to 14.29		
	2H2	14.29 to 15.34		
	2H3	15.34 to 15.75		
	2H4	15.75 to 16		
2I	2I1	16.0 to 16.5	Red in color, specimen is very wet.	
	2I2	16.5 to 17.55	Red in color, specimen is moist, top part is separated (2 inch), bottom part is separated (2 inch), middle part is broken into 2 halves.	Type 2
	2I3	17.55 to 18	Red in color, specimen is moist, few hair cracks.	

Table A3. Norman Site, Boring 3, Soil Description Based on Visual Inspection

Shelby Tube	Soil Segment	Depth (feet)	Soil Description	Soil Type
3A	3A1	0.0 to 1.1	Entirely disturbed (collapsed), brown in color, root fibers.	Type 1
	3A2	1.1 to 2.0	Disturbed, brown in color, root fibers.	
3B	3B1	2.0 to 2.9	Slightly disturbed, fallen parts from top, light brown in color, broken into 2 halves while unwrapping.	
	3B2	2.9 to 3.75	Light brown in color, black spots, slightly disturbed.	
3C	3C1	4.0 to 4.83	Red in color for 3C1 and 3C2. Top surface of 3C1 is disturbed (fallen particles) and dark brown in color. Some disturbance for the rest of 3C1 and all 3C2.	Type 2
	3C2	4.83 to 5.90		
3D	3D1	6.0 to 7.15	Red in color (whole push-tube). For 3D1, length of 6 cm is separated from rest of segment. Fallen particles from top end of 3D1, minimal disturbance for rest of 3D1. Top part of 3D2 is totally disturbed, rest of 3D2 is undisturbed, moisture appears.	
	3D2	7.15 to 8		
3E	3E1	8.0 to 8.95	Red in color. 3E1 is partially disturbed. Top part of 3E2 is separated, rest of 3E2 is undisturbed.	
	3E2	8.95 to 9.85		
3F	3F1	10.0 to 10.97	Red in color, slightly disturbed in general, cross-sectional crack in the middle of 3F2.	
	3F2	10.97 to 11.60		
3G	3G1	12.0 to 12.91	Red in color, undisturbed, one visible crack near top of 3G2.	
	3G2	12.91 to 13.78		
3H	3H1	14.0 to 14.07	Red in color, 3H1 disturbed from bottom end, 3H2 highly disturbed.	
	3H2	14.07 to 15.90		
3I	3I1	16.0 to 16.75	Red in color, highly disturbed, cross-section is not uniform along 3I1, cross-sectional crack in bottom of 3I1, 3I2 already broken into 4 pieces.	
	3I2	16.75 to 17.69		

Table A4. Norman Site, Boring 4, Soil Description Based on Visual Inspection

Shelby Tube	Soil Segment	Depth (feet)	Soil Description	Soil Type
4A	4A1	0 to 0.87	Very dark brown, root fibers, few small cracks.	Type 1
	4A2	0.87 to 1.62	Brown in color, traces of root fibers, few thin cracks.	
4B	4B1	2.0 to 3.0	Brown in color, highly disturbed, top part of 4B1 is separated.	
	4B2	3.0 to 3.25		
	4B3	3.25 to 3.87		
	4B4	3.87 to 4.0		
4C	4C1	4.0 to 5.0	Red in color, top part of 4C1 is brown in color, cracks in general, top part of 4C1 is highly disturbed, top part of 4C2 is separated.	Type 2
	4C2	5.0 to 5.95		
4D	4D1	6.0 to 7.17	Red in color. For 4D1 only, root fibers 4D1, cracked. For 4D2 only, minimum cracks, top part is separated.	
	4D2	7.17 to 7.77		
4E	4E1	8.0 to 9.0	Red in color, slightly disturbed.	
	4E2	9.0 to 9.77		
4F	4F1	10.0 to 11.0	Red in color, cracked and disturbed.	
	4F2	11.0 to 12.0	Red in color, undisturbed.	
4G	4G1	12.0 to 13.2	Red in color, slightly disturbed.	
	4G2	13.2 to 14.0		
4H	4H1	14.0 to 15.0	Red in color, disturbed (squeezed).	
	4H2	15.0 to 15.73		
4I	4I1	16.0 to 17.0	Red in color, highly disturbed.	
	4I2	17.0 to 17.85		

APPENDIX B

Table B1. Lake Hefner Site, Boring 1, Soil Description Based on Visual Inspection

Shelby Tube	Soil Segment	Depth (feet)	Soil Description	Soil Type
1A	1A1	0 to 0.8	Dark brown in color, disturbed. For 1A1 only, root fibers, slightly disturbed.	Type 1
	1A2	0.8 to 1.37		
	1A3	1.37 to 1.92		
1B	1B1	2.0 to 2.77	Light red, highly disturbed, similar to tennis court soil.	Type 2
	1B2	2.77 to 3.55		
	1B3	3.55 to 3.98		
1C	1C1	4.0 to 4.70	Dark red, disturbed.	
	1C2	4.70 to 5.58		
	1C3	5.58 to 5.99		
1D	1D1	6.0 to 6.99	Dark red, top part is greenish, highly disturbed.	
	1D2	6.99 to 7.81	Dark red, disturbed.	
1E	1E1	8.0 to 0.74	Dark red, slightly disturbed.	

Table B2. Lake Hefner Site, Boring 2, Soil Description Based on Visual Inspection

Shelby Tube	Soil Segment	Depth (feet)	Soil Description	Soil Type
2A	2A1	0 to 1.0	Root fibers, dark brown, disturbed	Type 2
	2A2	1.0 to 1.86	Red, traces of root fibers, disturbed.	
2B	2B1	2.0 to 2.94	Light red, traces of root fibers, disturbed.	
	2B2	2.94 to 3.64		
2C	2C1	4.0 to 4.87	Red, disturbed.	
	2C2	4.87 to 4.97		
	2C3	4.97 to 5.95		
2D	2D1	6 to 6.98		
	2D2	6.98 to 7.96		
2E	2E1	8 to 8.82		

Table B3. Lake Hefner Site, Boring 3, Soil Description Based on Visual Inspection

Shelby Tube	Soil Segment	Depth (feet)	Soil Description	Soil Type
3A	3A1	0 to 0.80	Living insects, brown, root fibers, disturbed.	Type 2
	3A2	0.80 to 1.50	Reddish brown, traces of root fibers, disturbed.	
3B	3B1	1.5 to 2.5	Light orange/red, traces of root fibers, disturbed.	
	3B2	2.5 to 3.35		
3C	3C1	3.5 to 4.5	Light orange/red, disturbed.	
	3C2	4.5 to 5.45	Red, slightly disturbed.	
3D	3D1	5.5 to 6.38	Dark red, highly disturbed.	
3E	3E1	–	Specimen not received.	

APPENDIX C

Table C1. Ardmore Site, Boring 1, Soil Description Based on Visual Inspection

Shelby Tube	Soil Segment	Depth (feet)	Soil Description (Visual Inspection)	Soil Type
1A	1A1	0 to 0.95	Root fibers, black, slightly disturbed.	Type 1
	1A2	0.95 to 1.95	Root fibers, black, disturbed.	
1B	1B1	2.0 to 2.80	Traces of root fibers, brownish, disturbed.	Type 2
	1B2	2.80 to 3.57	Root fibers, brownish, disturbed.	

Table C2. Ardmore Site, Boring 2, Soil Description Based on Visual Inspection

Shelby Tube	Soil Segment	Depth (feet)	Soil Description (Visual Inspection)	Soil Type
2A	2A1	0 to 0.90	Root fibers, black, disturbed.	Type 1
	2A2	0.90 to 1.90	Root fibers, black with brown stains, disturbed.	
2B	2B1	2.0 to 3.0	Root fibers traces, brownish, disturbed.	Type 2
	2B2	3.0 to 3.45	Light brown, highly disturbed/collapsed.	

Table C3. Ardmore Site, Boring 3, Soil Description Based on Visual Inspection

Shelby Tube	Soil Segment	Depth (feet)	Soil Description (Visual Inspection)	Soil Type
3A	3A1	0 to 1.1	Root fibers, black, disturbed, moisture appears.	Type 1
	3A2	1.1 to 1.85	Brownish, cracked, moisture appears.	Type 2
3B	3B1	2.0 to 2.90	Brownish, disturbed, sample cross-section is not fully cylindrical.	
	3B2	2.90 to 3.45	Dark brown, slightly disturbed.	
	3B3	3.45 to 4.0		
3C	3C1	4.0 to 4.90	Light black, highly disturbed.	Type 3
	3C2	4.90 to 6.0	Light black, undisturbed.	

Table C4. Ardmore Site, Boring 4, Soil Description Based on Visual Inspection

Shelby Tube	Soil Segment	Depth (feet)	Soil Description (Visual Inspection)	Soil Type
1AA	1AA1	0 to 1.0	Root fibers, brownish, slightly disturbed.	Type 2
	1AA2	1.0 to 2.0	Brownish, disturbed.	
1BB	1BB1	2.0 to 2.5	Root fibers, brownish, disturbed.	
	1BB2	2.5 to 3.4	Dark brown, undisturbed, cracked, small white aggregates.	
	1BB3	3.4 to 3.5	Brown, hollow.	
	1BB4	3.5 to 3.90	Dark brown, undisturbed.	
1CC	1CC1	4.0 to 4.88	Dark brown, partially disturbed.	
	1CC2	4.88 to 5.80	Brown, undisturbed, few cracks.	
	1CC3	5.80 to 6.0		
1DD	1DD1	6.0 to 6.50	Brown, partially disturbed, separated.	
	1DD2	6.50 to 7.50	Brown, disturbed.	
	1DD3	7.50 to 8.0	Brown, undisturbed.	

Table C5. Ardmore Site, Boring 5, Soil Description Based on Visual Inspection

Shelby Tube	Soil Segment	Depth (feet)	Soil Description (Visual Inspection)	Soil Type
2AA	2AA1	0 to 0.90	Root fibers, brown, undisturbed	Type 2
	2AA2	0.90 to 1.90	Brown, undisturbed, small white aggregates.	
	2AA3	1.90 to 2.0	Brown, undisturbed	
2BB	2BB1	2.0 to 2.90	Black, partially disturbed, small white aggregates.	Type 1
	2BB2	2.90 to 4.0	Dark brown, undisturbed, small white aggregates.	Type 2
2CC	2CC1	4.0 to 4.86	Root fibers, brown, partially disturbed.	
	2CC2	4.86 to 5.86	Brown, undisturbed.	
	2CC3	5.86 to 6.0		
2DD	2DD1	6.0 to 6.5	Brown to light black, disturbed, red particles.	Type 3
	2DD2	6.5 to 7.10	Brownish, undisturbed.	Type 2
	2DD3	7.10 to 7.50		
	2DD4	7.50 to 8.0	Brownish, disturbed.	

Table C6. Ardmore Site, Boring 6, Soil Description Based on Visual Inspection

Shelby Tube	Soil Segment	Depth (feet)	Soil Description (Visual Inspection)	Soil Type
3AA	3AA1	0 to 0.1	Root fibers, brown, undisturbed.	Type 2
	3AA2	0.1 to 1.1	Root fibers, brown with black stains, undisturbed.	
3BB	3BB1	2.0 to 3.15	Black, disturbed, small white aggregates.	Type 1
	3BB2	3.15 to 3.85	Dark brown, undisturbed, cracked, small white aggregates.	Type 2
3CC	3CC1	4.0 to 4.95	Root fibers, brown, disturbed, small white aggregates.	
	3CC2	4.95 to 6.0	Brown, partially disturbed, small white aggregates.	
3DD	3DD1	6.0 to 6.50	Brown, undisturbed.	
	3DD2	6.50 to 7.45	Brown, undisturbed, separated, red particles.	
	3DD3	7.45 to 8.0	Brown, disturbed, red particles.	

Table C7. Ardmore Site, Boring 7, Soil Description Based on Visual Inspection

Shelby Tube	Soil Segment	Depth (feet)	Soil Description (Visual Inspection)	Soil Type
4AA	4AA1	0 to 0.95	Living insects, root fibers, brown, disturbed.	Type 2
	4AA2	0.95 to 2.0	Dark brown, partially disturbed.	
4BB	4BB1	2.0 to 3.0	Brownish, disturbed, small white aggregates.	
	4BB2	3.0 to 4.0		
4CC	4CC1	4.0 to 4.85	Root fibers, brownish, disturbed, small white aggregates.	
	4CC2	4.85 to 5.5	Brown, undisturbed.	
	4CC3	5.5 to 6.0	Brown, disturbed.	
4DD	4DD1	6.0 to 6.50	Brown, undisturbed, cracked.	
	4DD2	6.50 to 6.85	Brown, undisturbed.	
	4DD3	6.85 to 7.50	Brownish, undisturbed.	
	4DD4	7.50 to 8.0	Brownish, disturbed, small white aggregates.	

APPENDIX D

Table D1. Idabel Site, Boring 1, Soil Description Based on Visual Inspection

Shelby Tube	Soil Segment	Depth (feet)	Soil Description	Soil Type
4A	4A1	0.00 to 0.55	Brown colored soil, Disturbed, Root fibers	Type 1
	4A2	0.55 to 1.13	Brown colored soil, Undisturbed	
4B	4B1	2.00 to 2.55		
	4B2	2.55 to 3.86		
4C	4C1	4.00 to 4.35		
	4C2	4.35 to 4.95		
4D	4D1	6.00 to 6.30		
	4D2	6.30 to 6.80		
4E	4E1	8.00 to 8.35		
	4E2	8.45 to 8.95		

Table D2. Idabel Site, Boring2, Soil Description Based on Visual Inspection

Shelby Tube	Soil Segment	Depth (feet)	Soil Description	Soil Type
5A	5A1	0.00 to 0.35	Brown colored soil, Disturbed, Root fibers	Type 1
	5A2	0.35 to 1.00	Brown colored soil, Undisturbed	
5B	5B1	2.00 to 2.30	Black colored soil, Undisturbed	Type 2
	5B2	2.30 to 3.05		
5C	5C1	4.00 to 4.25	Brown colored soil, Undisturbed	Type 1
	5C2	4.25 to 4.85		
5D	5D1	6.00 to 6.50		
	5D2	6.50 to 6.60		
5E	5E1	8.00 to 8.35		
	5E2	8.35 to 8.97		

Table D3. Idabel Site, Boring 3, Soil Description Based on Visual Inspection

Shelby Tube	Soil Segment	Depth (feet)	Soil Description	Soil Type
6A	6A1	0.00 to 0.55	Brown colored soil, Disturbed, Root fibers	Type 1
	6A2	0.55 to 1.10	Brown colored soil, Undisturbed	
6B	6B1	2.00 to 2.45	Black colored soil, Undisturbed	Type 2
	6B2	2.45 to 3.00		
	6B3	3.00 to 3.90		
6C	6C1	4.00 to 4.60		
	6C2	4.60 to 5.20		
6D	6D1	6.00 to 6.73	Brown colored soil, Undisturbed	Type 1
	6D2	6.30 to 6.80		
6E	6E1	8.00 to 8.27		
	6E2	8.27 to 8.93		

APPENDIX E

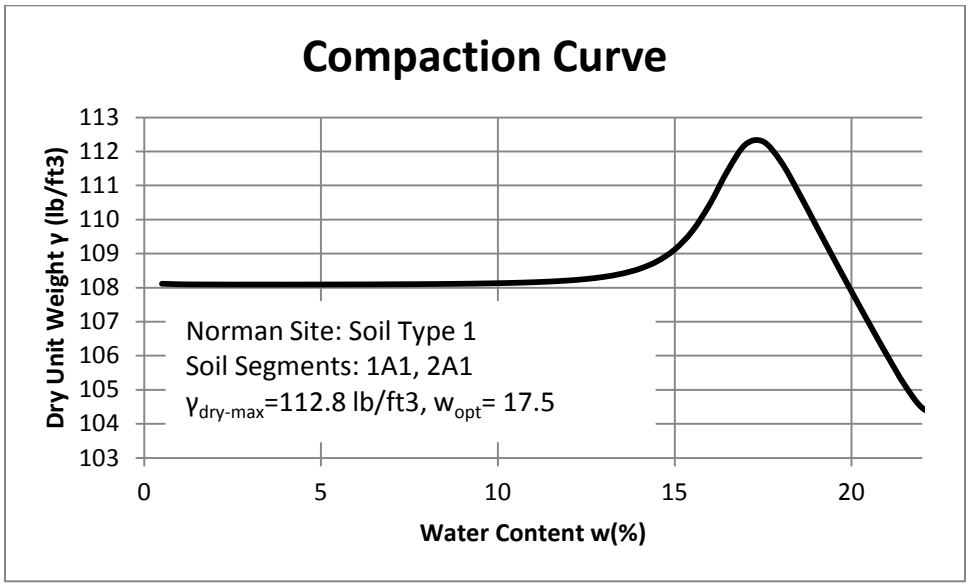

Figure E1. Relation between the Dry Unit Weight and the Water Content for the Soil from Segments 1A1, 2A1 of Type 1 of Norman Site

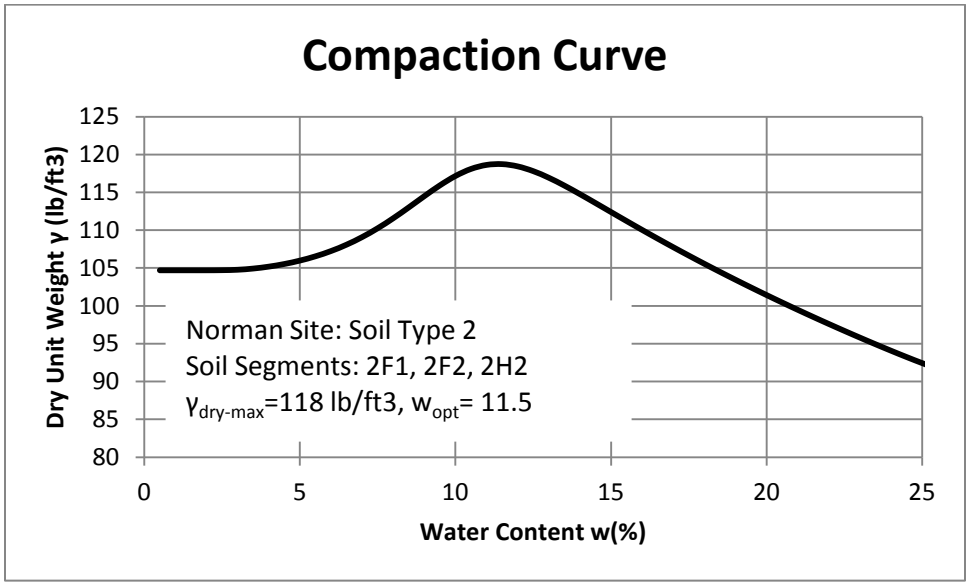

Figure E2. Relation between the Dry Unit Weight and the Water Content for the Soil from Soil Segments 2F1, 2F2, 2H2 of Type 2 of Norman Site

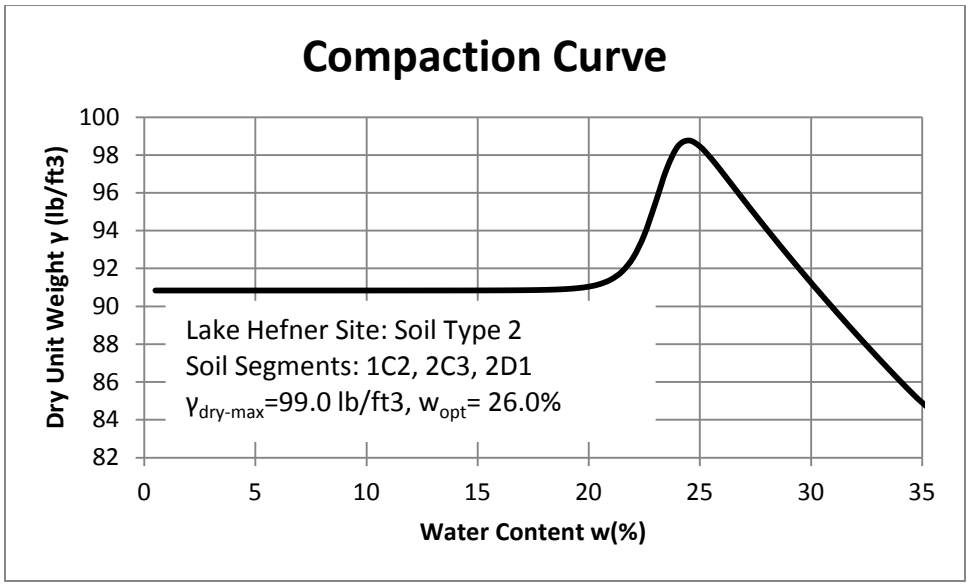

Figure E3. Relation between the Dry Unit Weight and the Water Content for the Soil from Soil Segments 1C2, 2C3, 2D1 of Type 2 of Lake Hefner Site

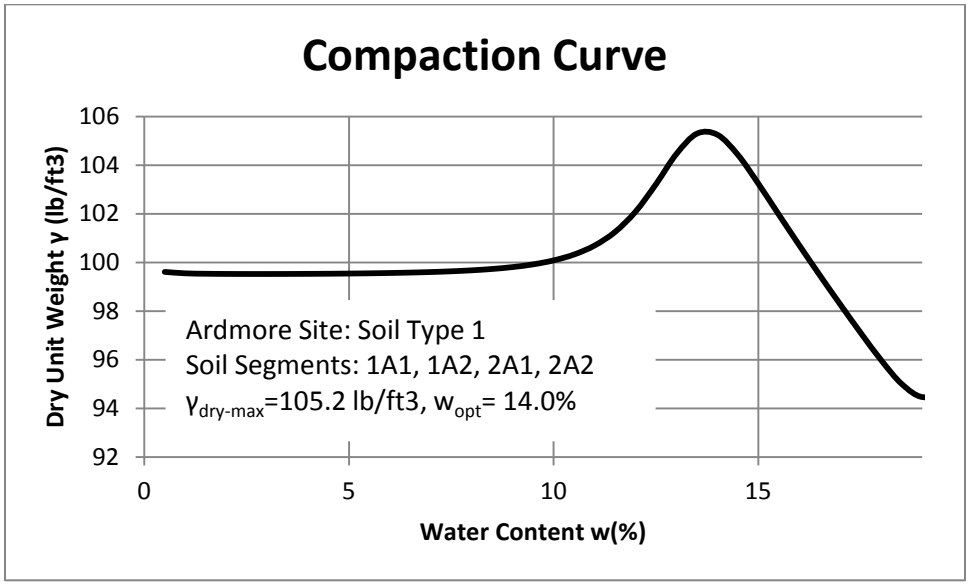

Figure E4. Relation between the dry unit weight and the water content for the soil from soil segments 1A1, 1A2, 2A1, 2A2 of type 2 of Ardmore site

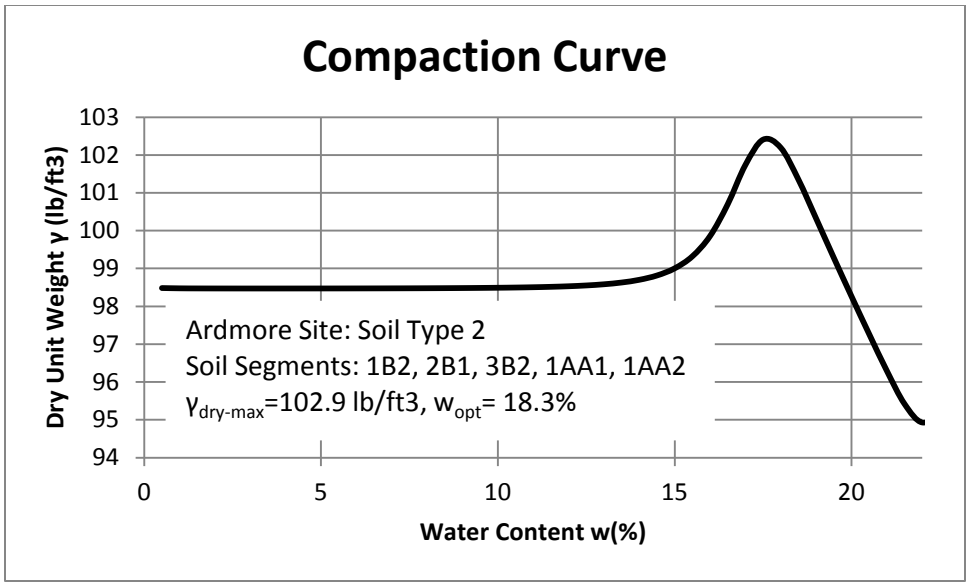

Figure E5. Relation between the Dry Unit Weight and the Water Content for the Soil from Soil Segments 1B2, 2B1, 3B2, 1AA1, 1AA2 of type 2 of Ardmore Site

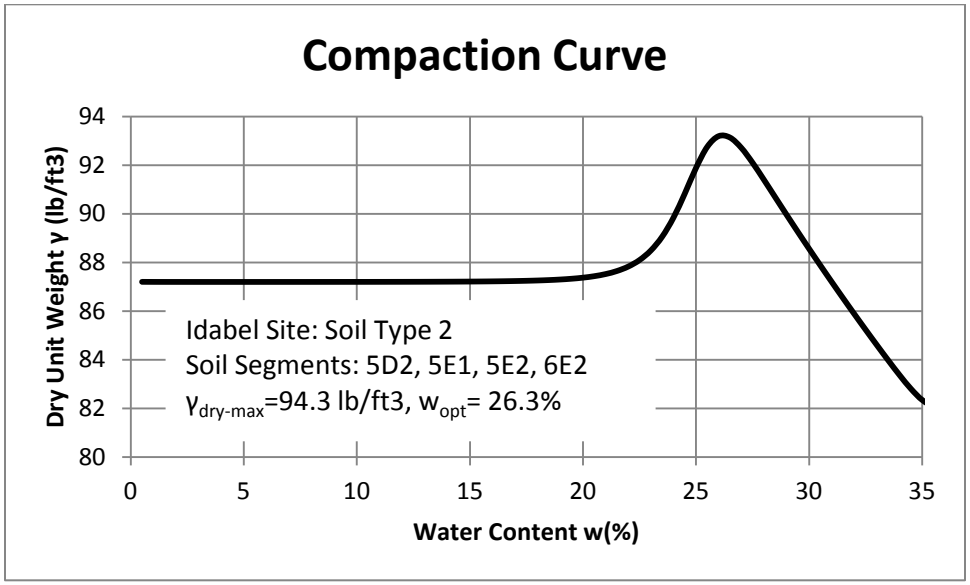

Figure E6. Relation between the Dry unit Weight and the Water Content for the Soil from Soil Segments 5D2, 5E1, 5E2, 6E2 of type 2 of Idabel Site

APPENDIX F

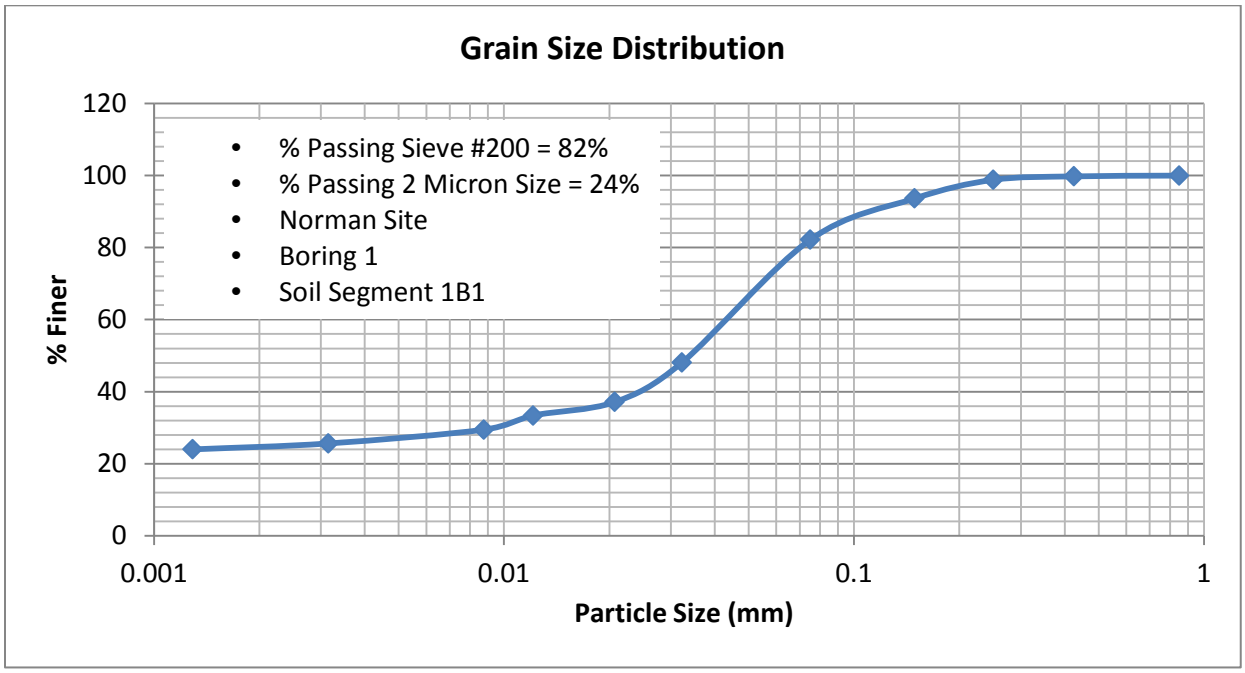

Figure F1. Grain Size Distribution Curve for the Soil from Boring 1, Soil Segment 1B1 of Norman Site

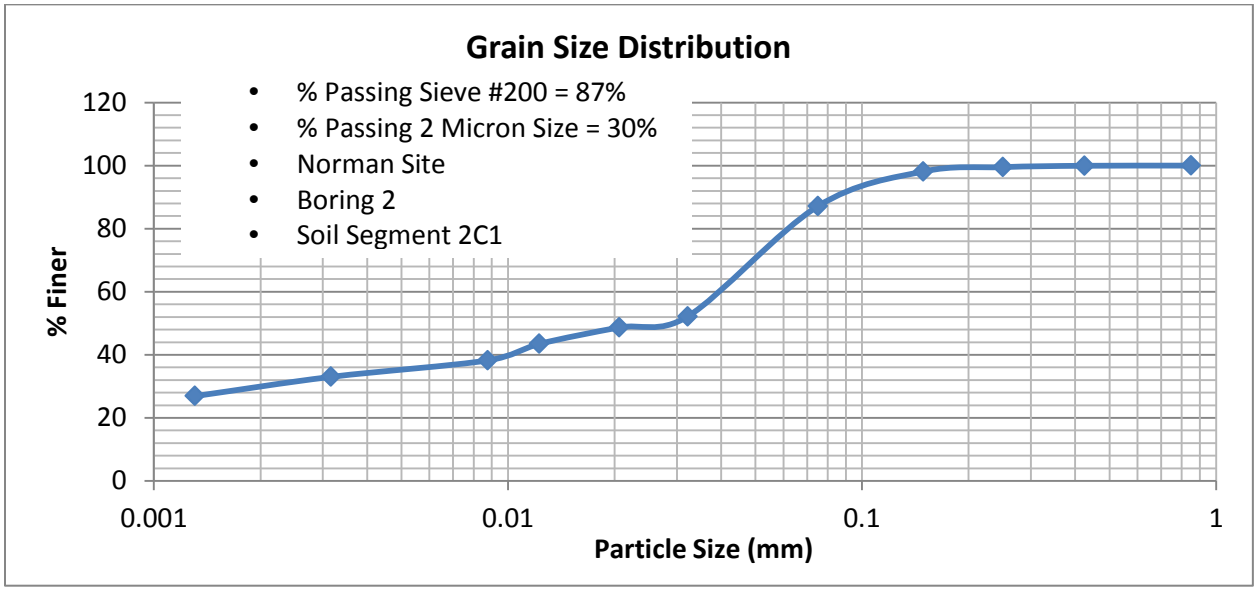

Figure F2. Grain Size Distribution Curve for the Soil from Boring 1, Soil Segment 2C1 of Norman Site

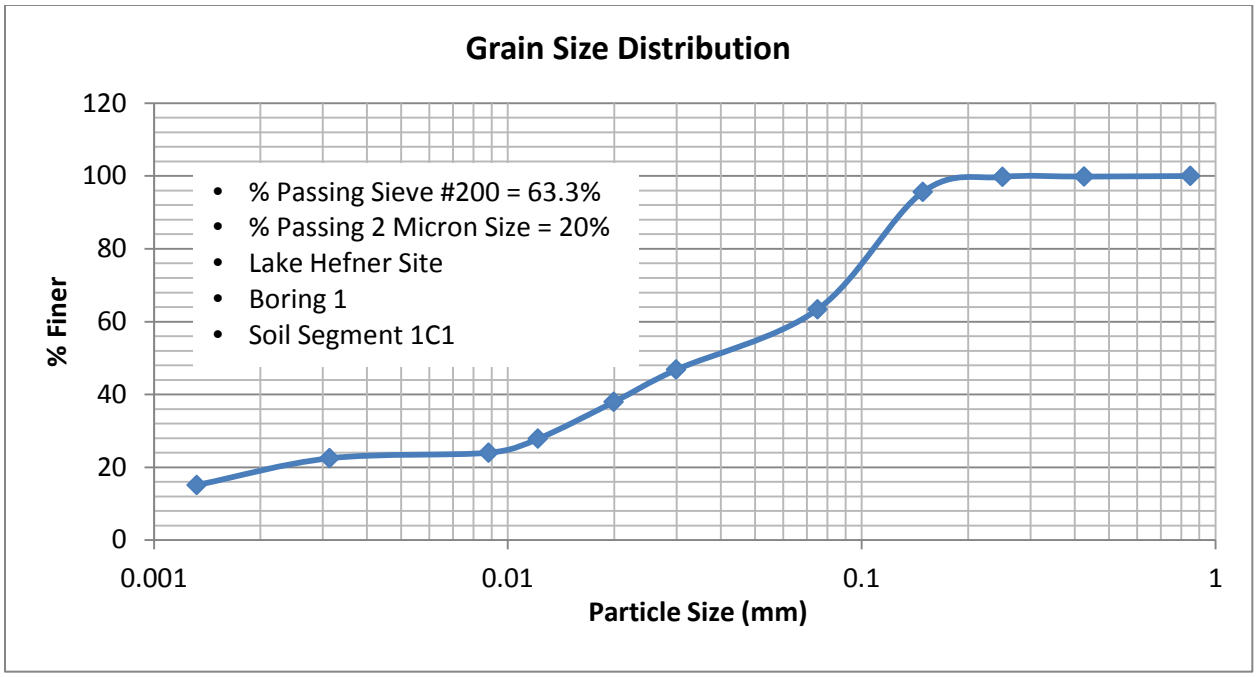

Figure F3. Grain Size Distribution Curve for the Soil from Boring 1, Soil Segment 1C1 of Lake Hefner Site

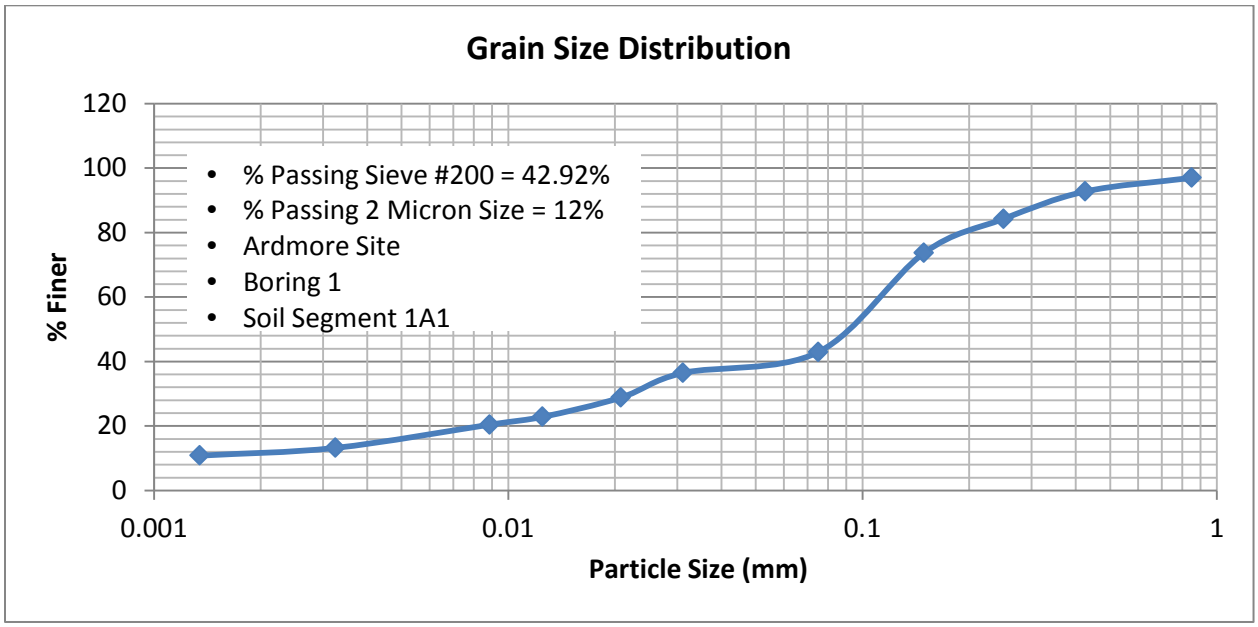

Figure F4. Grain Size Distribution Curve for the Soil from Boring 1, Soil Segment 1A1 of Ardmore Site

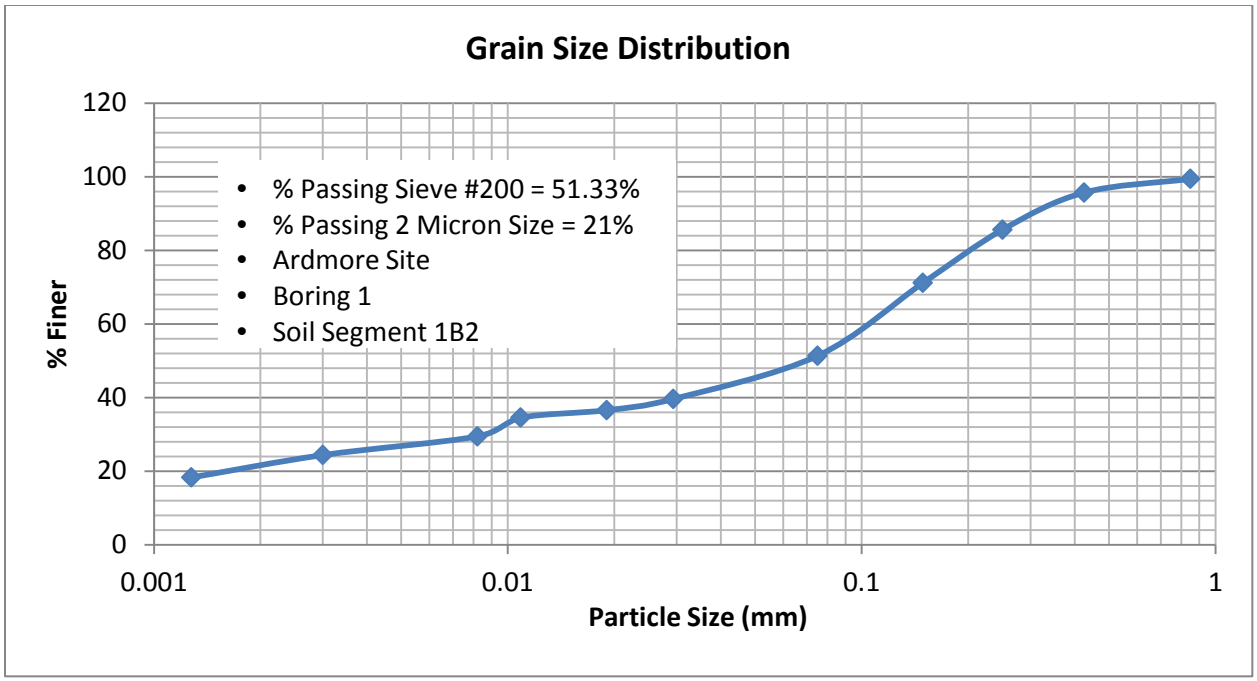

Figure F5. Grain Size Distribution Curve for the Soil from Boring 1, Soil Segment 1B2 of Ardmore Site

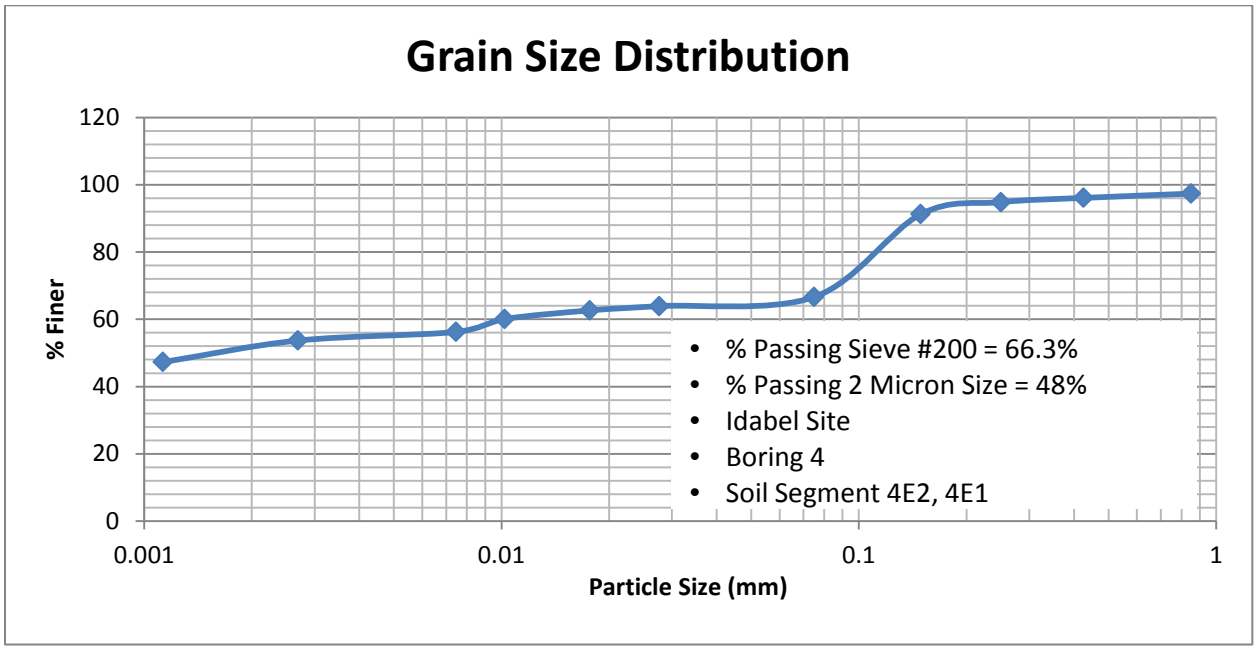

Figure F6. Grain Size Distribution Curve for the Soil from Boring 4, Soil Segments 4E2, 4E1 of Idabel Site

APPENDIX G

Table G1. Norman Site, Boring 1, Soil Segment 1A3, Depth 1.04 to 1.98 feet

Parameter	Value	Units
Evaporation Coefficient (he)	0.54	cm^{-1}
Atmospheric Suction (Ua)	6.29	pF
Initial Suction (Uo)	3.176	pF
Psychrometer Location (x)	9.2	cm
Sample Length (L)	11.1	cm

Drying Diffusion Coefficient, α_{dry} = 3.2 x 10^{-5} cm^2/sec (1.92 x 10^{-3} cm^2/min)

Laboratory Suction Measurements

Time	Suction
(min)	(pF)
2730	3.944
2880	3.988
3030	4.131
3180	4.189
3330	4.252
3480	4.316
3630	4.373
3780	4.415
3930	4.457
4080	4.493

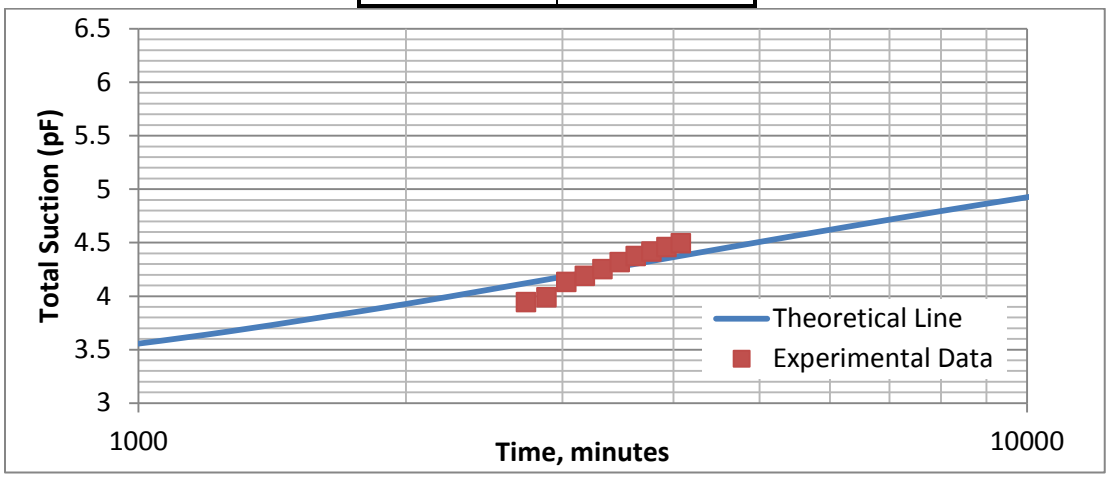

Figure G1. Variation of Total Suction with Time for the Soil of Norman Site from Boring 1, Soil Segment 1A3 at a Depth of 1.04 to 1.98 Feet

Table G2. Norman Site, Boring 2, Soil Segment 2B1, Depth 2.11 to 2.88 feet

Parameter	Value	Units
Evaporation Coefficient (he)	0.54	cm-1
Atmospheric Suction (Ua)	6.292	pF
Initial Suction (Uo)	3.962	pF
Psychrometer Location (x)	18.7	cm
Sample Length (L)	20.7	cm

Drying Diffusion Coefficient, α_{dry} = 4.33 x 10^{-6} cm^2/sec (2.60 x 10^{-4} cm^2/min)

Laboratory Suction Measurements

Time	Suction
min	pF
7815	3.964
8185	4.179
8550	4.317
8915	4.426
9285	4.501

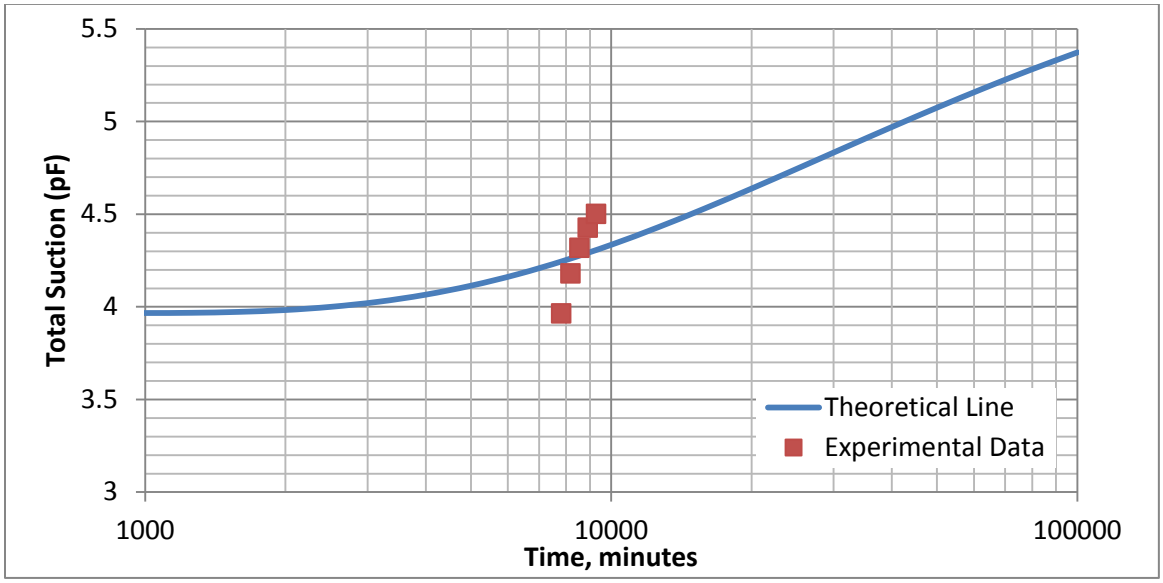

Figure G2. Variation of Total Suction with Time for the Soil of Norman Site from Boring 2, Soil Segment 2B1 at a Depth of 2.11 to 2.88 Feet

Table G3. Norman Site, Boring 2, Soil Segment 2C2, Depth 4.81 to 5.42 feet

Parameter	Value	Units
Evaporation Coefficient (he)	0.54	cm-1
Atmospheric Suction (Ua)	6.140	pF
Initial Suction (Uo)	3.962	pF
Psychrometer Location (x)	5.3	cm
Sample Length (L)	7.0	cm

Drying Diffusion Coefficient, α_{dry} = 1.17 x 10^{-5} cm^2/sec (7.0 x 10^{-4} cm^2/min)

Laboratory Suction Measurements

Time	Suction
min	pF
1805	3.967
1905	4.110
2010	4.217
2115	4.293
2215	4.332

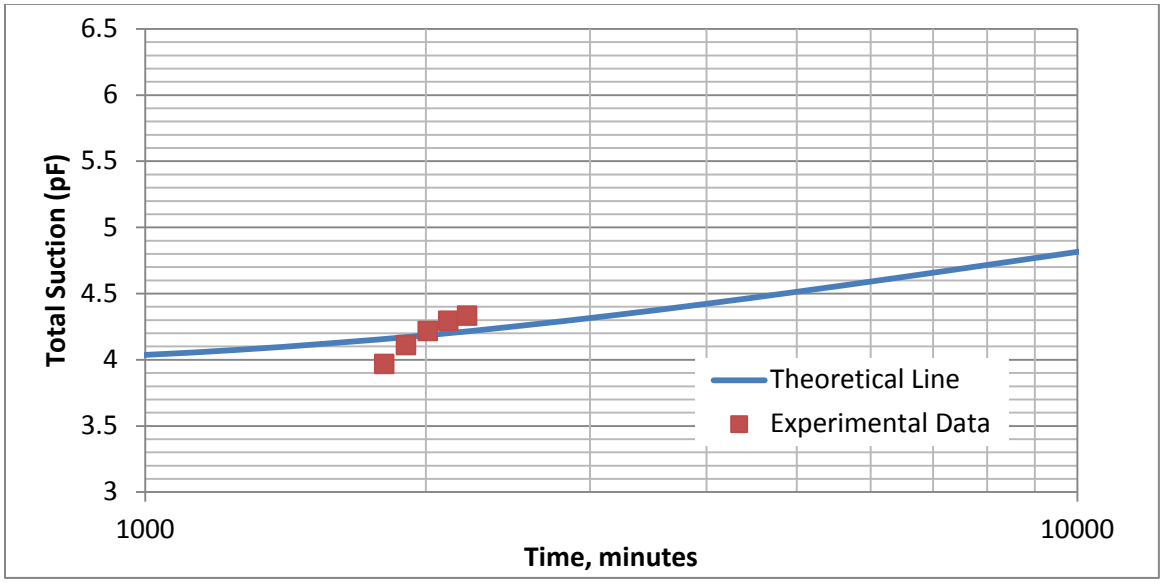

Figure G3. Variation of Total suction with Time for the Soil of Norman Site from Boring 2, Soil Segment 2C2 at a Depth of 4.81 to 5.42 Feet

Table G4. Norman Site, Boring 2, Soil Segment 2H2, Depth 14.29 to 15.34 feet

Parameter	Value	Units
Evaporation Coefficient (he)	0.54	cm^{-1}
Atmospheric Suction (Ua)	6.279	pF
Initial Suction (Uo)	3.599	pF
Psychrometer Location (x)	16.2	cm
Sample Length (L)	17.2	cm

Drying Diffusion Coefficient, α_{dry} = 2.17 x 10^{-6} cm^2/sec (1.30 x 10^{-4} cm^2/min)

Laboratory Suction Measurements

Time	Suction
min	pF
6250	3.599
6290	3.742
6330	3.830
6380	3.909
6420	3.964
6470	4.040
6520	4.069
6560	4.133
6610	4.169

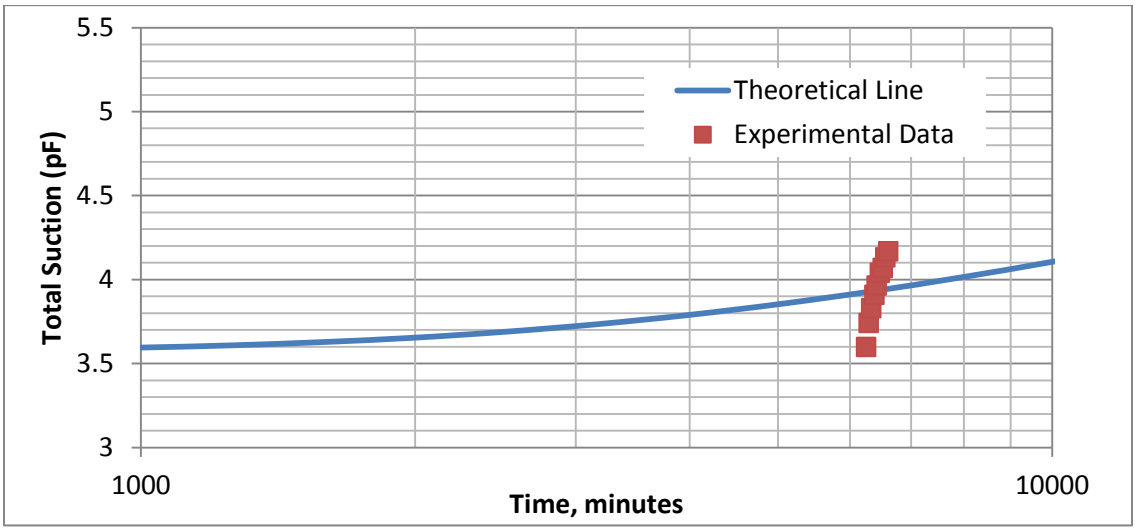

Figure G4. Variation of Total suction with Time for the Soil of Norman Site from Boring 2, Soil Segment 2H2 at a Depth of 14.29 to 15.34 Feet

Table G5. Norman Site, Boring 3, Soil Segment 3B2, Depth 2.90 to 3.75 feet

Parameter	Value	Units
Evaporation Coefficient (he)	0.54	cm^{-1}
Atmospheric Suction (Ua)	6.275	pF
Initial Suction (Uo)	3.809	pF
Psychrometer Location (x)	17.6	cm
Sample Length (L)	19.1	cm

Drying Diffusion Coefficient, α_{dry} = 1.72 x 10^{-5} cm^2/sec (1.03 x 10^{-3} cm^2/min)

Laboratory Suction Measurements

Time	Suction
min	pF
715	3.809
1065	4.024
1415	4.172
1765	4.261
2125	4.326
2475	4.382
2825	4.433
3175	4.463
3525	4.490

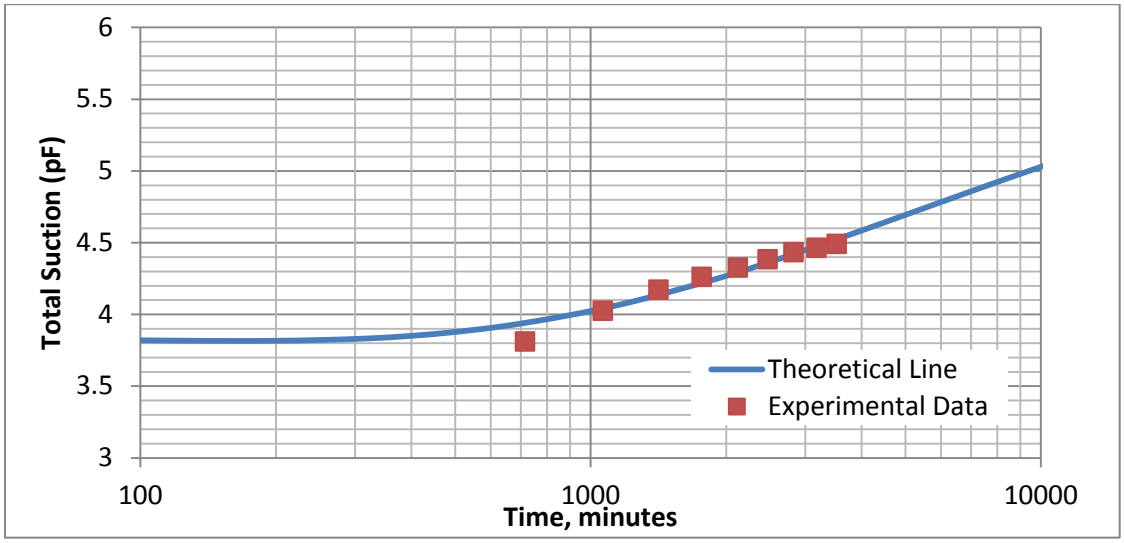

Figure G5. Variation of Total Suction with Time for the Soil of Norman Site from Boring 3, Soil Segment 3B2 at a Depth of 2.90 to 3.75 Feet

Table G6. Norman Site, Boring 3, Soil Segment 3C2, Depth 4.83 to 5.90 feet

Parameter	Value	Units
Evaporation Coefficient (he)	0.54	cm^{-1}
Atmospheric Suction (Ua)	6.272	pF
Initial Suction (Uo)	3.582	pF
Psychrometer Location (x)	26.0	cm
Sample Length (L)	29.0	cm

Drying Diffusion Coefficient, α_{dry} = 9.0 x 10^{-5} cm^2/sec (5.40 x 10^{-3} cm^2/min)

Laboratory Suction Measurements

Time	Suction
min	pF
510	3.582
780	4.061
1050	4.244
1320	4.352
1590	4.415
1850	4.459
2120	4.489
2390	4.514
2660	4.524
2930	4.527

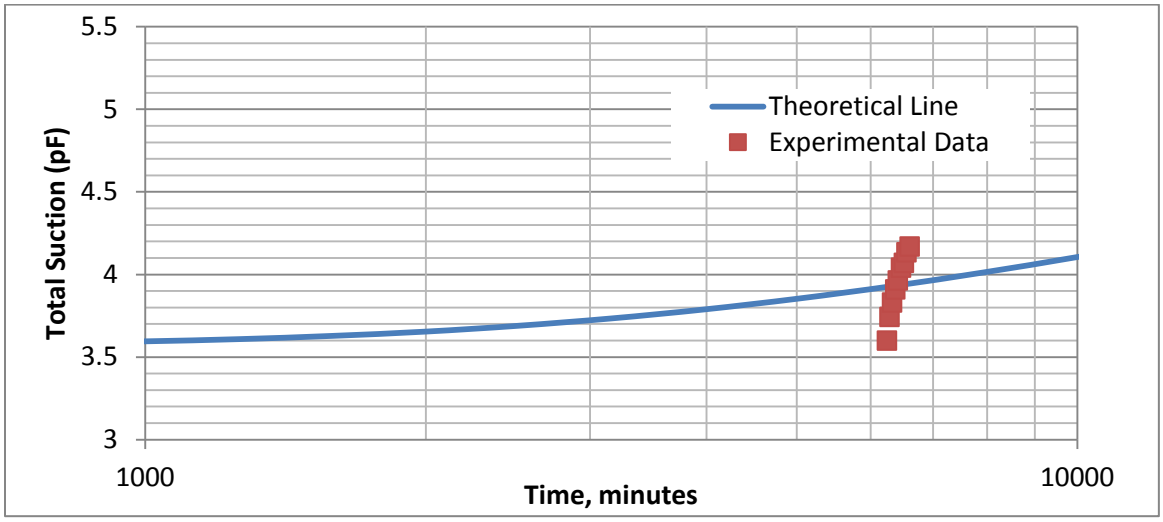

Figure G6. Variation of Total Suction with Time for the Soil of Norman Site from Boring 3, Soil Segment 3C2 at a Depth of 4.83 to 5.90 Feet

Table G7. Norman Site, Boring 4, Soil Segment 4A1, Depth 0 to 0.87 feet

Parameter	Value	Units
Evaporation Coefficient (he)	0.54	cm^{-1}
Atmospheric Suction (Ua)	6.31	pF
Initial Suction (Uo)	3.61	pF
Psychrometer Location (x)	22.9	cm
Sample Length (L)	24.9	cm

Drying Diffusion Coefficient, α_{dry} = 1.68 x 10^{-5} cm^2/sec (1.01 x 10^{-3} cm^2/min)

Laboratory Suction Measurements

Time	Suction
min	pF
2950	3.61
3230	3.85
3520	4.04
3810	4.21
4090	4.34
4380	4.43
4670	4.50
4950	4.57
5240	4.61

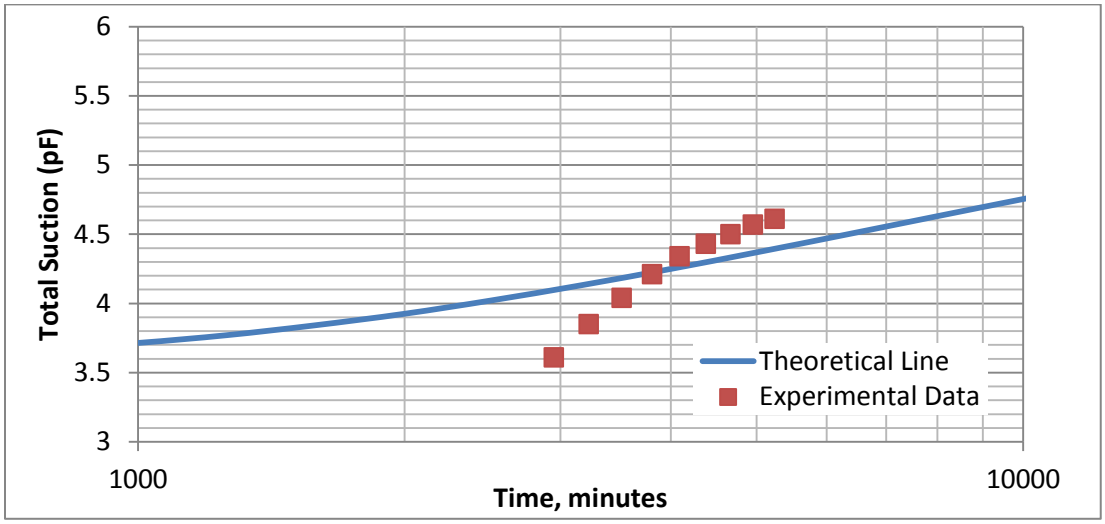

Figure G7. Variation of Total Suction with Time for the Soil of Norman Site from Boring 4, Soil Segment 4A1 at a Depth of 0 to 0.87 Feet

Table G8. Norman Site, Soil Segment 4D2, Depth 7.40 to 8.0 feet

Parameter	Value	Units
Evaporation Coefficient (he)	0.54	cm^{-1}
Atmospheric Suction (Ua)	6.29	pF
Initial Suction (Uo)	3.69	pF
Psychrometer Location (x)	14.9	cm
Sample Length (L)	17.9	cm

Drying Diffusion Coefficient, α_{dry} = 4.33 x 10^{-5} cm^2/sec (2.60 x 10^{-3} cm^2/min)

Laboratory Suction Measurements

Time	Suction
min	pF
1540	3.75
1810	4.02
2080	4.19
2350	4.27
2630	4.35
2900	4.40
3170	4.45
3440	4.49
3710	4.51

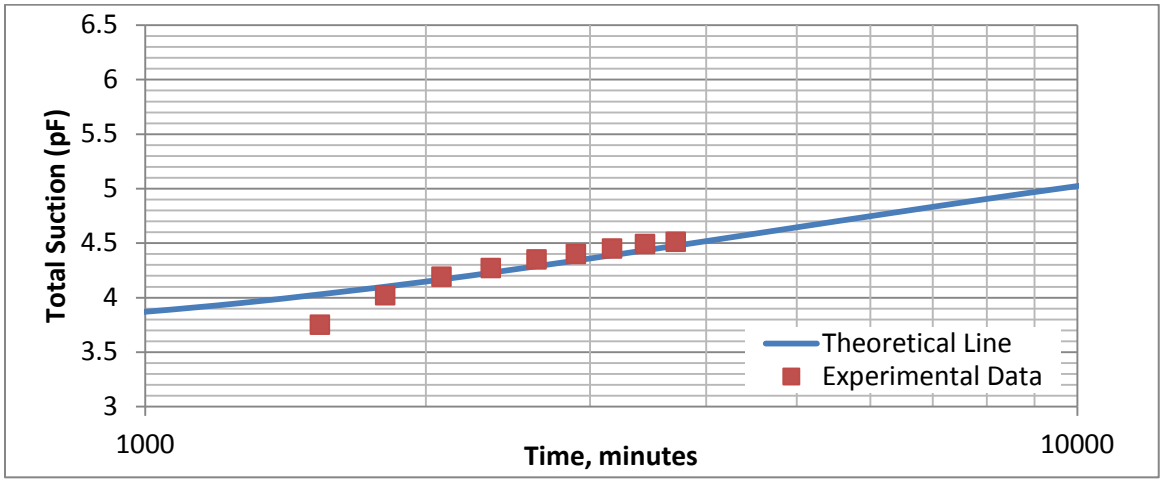

Figure G8. Variation of Total Suction with Time for the Soil of Norman Site from Boring 4, Soil Segment 4D2 at a Depth of 7.40 to 8.0 Feet

Table G9. Norman Site, Compacted Sample, Soil Segments 2F1, 2F2, 2H2, Soil Type 2

Parameter	Value	Units
Evaporation Coefficient, h_e	0.54	cm^{-1}
Atmospheric Suction, U_a	6.29	pF
Initial Suction, U_o	3.59	pF
Psychrometer Location, X	14.3	cm
Sample Length, L	16.8	cm

Drying Diffusion Coefficient, α_{dry} = 8.0 x 10^{-5} cm^2/sec (4.80 x 10^{-3} cm^2/min)

Laboratory Suction Measurements

Time	Suction
min	pF
470	3.59
500	3.68
550	3.80
600	3.91
680	4.02
770	4.13
920	4.24
1150	4.35
1500	4.46
2640	4.56

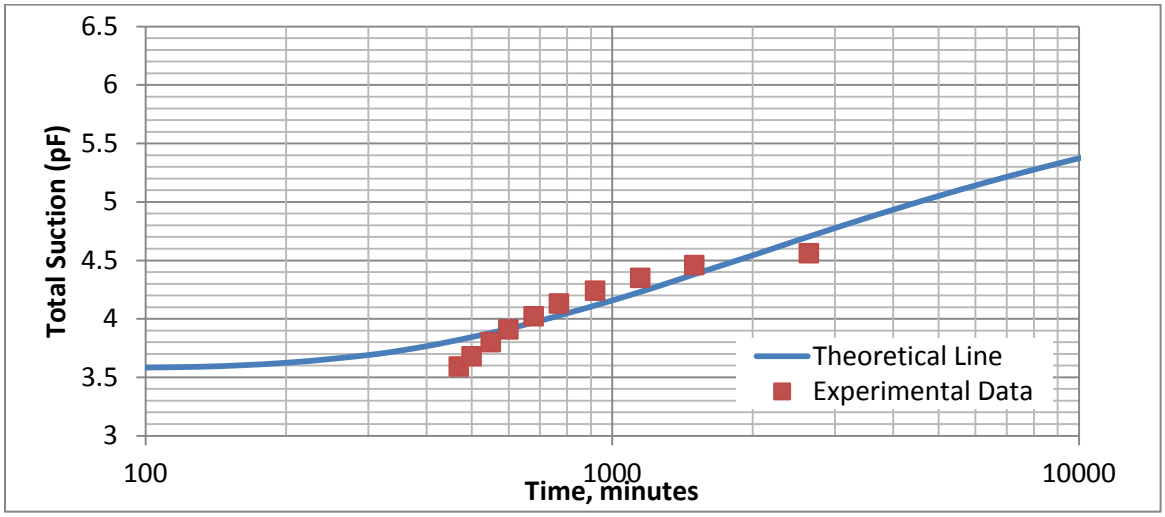

Figure G9. Variation of Total Suction with Time for Compacted Samples of Norman Site Soil from the Segments 2F1, 2F2, 2H2 of Soil Type 2

Table G10. Norman Site, Compacted Sample, Soil Segments 1A1, 2A1, Soil Type 1

Parameter	Value	Units
Evaporation Coefficient, h_e	0.54	cm^{-1}
Atmospheric Suction, U_a	6.21	pF
Initial Suction, U_o	3.38	pF
Psychrometer Location, X	14.6	cm
Sample Length, L	16.6	cm

Drying Diffusion Coefficient, α_{dry} = 4.45 x 10^{-5} cm^2/sec (2.67 x 10^{-3} cm^2/min)

Laboratory Suction Measurements

Time	Suction
Min	pF
10	4.38
450	4.40
1200	4.42
1950	4.44
2600	4.45
3450	4.47
4760	4.50
4820	4.50
6230	4.53
6930	4.54

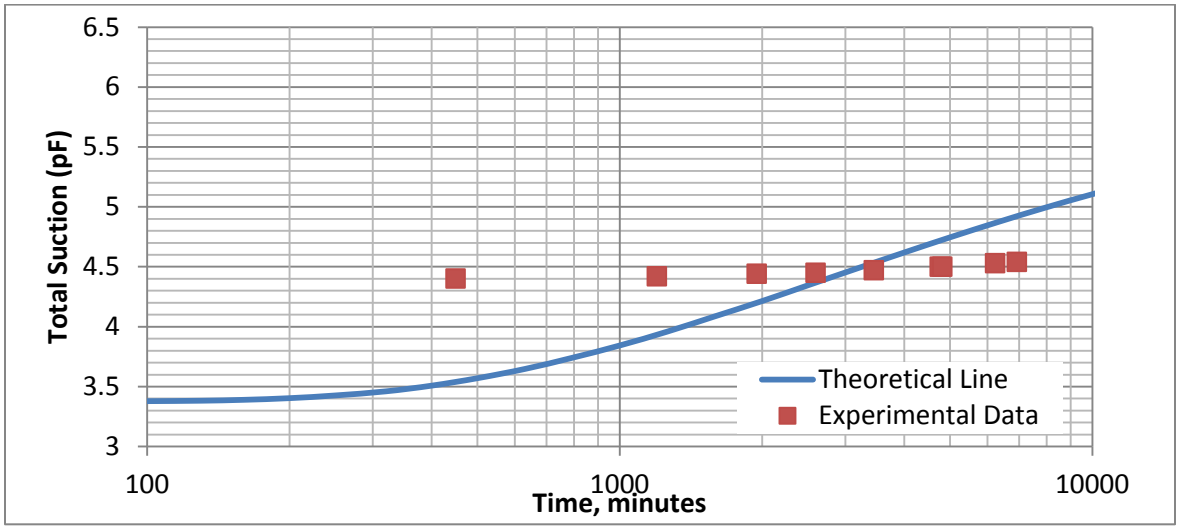

Figure G10. Variation of Total Suction with Time for Compacted Samples of Norman Site Soil from the Segments 1A1, 2A1 of Soil Type 1

APPENDIX H

Table H1. Lake Hefner Site, Boring 1, Soil Segment 1A1, Depth 0 to 0.80 Feet

Parameter	Value	Unit
Evaporation Coefficient, h_e	0.54	cm^{-1}
Atmospheric Suction, U_a	6.30	pF
Initial Suction, U_o	3.01	pF
Psychrometer Location, X	21.5	cm
Sample Length, L	23	cm

Drying Diffusion Coefficient, α_{dry} = 6.67 x 10^{-5} cm^2/sec (4.00 x 10^{-3} cm^2/min)

Laboratory Suction Measurements

Time	Suction
min	pF
1020	3.71
1060	3.86
1110	3.98
1160	4.08
1200	4.15
1250	4.21
1300	4.32
1340	4.37
1390	4.39

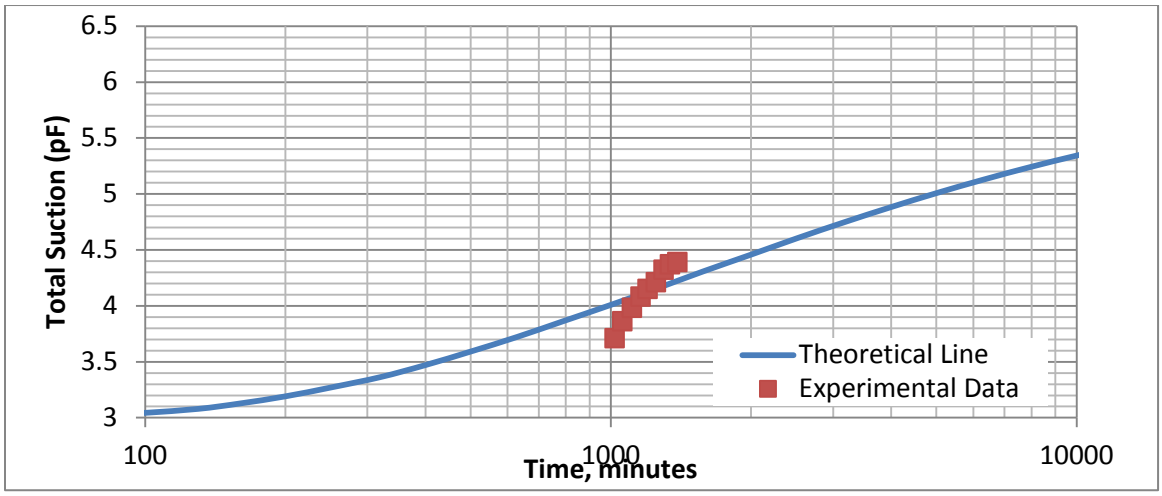

Figure H1. Variation of Total Suction with Time for the Soil of Lakehefner Site from Boring 1, Soil Segment 1A1 at a Depth of 0 to 0.80 Feet

Table H2. Lake Hefner Site, Boring 2, Soil Segment 2C1, Depth 4 to 4.87 Feet

Parameter	Value	Unit
Evaporation Coefficient, h_e	0.54	cm^{-1}
Atmospheric Suction, U_a	6.29	pF
Initial Suction, U_o	3.66	pF
Psychrometer Location, X	19.7	cm
Sample Length, L	22.7	cm

Drying Diffusion Coefficient, α_{dry} = 8.83 x 10^{-5} cm^2/sec (5.30 x 10^{-3} cm^2/min)

Laboratory Suction Measurements

Time	Suction
min	pF
700	3.66
820	3.90
930	4.07
1040	4.17
1160	4.28
1270	4.33
1380	4.39
1500	4.43
1610	4.45

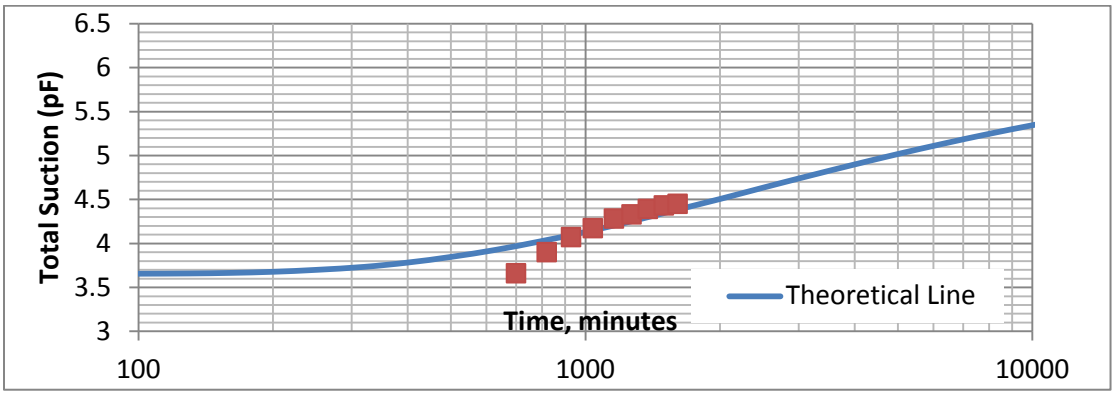

Figure H2. Variation of Total Suction with Time for the Soil of Lakehefner Site from Boring 2, Soil Segment 2C1 at a Depth of 4 to 4.87 Feet

Table H3. Lake Hefner Site, Boring 2, Soil Segment 2D2, Depth 6.98 to 7.96 Feet

Parameter	Value	Unit
Evaporation Coefficient, h_e	0.54	cm^{-1}
Atmospheric Suction, U_a	6.30	pF
Initial Suction, U_o	3.30	pF
Psychrometer Location, X	12	cm
Sample Length, L	15	cm

Drying Diffusion Coefficient, α_{dry} = 8.92 x 10^{-5} cm^2/sec (5.35 x 10^{-3} cm^2/min)

Laboratory Suction Measurements

Time	Suction
min	pF
1400	3.84
1680	4.07
1960	4.22
2240	4.32
2530	4.40
2810	4.47
3090	4.53
3370	4.57
3650	4.59

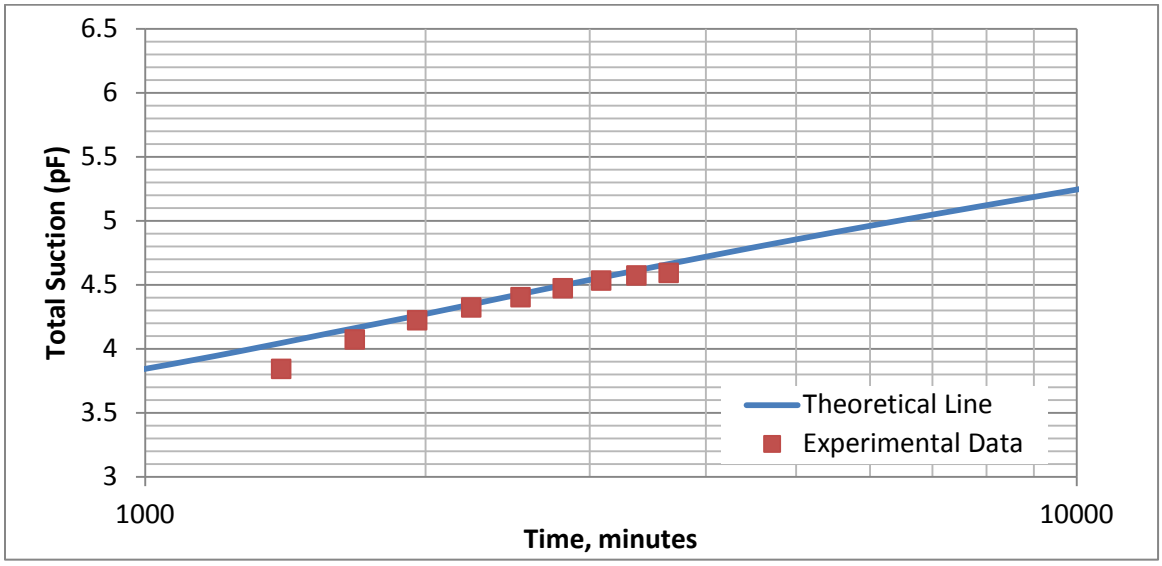

Figure H3. Variation of Total Suction with Time for the Soil of Lakehefner Site from Boring 2, Soil Segment 2D2 at a Depth of 6.98 to 7.96 Feet

Table H4. Lake Hefner Site, Boring 3, Soil Segment 3A2, Depth 0.80 to 1.5 Feet

Parameter	Value	Unit
Evaporation Coefficient, h_e	0.54	cm^{-1}
Atmospheric Suction, U_a	6.27	pF
Initial Suction, U_o	3.29	pF
Psychrometer Location, X	12.3	cm
Sample Length, L	14.8	cm

Drying Diffusion Coefficient, α_{dry} = 3.67 x 10^{-5} cm^2/sec (2.20 x 10^{-3} cm^2/min)

Laboratory Suction Measurements

Time	Suction
min	pF
1960	3.65
2300	3.91
2630	4.06
2970	4.16
3300	4.22
3640	4.29
3970	4.33
4310	4.35
4640	4.37

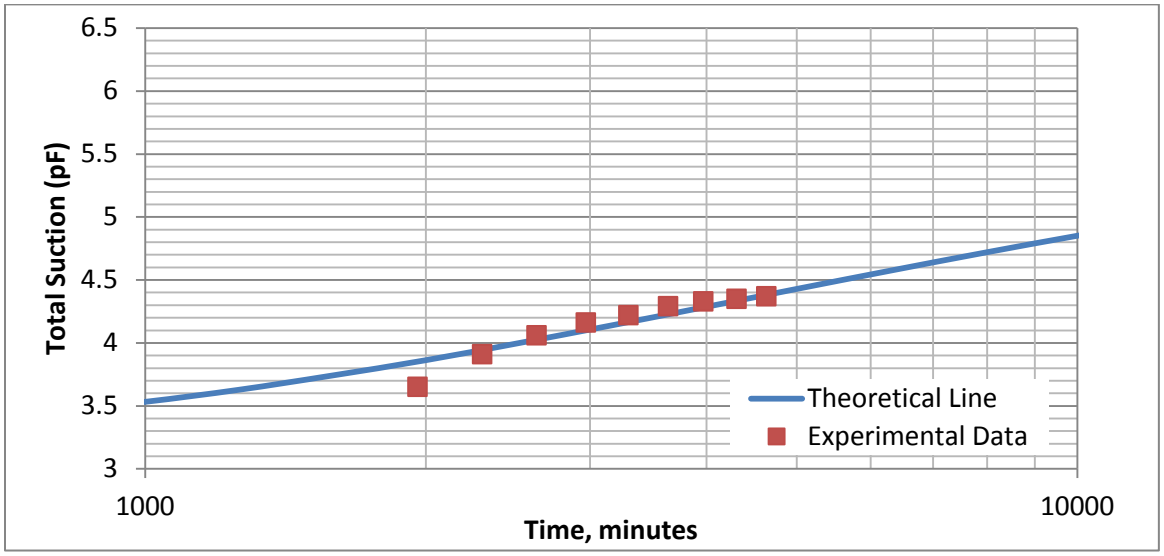

Figure H4. Variation of Total Suction with Time for the Soil of Lakehefner Site from Boring 3, Soil Segment 3A2 at a Depth of 0.80 to 1.5 Feet

Table H5. Lake Hefner Site, Boring 3, Soil Segment 3C2, Depth 4.50 to 5.45 Feet

Parameter	Value	Unit
Evaporation Coefficient, h_e	0.54	cm^{-1}
Atmospheric Suction, U_a	6.32	pF
Initial Suction, U_o	3.74	pF
Psychrometer Location, X	16	cm
Sample Length, L	18	cm

Drying Diffusion Coefficient, α_{dry} = 5.33 x 10^{-5} cm^2/sec (3.20 x 10^{-3} cm^2/min)

Laboratory Suction Measurements

Time	Suction
min	pF
510	3.74
580	3.90
660	4.02
740	4.12
810	4.20
890	4.27
970	4.33
1040	4.37
1120	4.39

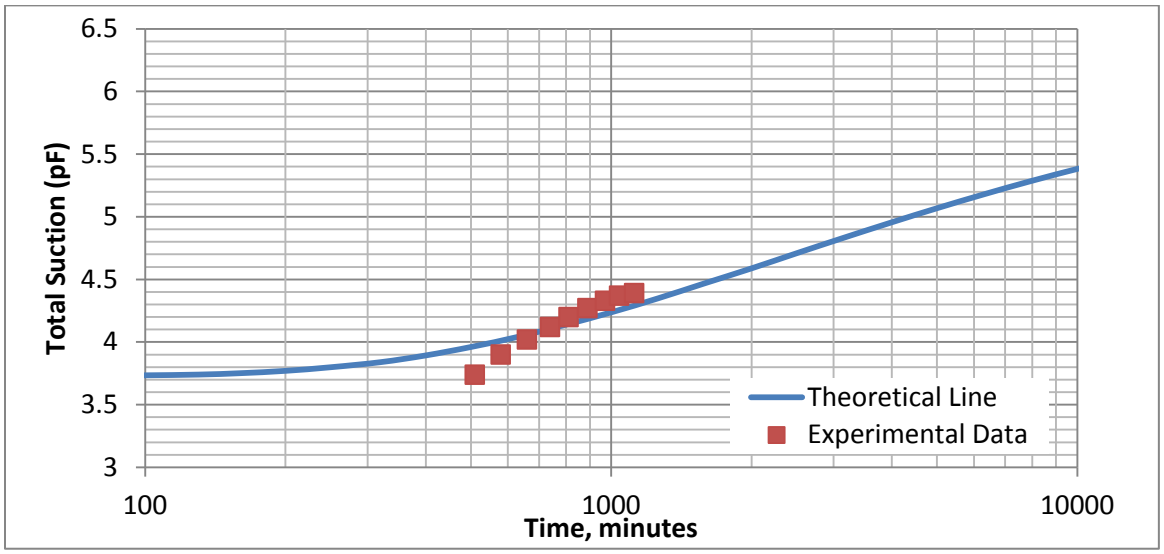

Figure H5 Variation of Total Suction with Time for the Soil of Lakehefner Site from Boring 3, Soil Segment 3C2 at a Depth of 4.50 to 5.45 Feet

Table H6. Lake Hefner Site, Compacted Sample, Soil Segments 1C2, 2C3, 2D1, Soil Type 2

Parameter	Value	Unit
Evaporation Coefficient, h_e	0.54	cm^{-1}
Atmospheric Suction, U_a	6.19	pF
Initial Suction, U_o	3.53	pF
Psychrometer Location, x	1.5	cm
Sample Length, L	16.7	cm

Drying Diffusion Coefficient, α_{dry} = 4.66 x 10^{-6} cm^2/sec (2.80 x 10^{-4} cm^2/min)

Laboratory Suction Measurements

Time	Suction
min	pF
4150	3.53
4240	3.61
4280	3.66
4400	3.75
4460	3.79
4530	3.88
4600	3.93
4670	3.97
4930	4.07
5200	4.13

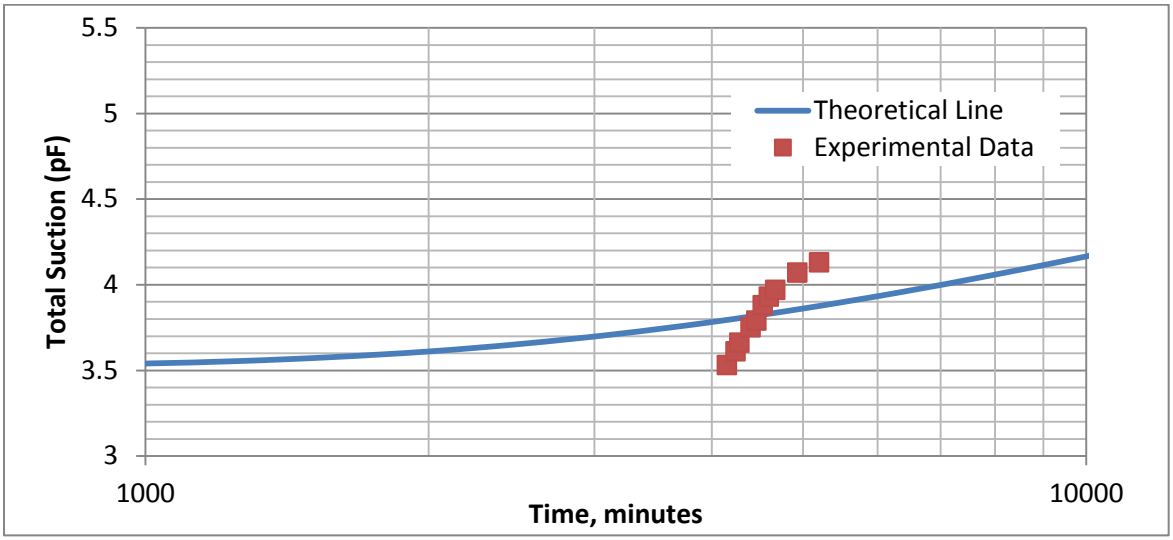

Figure H6. Variation of Total Suction with Time for Compacted Samples of Lakehefner Site Soil from the Segments 1C2, 2C3, 2D1 of Soil Type 2

APPENDIX I

Table I1. Ardmore Site, Boring 1, Soil Segment 1B1, Depth 2.0 to 2.80 Feet

Parameter	Value	Unit
Evaporation Coefficient, h_e	0.54	cm^{-1}
Atmospheric Suction, U_a	6.25	pF
Initial Suction, U_o	3.42	pF
Psychrometer Location, x	15.5	cm
Sample Length, L	17.5	cm

Drying Diffusion Coefficient, α_{dry} = 3.30 x 10^{-5} cm^2/sec (1.98 x 10^{-3} cm^2/min)

Laboratory Suction Measurements

Time	Suction
min	pF
1640	3.42
1700	3.70
1760	3.88
1820	4.00
1880	4.11
1950	4.19
2010	4.25
2070	4.30
2130	4.33
2190	4.35

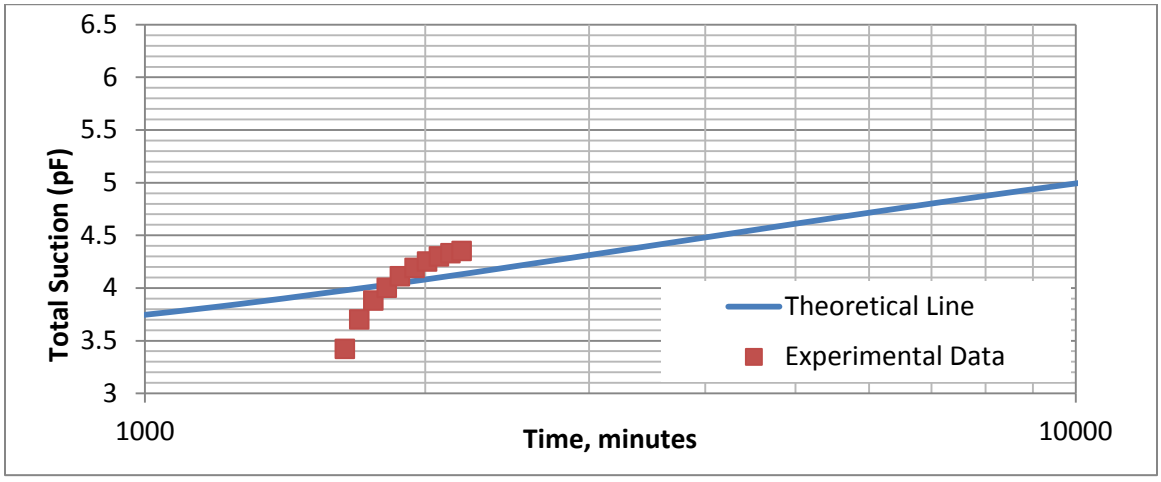

Figure I1. Variation of Total Suction with Time for the Soil of Ardmore Site from Boring 1, Soil Segment 1B1 at a Depth of 2.0 to 2.80 Feet

Table I2. Ardmore Site, Boring 3, Soil Segment 3C2, Depth 4.90 to 6.0 Feet

Parameter	Value	Unit
Evaporation Coefficient, h_e	0.54	cm^{-1}
Atmospheric Suction, U_a	6.22	pF
Initial Suction, U_o	3.37	pF
Psychrometer Location, x	26.1	cm
Sample Length, L	28.6	cm

Drying Diffusion Coefficient, α_{dry} = 1.02 x 10^{-4} cm^2/sec (6.11 x 10^{-3} cm^2/min)

Laboratory Suction Measurements

Time	Suction
min	pF
450	3.37
480	3.50
520	3.64
580	3.78
660	3.90
760	4.04
910	4.17
1100	4.30
1440	4.44
2010	4.57

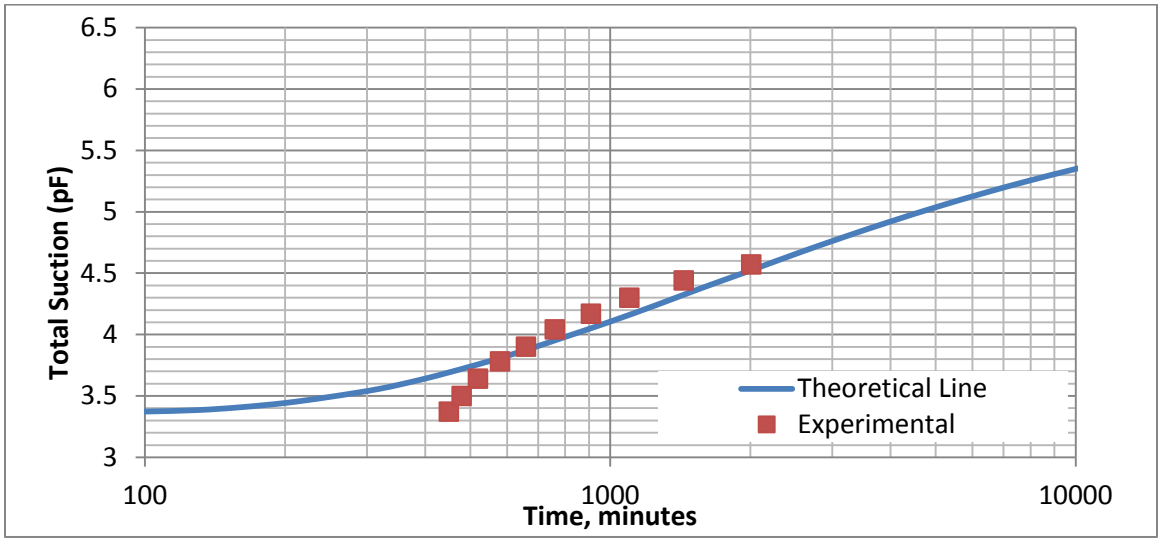

Figure I2. Variation of Total Suction with Time for the Soil of Ardmore Site from Boring 3, Soil Segment 3C2 at a Depth of 4.90 to 6.0 Feet

Table I3. Ardmore Site, Boring 4, Soil Segment 1BB2, Depth 2.50 to 3.40 Feet

Parameter	Value	Unit
Evaporation Coefficient, h_e	0.54	cm^{-1}
Atmospheric Suction, U_a	6.29	pF
Initial Suction, U_o	3.91	pF
Psychrometer Location, x	20.2	cm
Sample Length, L	23.2	cm

Drying Diffusion Coefficient, α_{dry} = 7.08 x 10^{-5} cm^2/sec (4.25 x 10^{-3} cm^2/min)

Laboratory Suction Measurements

Time	Suction
min	pF
100	3.91
220	3.99
330	4.06
490	4.14
710	4.22
1000	4.29
1290	4.37
1630	4.44
2000	4.52
2560	4.60

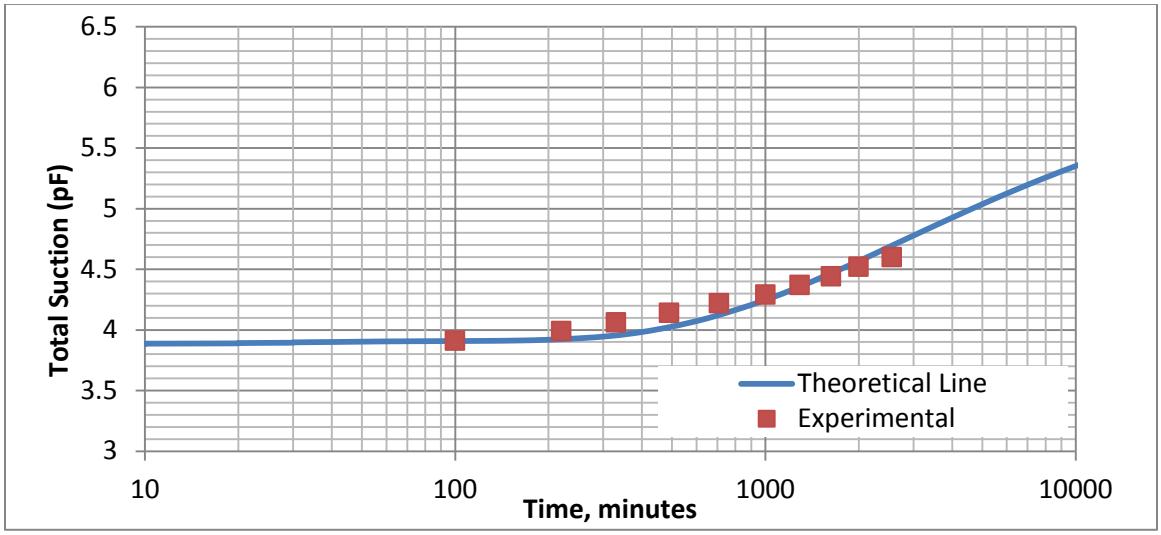

Figure I3. Variation of Total Suction with Time for the Soil of Ardmore Site from Boring 4, Soil Segment 1BB2 at a Depth of 2.50 to 3.40 Feet

Table I4. Ardmore Site, Boring 4, Soil Segment 1CC1, Depth 4.0 to 4.88 Feet

Parameter	Value	Unit
Evaporation Coefficient, h_e	0.54	cm^{-1}
Atmospheric Suction, U_a	6.29	pF
Initial Suction, U_o	3.0	pF
Psychrometer Location, x	17.5	cm
Sample Length, L	21.0	cm

Drying Diffusion Coefficient, α_{dry} = 1.55 x 10^{-4} cm^2/sec (9.30 x 10^{-3} cm^2/min)

Laboratory Suction Measurements

Time	Suction
min	pF
460	3.13
510	3.30
570	3.47
660	3.63
820	3.80
1060	3.96
1410	4.11
1980	4.28
2660	4.44
3860	4.61

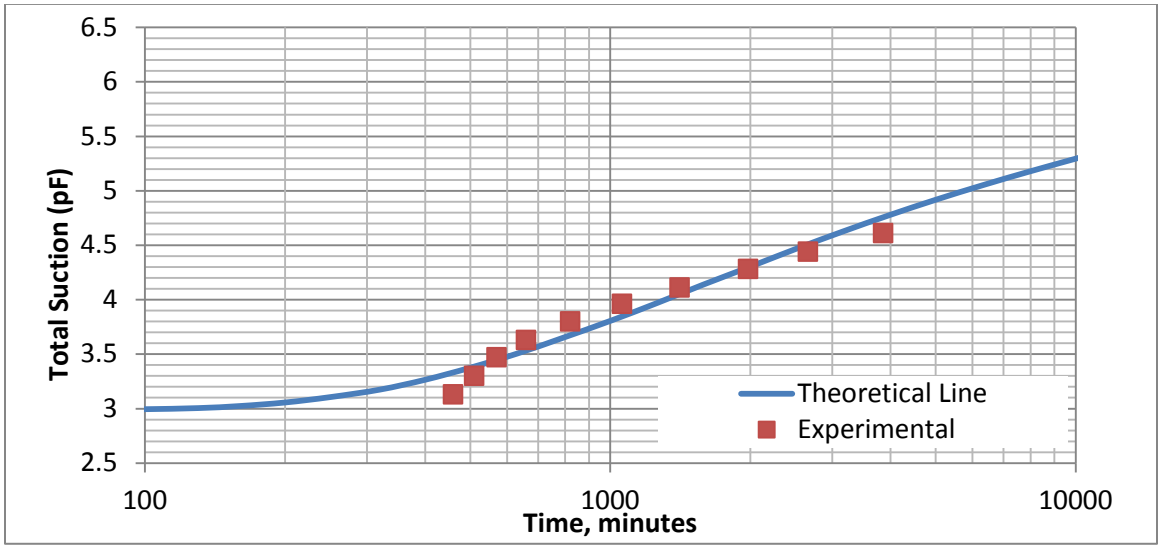

Figure I4. Variation of Total Suction with Time for the Soil of Ardmore Site from Boring 4, Soil Segment 1CC1 at a Depth of 4.0 to 4.88 Feet

Table I5. Ardmore Site, Boring 5, Soil Segment 2BB2, Depth 2.90 to 4.0 Feet

Parameter	Value	Unit
Evaporation Coefficient, h_e	0.54	cm^{-1}
Atmospheric Suction, U_a	6.21	pF
Initial Suction, U_o	3.54	pF
Psychrometer Location, x	16.5	cm
Sample Length, L	18.0	cm

Drying Diffusion Coefficient, α_{dry} = 1.08 x 10^{-5} cm^2/sec (6.50 x 10^{-4} cm^2/min)

Laboratory Suction Measurements

Time	Suction
min	pF
2740	3.54
2790	3.65
2840	3.75
2910	3.86
3000	3.97
3130	4.09
3280	4.18
3500	4.29
3810	4.40
4420	4.51

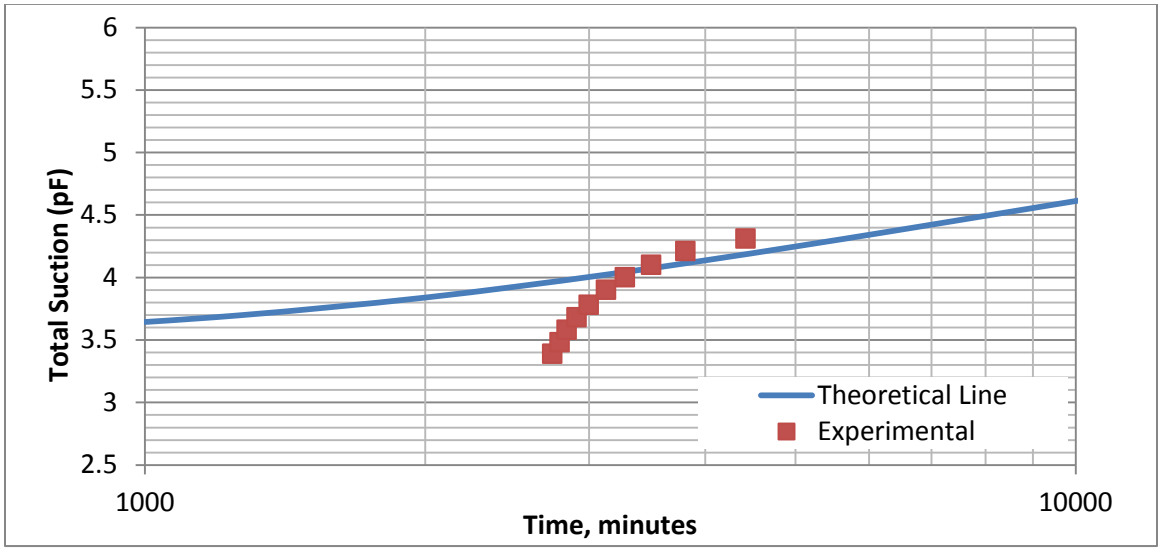

Figure I5. Variation of Total Suction with Time for the Soil of Ardmore Site from Boring 5, Soil Segment 2BB2 at a Depth of 2.90 to 4.0 Feet

Table I6. Ardmore Site, Boring 5, Soil Segment 2CC2, Depth 4.86 to 5.86 Feet

Parameter	Value	Unit
Evaporation Coefficient, h_e	0.54	cm^{-1}
Atmospheric Suction, U_a	6.13	pF
Initial Suction, U_o	3.39	pF
Psychrometer Location, x	19.6	cm
Sample Length, L	21.6	cm

Drying Diffusion Coefficient, α_{dry} = 1.30 x 10^{-5} cm^2/sec (7.80 x 10^{-4} cm^2/min)

Laboratory Suction Measurements

Time	Suction
min	pF
3190	3.39
3210	3.48
3300	3.58
3350	3.68
3460	3.78
3590	3.90
3730	4.00
3880	4.10
4100	4.21
4570	4.31

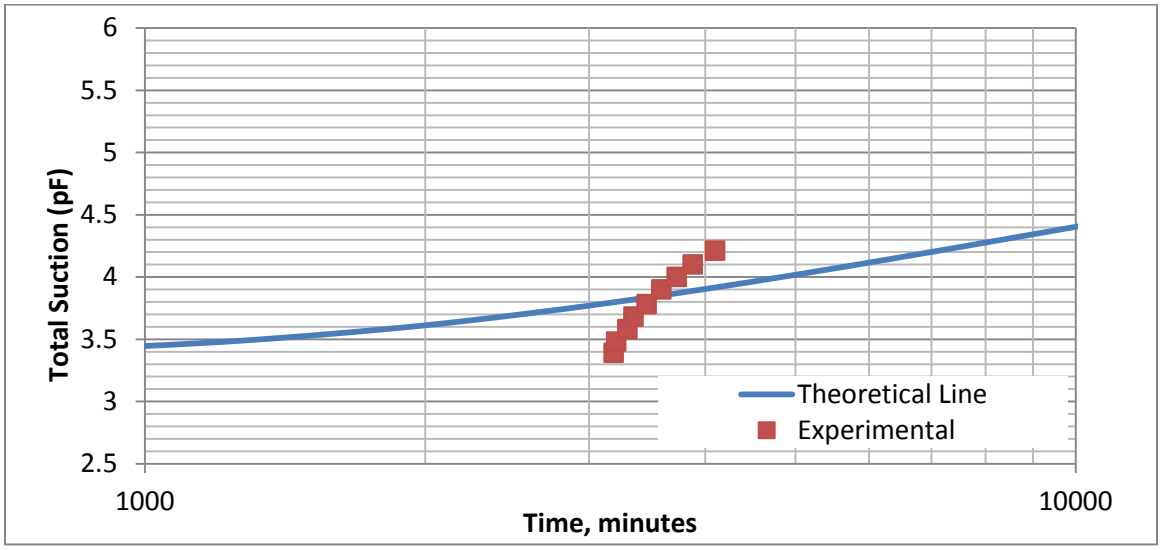

Figure I6. Variation of Total Suction with Time for the Soil of Ardmore Site from Boring 5, Soil Segment 2CC2 at a Depth of 4.86 to 5.86 Feet

Table I7. Ardmore Site, Boring 6, Soil Segment 3AA2, Depth 0.1 to 1.1 Feet

Parameter	Value	Unit
Evaporation Coefficient, h_e	0.54	cm^{-1}
Atmospheric Suction, U_a	6.19	pF
Initial Suction, U_o	3.52	pF
Psychrometer Location, x	21.0	cm
Sample Length, L	23.0	cm

Drying Diffusion Coefficient, α_{dry} = 3.43 x 10^{-5} cm^2/sec (2.06x10^{-3} cm^2/min)

Laboratory Suction Measurements

Time	Suction
min	pF
990	3.52
1020	3.61
1090	3.70
1210	3.85
1360	3.97
1540	4.08
1800	4.21
2110	4.32
2550	4.44
3400	4.59

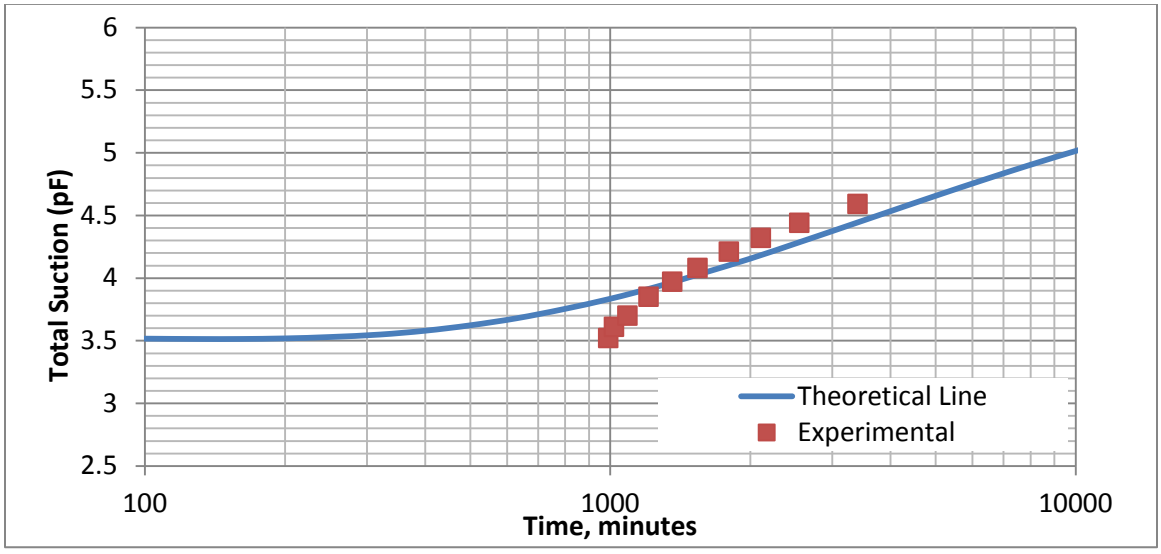

Figure I7. Variation of Total Suction with Time for the Soil of Ardmore Site from Boring 6, Soil Segment 3AA2 at a Depth of 0.1 to 1.1 Feet

Table I8. Ardmore Site, Boring 6, Soil Segment 3DD1, Depth 6.0 to 6.5 Feet

Parameter	Value	Unit
Evaporation Coefficient, h_e	0.54	cm^{-1}
Atmospheric Suction, U_a	6.21	pF
Initial Suction, U_o	3.51	pF
Psychrometer Location, x	12.4	cm
Sample Length, L	14.9	cm

Drying Diffusion Coefficient, α_{dry} = 1.62 x 10^{-5} cm^2/sec (9.7 x 10^{-4} cm^2/min)

Laboratory Suction Measurements

Time	Suction
min	pF
3590	3.51
3690	3.63
3800	3.73
3950	3.85
4150	3.96
4360	4.07
4640	4.18
4980	4.29
5430	4.40
6070	4.52

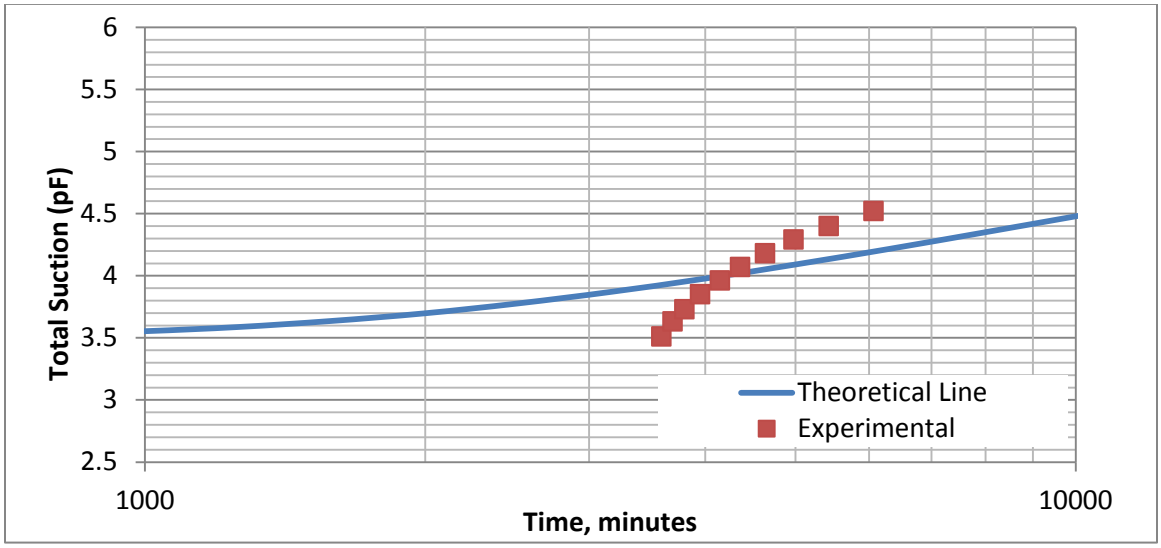

Figure I8. Variation of Total Suction with Time for the Soil of Ardmore Site from Boring 6, Soil Segment 3DD1 at a Depth of 6.0 to 6.5 Feet

Table I9. Ardmore Site, Boring 7, Soil Segment 4AA2, Depth 0.95 to 2.0 Feet

Parameter	Value	Unit
Evaporation Coefficient, h_e	0.54	cm^{-1}
Atmospheric Suction, U_a	6.08	pF
Initial Suction, U_o	3.68	pF
Psychrometer Location, x	15	cm
Sample Length, L	17.5	cm

Drying Diffusion Coefficient, α_{dry} = 9.0 x 10^{-6} cm^2/sec (5.4 x 10^{-4} cm^2/min)

Laboratory Suction Measurements

Time	Suction
min	pF
6140	3.68
6410	3.78
6700	3.89
7030	3.98
7500	4.09
8080	4.19
8660	4.29
9510	4.39
10660	4.50
12600	4.61

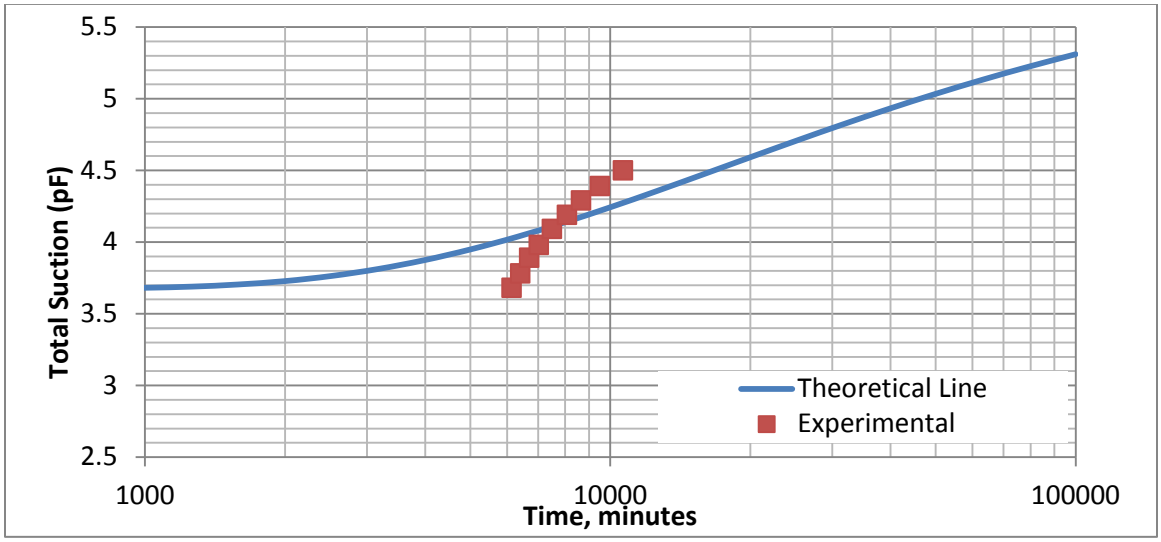

Figure I9. Variation of Total Suction with Time for the Soil of Ardmore Site from Boring 7, Soil Segment 4AA2 at a Depth of 0.95 to 2.0 Feet

Table I10. Ardmore Site, Boring 7, Soil Segment 4DD3, Depth 6.85 to 7.50 Feet

Parameter	Value	Unit
Evaporation Coefficient, h_e	0.54	cm^{-1}
Atmospheric Suction, U_a	6.13	pF
Initial Suction, U_o	3.69	pF
Psychrometer Location, x	15	cm
Sample Length, L	17	cm

Drying Diffusion Coefficient, α_{dry} = 9.83 x 10^{-6} cm^2/sec (5.9 x 10^{-4} cm^2/min)

Time	Suction
min	pF
3190	3.69
3310	3.76
3400	3.83
3520	3.90
3630	3.98
3800	4.05
3930	4.12
4050	4.19
4360	4.26
5070	4.34

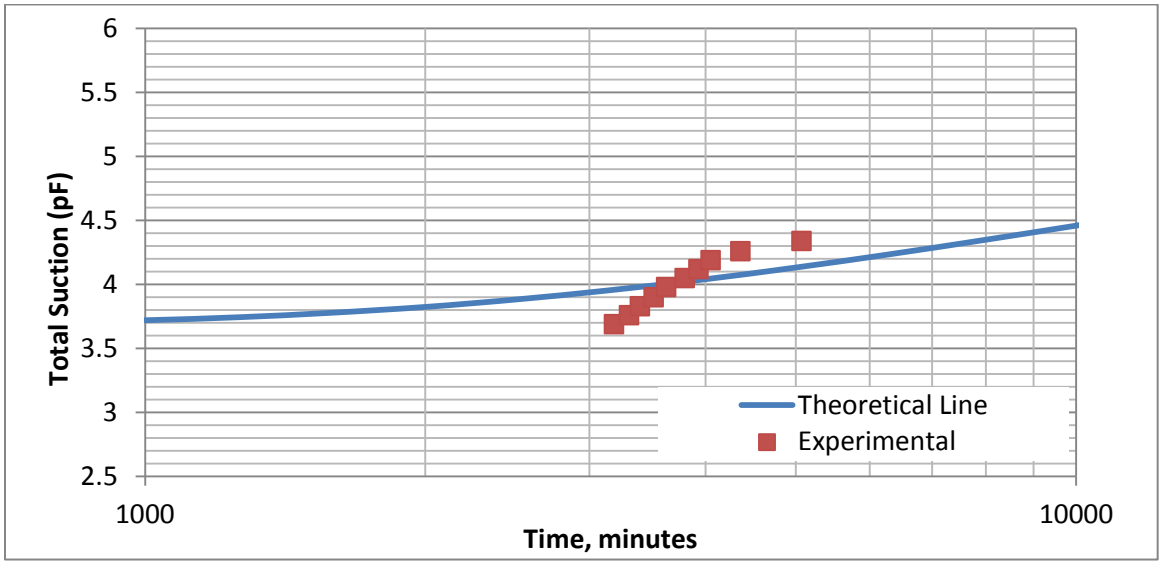

Figure I10. Variation of Total Suction with Time for the Soil of Ardmore Site from Boring 7, Soil Segment 4DD3 at a Depth of 6.85 to 7.50 Feet

Table I11. Ardmore Site, Compacted Sample, Soil Segments 1A1, 1A2, 2A1, 2A2, Soil Type 1

Parameter	Value	Unit
Evaporation Coefficient, h_e	0.54	cm^{-1}
Atmospheric Suction, U_a	6.09	pF
Initial Suction, U_o	4.03	pF
Psychrometer Location, x	11.8	cm
Sample Length, L	16.8	cm

Drying Diffusion Coefficient, α_{dry} = 1.41 x 10^{-5} cm^2/sec (8.5 x 10^{-4} cm^2/min)

Laboratory Suction Measurements

Time	Suction
min	pF
610	4.03
1610	4.10
2770	4.17
4000	4.25
5160	4.31
6600	4.38
8200	4.45
9700	4.52
11600	4.59
14690	4.66

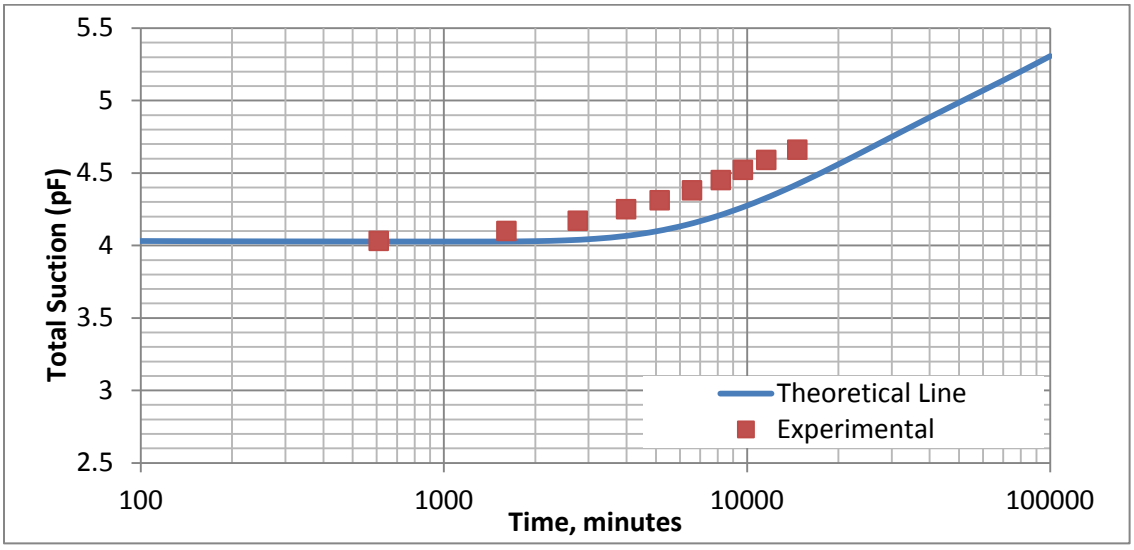

Figure I11. Variation of Total Suction with Time for Compacted Samples of Ardmore Site Soil from the Segments 1A1, 1A2, 2A1, 2A2 of Soil Type 1

Table I12. Ardmore Site, Compacted Sample, Soil Segments 1B2, 2B1, 3B2, 1AA1, 1AA2, Soil Type 2

Parameter	Value	Unit
Evaporation Coefficient, h_e	0.54	cm^{-1}
Atmospheric Suction, U_a	6.09	pF
Initial Suction, U_o	3.69	pF
Psychrometer Location, x	13.5	cm
Sample Length, L	16.5	cm

Drying Diffusion Coefficient, α_{dry} = 1.22 x 10^{-5} cm^2/sec (7.3 x 10^{-4} cm^2/min)

Laboratory Suction Measurements

Time	Suction
min	pF
2760	3.69
3270	3.79
3770	3.87
4390	3.95
5290	4.03
6490	4.12
8040	4.19
10090	4.28
12640	4.36
15890	4.44

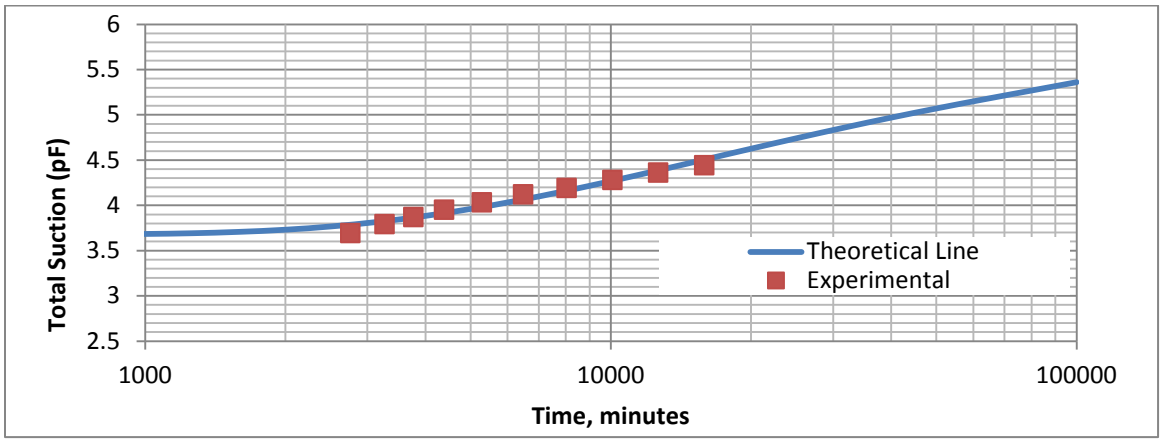

Figure I12. Variation of Total Suction with Time for Compacted Samples of Ardmore Site Soil from the Segments 1B2, 2B1, 3B2, 1AA1, 1AA2 of Soil Type 2

APPENDIX J

Table.J1. Idabel Site, Boring 4, Soil Segment 4A2IDB, Depth 0.45 to 1.13 Feet

Parameter	Value	Unit
Evaporation Coefficient, he	0.54	cm-1
Atmospheric Suction, Ua	6.09	pF
Initial Suction, Uo	3.11	pF
Psychrometer Location, x	13.5	cm
Sample Length, L	15.5	cm

Drying Diffusion Coefficient, α_{dry} = 1.57 x 10^{-3} cm^2/sec (2.619 x 10^{-5} cm^2/min)

Laboratory Suction Measurements

Time	Suction
min	pF
2830	3.68
3000	3.77
3090	3.83
3250	3.92
3370	3.98
3560	4.06
3740	4.13
4000	4.21
4240	4.28
5050	4.36

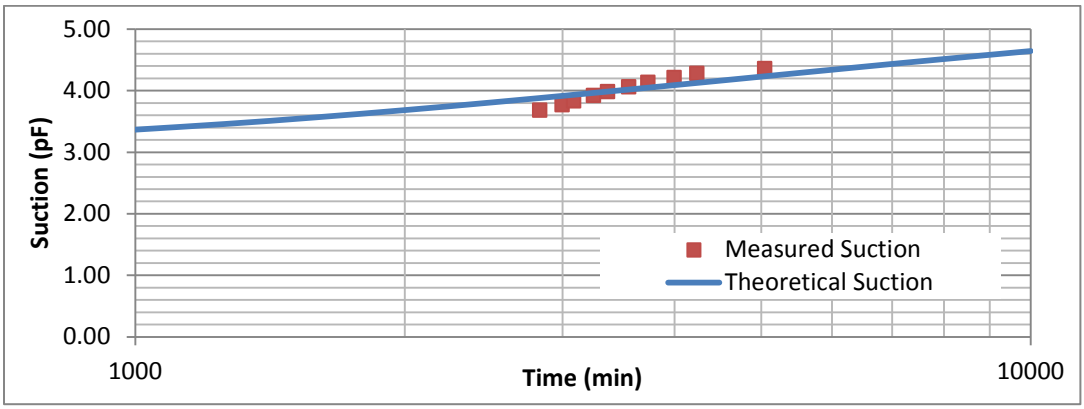

Figure J1. Variation of Total Suction with Time for the Soil of Idabel Site from Boring 4, Soil Segment 4A2 at a Depth of 0.45 to 1.13 Feet

Table J2. Idabel Site, Brown, Boring 4, Soil Segment 4C2, Depth 4.35 to 4.95 Feet

Parameter	Value	Unit
Evaporation Coefficient, he	0.54	cm-1
Atmospheric Suction, Ua	6.08	pF
Initial Suction, Uo	2.47	pF
Psychrometer Location, x	13.5	cm
Sample Length, L	16.5	cm

Drying Diffusion Coefficient, α_{dry} = 5.47 x 10^{-3} cm^2/min (9.127 x 10^{-5} cm^2/sec)

Laboratory Suction Measurements

Time	Suction
min	pF
2740	3.68
2880	3.78
3030	3.87
3190	3.97
3380	4.06
3570	4.16
3900	4.26
4250	4.35
4770	4.45
5690	4.55

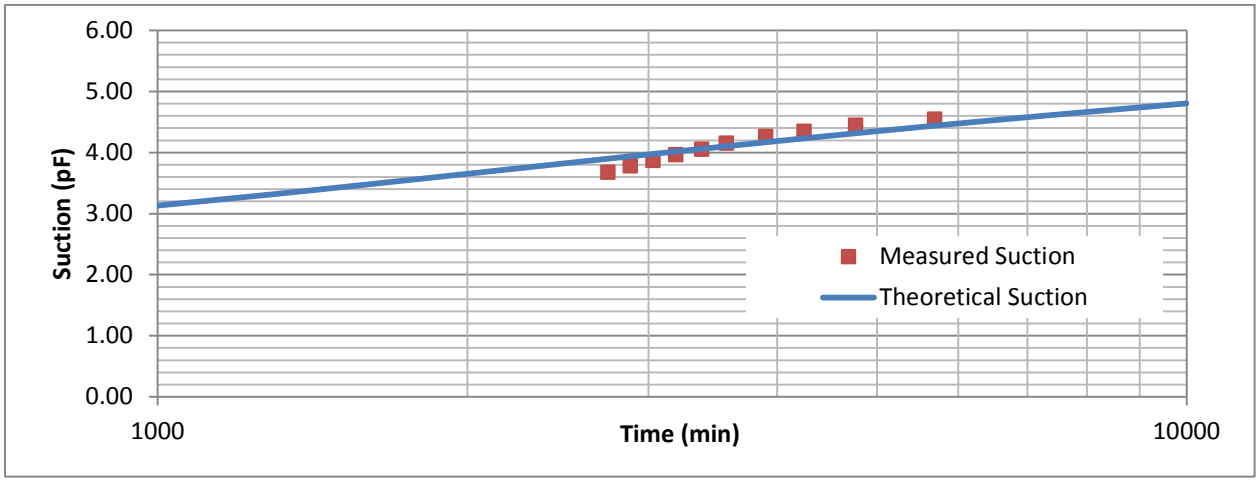

Figure J2. Variation of Total Suction with Time for the Soil of Idabel Site from Boring 4, Soil Segment 4C2 at a Depth of 4.35 to 4.95 Feet

Table J3. Idabel Site, Boring 4, Soil Segment 4D2, Depth 6.30 to 6.80 Feet

Parameter	Value	Unit
Evaporation Coefficient, he	0.54	cm-1
Atmospheric Suction, Ua	6.08	pF
Initial Suction, Uo	3.07	pF
Psychrometer Location, x	8.5	cm
Sample Length, L	14.5	cm

Drying Diffusion Coefficient, α_{dry} = 7.21 x 10^{-3} cm^2/min (1.20238 x 10^{-4} cm^2/sec)

Laboratory Suction Measurements

Time	Suction
min	pF
2060	3.67
2410	3.77
2900	3.87
3490	3.98
4140	4.08
5000	4.19
6000	4.29
7100	4.39
8800	4.50
9470	4.60

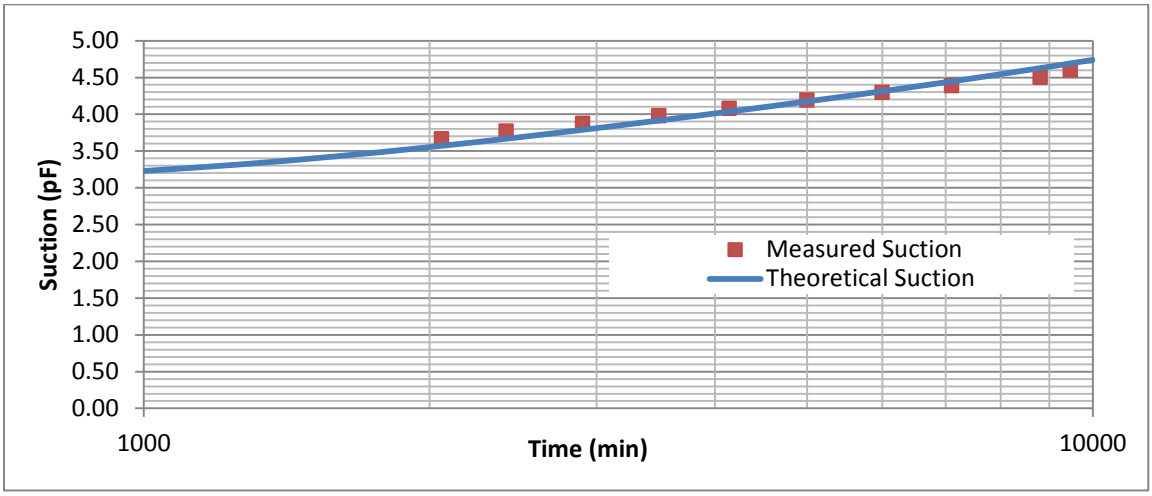

Figure J3. Variation of Total Suction with Time for the Soil of Idabel Site from Boring 4, Soil Segment 4D2 at a Depth of 6.30 to 6.80 Feet

Table J4. Idabel Site, Boring 5, Soil Segment 5A2, Depth 0.35 to 1.0 Feet

Parameter	Value	Unit
Evaporation Coefficient, he	0.54	cm-1
Atmospheric Suction, Ua	6.08	pF
Initial Suction, Uo	2.04	pF
Psychrometer Location, x	8.2	cm
Sample Length, L	14.2	cm

Drying Diffusion Coefficient, α_{dry} = 5.43 x 10^{-3} cm^2/min (9.0477 x 10^{-5} cm^2/sec)

Laboratory Suction Measurements

Time	Suction
min	pF
7100	3.67
7620	3.77
8320	3.88
9040	3.98
9970	4.08
11170	4.19
12760	4.29
14750	4.40
17420	4.50
21460	4.61

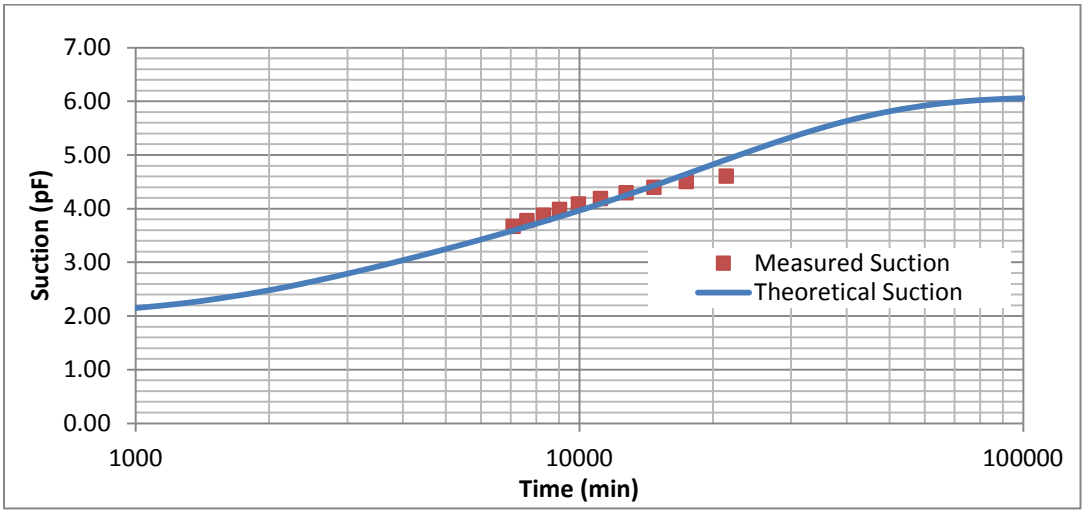

Figure J4. Variation of Total Suction with Time for the Soil of Idabel Site from Boring 5, Soil Segment 5A2 at a Depth of 0.35 to 1.00 Feet

Table J5. Idabel Site, Boring 5, Soil Segment 5B2, Depth 2.30 to 3.05 Feet

Parameter	Value	Unit
Evaporation Coefficient, he	0.54	cm-1
Atmospheric Suction, Ua	6.08	pF
Initial Suction, Uo	1.60	pF
Psychrometer Location, x	10.9	cm
Sample Length, L	16.9	cm

Drying Diffusion Coefficient, α_{dry} = 7.21 x 10^{-3} cm^2/min (1.202 x 10^{-4} cm^2/sec)

Laboratory Suction Measurements

Time	Suction
min	pF
7110	3.67
7490	3.78
8030	3.89
8930	4.00
9990	4.10
11470	4.21
13690	4.32
15850	4.43
18810	4.54
24420	4.67

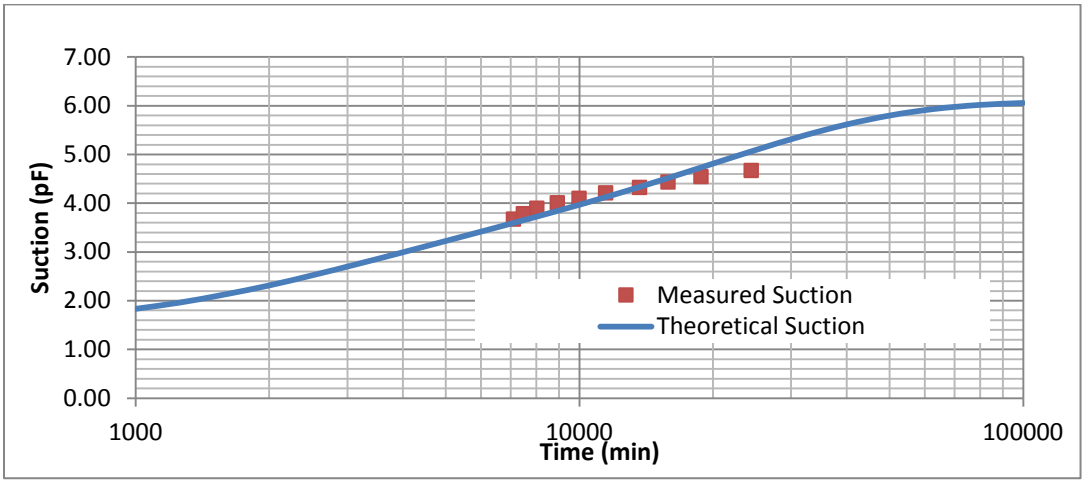

Figure J5. Variation of Total Suction with Time for the Soil of Idabel Site from Boring 4, Soil Segment 5B2 at a Depth of 2.30 to 3.05 Feet

Table J6. Idabel Site, Boring 6, Soil Segment 6D1, Depth 6.00 to 6.73 Feet

Parameter	Value	Unit
Evaporation Coefficient, he	0.54	cm-1
Atmospheric Suction, Ua	6.08	pF
Initial Suction, Uo	3.06	pF
Psychrometer Location, x	15.5	cm
Sample Length, L	21.5	cm

Drying Diffusion Coefficient, α_{dry} = 5.53 x 10^{-3} cm^2/min (9.22147 x 10^{-5} cm^2/sec)

Laboratory Suction Measurements

Time	Suction
min	pF
3370	3.67
3690	3.74
3840	3.78
4170	3.84
4270	3.88
4460	3.93
4850	3.98
5200	4.03
6140	4.09
6610	4.14

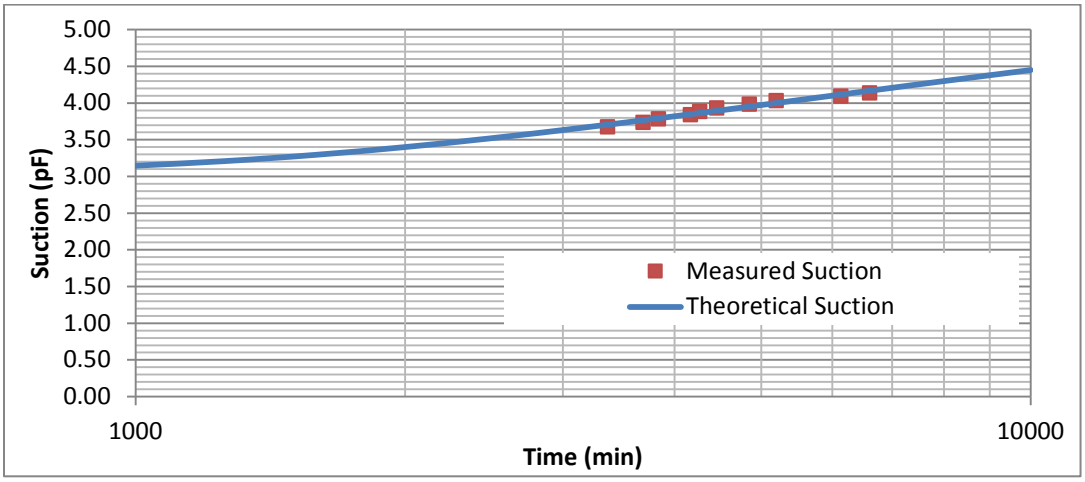

Figure J6. Variation of Total Suction with Time for the Soil of Idabel Site from Boring 6, Soil Segment 6D1 at a Depth of 6.00 to 6.73 Feet

Table J7. Idabel Site, Compacted Sample, Soil Segments 4E2, 5D2, 5E2, 5E2, 6E1, Soil Type 2

Parameter	Value	Unit
Evaporation Coefficient, he	0.54	cm-1
Atmospheric Suction, Ua	6.08	pF
Initial Suction, Uo	3.86	pF
Psychrometer Location, x	9.0	cm
Sample Length, L	13.0	cm

Drying Diffusion Coefficient, α_{dry} = 0.7786 x 10^{-3} cm^2/min (1.29767 x 10^{-5} cm^2/sec)

Laboratory Suction Measurements

Time	Suction
min	pF
6340	3.86
6500	3.90
7300	4.01
7720	4.06
8240	4.12
9510	4.23
10900	4.33
12480	4.44
14950	4.55
18240	4.66

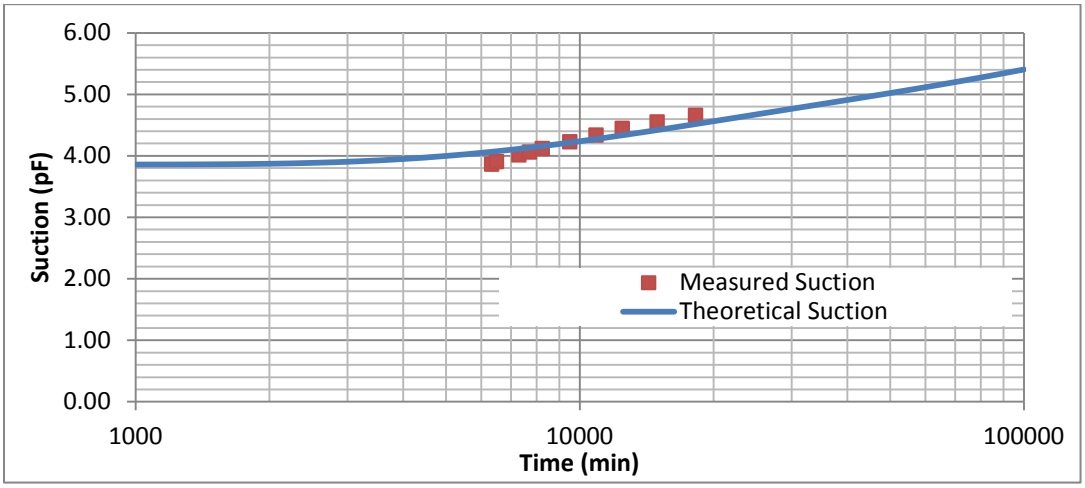

Figure J7. Variation of Total Suction with Time for Compacted Samples of Idabel Site Soil from the Segments 4D2, 5D2, 5E1, 5E2, 6E1 of oil type 2